TECHNISCHE UNIVERSITÄT WIEN
Vienna | Austria

Diploma Thesis

Combustion of Biofuels and Hydrocarbon Fuels in Nonpremixed Flows

carried out for the purpose of obtaining the degree of Dipl.-Ing.,
submitted at TU Wien, Faculty of Mechanical and Industrial Engineering, by

Moritz Öllerer

Mat.Nr.: 01425760

under the supervision of
Ao.Univ.Prof.i.R. Dipl.-Ing. Dr.techn. Ernst Pucher
Institute for Powertrains and Automotive Technology
Technical University Vienna, Austria

and

Prof. Dr. Kalyanasundaram Seshadri
Department of Mechanical and Aerospace Engineering
University of California San Diego, USA

Vienna, April 2022

Abstract

The transition away from fossil energies has important implications for the climate change to keep global temperature rise below 1.5°C. This goes hand in hand with ongoing research into combustion processes for a better understanding and more targeted application of existing fuel blends and novel alternative fuel components.
Emissions in the automotive technology sector go hand in hand with this issue. Even though the proportion of hybrid and electric vehicles has increased, conventional internal combustion engines respectively piston engines with internal combustion, still account for the majority of vehicles on the market.

As a consequence, fundamental investigations on combustion of hydrocarbon and alternative fuels, as they take part in this diploma thesis, provide knowledge for modeling combustion of jet fuels, gasoline, diesel and biofuels. Therefor critical conditions of extinction and autoignition of different fuel mixtures are measured to provide exact data values for further data bases. This reaction kinetic study investigates the experimental extinction behavior of different liquid fuel compositions from Decane with Heptane, Isobutanol with Heptane and Ethanol with Heptane as well as the autoignition behavior of Ethanol with Heptane. The study about autoignition consists of both, a numerical and experimental investigation.

All experiments were carried out at the counterflow burner setup used at UCSD aiming to analyze selected aspects of the combustion of hydrocarbon fuels and alternative fuels in non-premixed flows.
The counterflow setup at UCSD consists of the gas supply, the pump system, the control software and the counterflow burner itself, which is the most important component. A syringe pump filled with the fuel mixture provides the liquid level in the fuel duct which can be additionally observed by a camera. This duct faces axisymmetric the oxidizer duct. An oxidizer stream facing this fuel disc causes in optimal configuration a stagnation plane. During autoignition experiments the autoignition top of the burner is connected to a heating element and a thermocouple measures the temperature close to the ducts' outlet. The gas supply comes from N_2 cylinders and an air pipe. All measured flows are regulated by mass flow controller which operate together with the LabVIEW™ software.

Extinction is defined to take place at the value of a certain strain rate, when the stagnation plane is extinguished by a sudden transition from a reactive region to a non-reactive region. The strain rate is defined as the axial gradient of the axial component of the flow velocity. During experimental investigations, the strain rate a_2 is increased until the flame of the ignited fuel mixture is suddenly extinguished at the extinction strain rate $a_{2.E}$ for a fixed oxygen mass fraction $Y_{O_2.2}$.
The common finding of the extinction experiments for all fuels and volumetric mixtures is that an increase of the respective oxygen mass fraction $Y_{O_2.2}$ leads to an increase in the corresponding extinction strain rate $a_{2.E}$. Heptane is the hardest to extinguish followed in a linear trend by Decane–Heptane mixtures with a higher share of Heptane.
The critical conditions of extinction of burning Isobutanol–Heptane blends of different ratios are in general very similar regardless their volumetric mixing ratios shown by the relatively small deviations between them. Nonlinear effects occur, in particular a burning 50%Vol.Isobutanol–50%Vol.Heptane flame being the easiest to extinguish and consists of the lowest reactivity of the investigated Isobutanol–Heptane blends.
Comparing the critical conditions for a given extinction strain rate $a_{2.E}$ the value of the corresponding oxygen mass fraction $Y_{O_2.2}$ is the highest for Heptane, followed by a 50%Vol.Ethanol– 50%Vol.Heptane-, 20%Vol.Ethanol–80%Vol.Heptane-, 80%Vol.Ethanol–20%Vol.Heptane mixture and Ethanol.

Autoignition is defined to take place at the value of strain rate where an abrupt transition takes place from a weakly reactive region to a reactive region. In the research work, the temperature of the thermocouple, which measures the temperature of the gaseous oxidizer stream T_2, is measured at a constant strain rate a_2. In the event of a sudden flame, the autoignition temperature $T_{2.AI}$ is recorded.
Investigations show that for every mixing ratio of Ethanol and Heptane fuels the autoignition temperature $T_{2.AI}$ increases with an increased strain rate $a_{2.AI}$. Thus the fuel mixture becomes harder to ignite. Heptane is at all strain rate values $a_{2.AI}$ the easiest to ignite. The results indicate that at higher strain rates, Ethanol has the highest autoignition temperature $T_{2.AI}$ followed by descending shares of Ethanol in the mixture. At lower strain rates both numerical and experimental results observe in contrast, opposite results. Analyzing the autoignition behavior of mixtures of Ethanol and Heptane, it seems that already small shares of Ethanol inhibit the low temperature chemistry of Heptane.

Kurzfassung

Eine Verringerung der Abhängigkeit von fossilen Brennstoffen ist ein entscheidendes Ziel, um den globalen Temperaturanstieg unter 1.5°C zu halten. Damit einher geht die Forschung an Verbrennungsvorgängen, was zu einem besseren Verständnis und einer zielgerechteren Anwendung von bereits existierenden Kraftstoffmischungen und neuen alternativen Kraftstoffen führt. Die Emissionen des Automobilsektors spielen bei dieser Diskussion eine große Rolle. Obwohl es durch jüngste Entwicklungen zu einer deutlichen Zunahme von Hybrid- und Elektrofahrzeugen gekommen ist, bilden konventionelle interne Verbrennungsmaschinen immer noch die Mehrheit der Fahrzeuge des Marktes.

Unter Anbetracht dessen liefern fundamentale Verbrennungsanalysen von kohlenstoffhaltigen und alternativen Kraftstoffen, wie sie in dieser Diplomarbeit durchgeführt werden, Wissen über die Modellierung von Jet-Kraftstoffen, Benzin, Diesel und biogenen Kraftstoffen. Deshalb werden hier die kritischen Bedingungen des Auslöschungs- und Selbstzündungsverhalten für ausgewählte Kraftstoffzusammensetzungen gemessen, um exakte Datenwerte für die Verwertung in weiteren Datenbanken und spezifischen Programmen ermitteln zu können. Diese reaktionskinetische Studie untersucht definierte volumetrische Mischungen von Dekan mit Heptan, Isobutanol mit Heptan und Ethanol mit Heptan bezüglich deren Auslöschungsverhalten, als auch eine kombinierte numerische und experimentelle Studie des Selbstzündungsverhaltens von Ethanol mit Heptan. Um die Betriebsgrenzen für Energieumwandlungssysteme in komplexeren Systemen bestimmen zu können, setzt sich diese Arbeit das Ziel, die fundamentalen Stoffeigenschaften des Auslöschungs- und Selbstzündungsvorganges besagter Brennstoffe zu ermitteln.
Die Verbrennungseigenschaften dieser Kraftstoffe hängen einerseits von der charakteristischen chemischen Reaktionsdauer, welche wiederum von der adiabaten Flammentemperatur und der Stöchiometrie abhängt, als auch andererseits von der charakteristischen Verweilzeit ab, welche durch die Strömungsgeschwindigkeit und somit durch die sogenannte Strainrate bestimmt wird.

Die experimentellen Untersuchungen wurden an der University of California San Diego an einem sogenannten Gegenstrombrenner durchgeführt. Dieser Brenner ermöglicht eine einfache, vergleichbare und genaue Charakterisierung des Strömungsfeldes. Der Aufbau lässt sich durch zwei gegenüberliegende, vertikal angeordnete Düsen klassifizieren. Bei einem solchen Brenner treffen im Allgemeinen ein gasförmiger Oxidationsstrom und ein gasförmiger oder flüssiger Brennstoffstrom – hier im Speziellen ein zylindrischer Kraftstoffsammelbehälter, aus dem lediglich der Kraftstoff vaporisiert wird – an einer Stagnationsebene zusammen. Diese konzentrische Stagnationsebene, welche eine dünne, laminare, viskose Grenzschicht darstellt, lässt den Gasstrom in einem bestimmten stöchiometrischen Verhältnis stehen. Es bildet sich eine laminare, stabile und nicht vorgemischte Flamme an der Stagnationsebene zwischen den beiden Auslässen aus. Diese Ebene wird konzentrisch durch einen Stickstoffstrom umschlossen, welcher die Reaktionszone von der Umgebung abschirmt. Alle gemessenen Gasströme werden durch Kontrollventile geregelt und operieren zusammen mit der eigens designten LabVIEW^{TM} Umgebung.

Der Zustand der Erlöschung tritt ein, wenn zwischen den Strömungsgeschwindigkeiten beider Auslässe kein Gleichgewicht mehr besteht und somit die Flamme von der Diffusionsebene ausbricht und erlischt. Dabei wird experimentell der Sauerstoffmassenanteil des Brennstoffstroms bei Auslöschung $Y_{O_2.2}$ variiert, um den jeweiligen Wert der Auslöschungsstrainrate $a_{2.E}$ des korrespondierenden Sauerstoffmassenanteils genau zu bestimmen.
Gemeinsamkeit aller Auslöschexperimente unabhänig der Kraftstoffe und Volumengemische ist, dass eine Erhöhung des Sauerstoffmassenanteils bei Auslöschung $Y_{O_2.2}$ zu einer Erhöhung der Auslöschungsstrainrate $a_{2.E}$ führt. Eine Heptan-Flamme ist am schwersten auszulöschen, gefolgt in einem linearen Trend von Decan-Heptan-Gemischen mit einem höheren Anteil an Heptan. Die kritischen Bedingungen für das Erlöschen brennender Isobutanol-Heptan-Gemische verschiedener Verhältnisse sind sich im Allgemeinen sehr ähnlich, unabhängig von ihren volumetrischen Mischungsverhältnissen, wie die relativ geringen Abweichungen zeigen. Es treten nichtlineare Effekte auf, insbesondere ist eine brennende 50%Vol.Isobutanol–50%Vol.Heptan-Flamme am leichtesten auszulöschen und weist somit die geringste Reaktivität der untersuchten Isobutanol-Heptan-Gemische auf. Vergleicht man die kritischen Bedingungen für eine gegebene Strainrate $a_{2.E}$, so ist der Wert des Sauerstoffmassenanteils $Y_{O_2.2}$ für Heptan am höchsten, gefolgt von einem 50%Vol.Ethanol–50%Vol.Heptan-, 20%Vol.Ethanol–80%Vol.Heptan-, 80%Vol.Ethanol–20%Vol.Heptan-Gemisch und Ethanol.

Das Phänomen der Selbstzündung tritt auf, wenn die entstehende Wärmeentwicklung ein charakteristisches Limit übersteigt und somit die chemische Verweilzeit der Reaktanten schlagartig ansteigen lässt. Die Selbstzündungsexperimente werden bei atmosphärischem Druck p_{atm} unter konstant gehaltenem Sauerstoffmassenanteil des Brennstoffstroms $Y_{O_2.2}$, konstant gehaltener Strainrate a_2 und konstant gehaltenem stöchiometrischen Massenanteil der Kraftstoffrate Y_F durchgeführt. Ziel ist die Bestimmung der Temperatur des Oxidationsmittelstromes T_2 bei Selbstzündung.

Untersuchungen zeigen, dass für jedes Mischungsverhältnis von Ethanol–Heptan-Kraftstoffen die Selbstzündungstemperatur $T_{2.AI}$ mit zunehmender Strainrate $a_{2.AI}$ ansteigt. Dadurch wird das Kraftstoffgemisch schwieriger zu entzünden. Heptan zeigt über jede Strainrate $a_{2.AI}$ hinweg die leichteste Selbstentzündbarkeit. Die Ergebnisse zeigen, dass Ethanol bei höheren Strainrates die höchste Selbstentzündungstemperatur $T_{2.AI}$ aufweist, gefolgt von Kompositionen mit abnehmendem Ethanolanteil in linearem Verhältnis. Bei niedrigeren Strainrates zeigen sowohl die numerischen, als auch die experimentellen Ergebnisse entgegengesetzte Resultate. Die Analyse des Selbstzündungsverhaltens von Ethanol–Heptan-Gemischen zeigt, dass bereits geringe Ethanolanteile die Niedertemperaturchemie von Heptan zu hemmen scheint.

Affidavit

This work was supported by the Austrian Marshall Plan Foundation within the framework of the Marshall Plan Scholarship.

I confirm, that going to press of this thesis needs the confirmation of the examination committee.

Affidavit

I declare in lieu of oath, that I wrote this thesis and performed the associated research myself, using only literature cited in this volume. If text passages from sources are used literally, they are marked as such.

I confirm that this work is original and has not been submitted elsewhere for any examination, nor is it currently under consideration for a thesis elsewhere.

I acknowledge that the submitted work will be checked electronically-technically using suitable and state-of-the-art means (plagiarism detection software). On the one hand, this ensures that the submitted work was prepared according to the high-quality standards within the applicable rules to ensure good scientific practice "Code of Conduct" at the TU Wien. On the other hand, a comparison with other student theses avoids violations of my personal copyright.

San Diego, March 2022

City and Date

Signature

Acknowledgements

First of all, I would like to thank my advisor from my home university TU Wien, Prof. Dr. Ernst Pucher, for his interesting lectures in the field of automotive, energy environment and his practical explanations about research projects in connection with UCSD, without which I would never have had the idea to go to California. As one of his students, I really appreciate the support he has given me in various situations. I am very grateful for the advice he has given me along the way.

I would also like to thank Prof. Dr. Kalyanasundaram Seshadri, who welcomed me very warmly at the university and with whom I had some interesting conversations. I am very grateful to him for asking me which fuels I would like to perform investigations with and for his confidence in performing them in one of his laboratories. because of his trust and calmness, I enjoyed my work at UCSD very much and i was able to develop freely in my work design which was a big advantage for my creativity. Thanks for having me here.

I would like to express my gratitude toward the Austrian Marshallplan Foundation and the TU Wien for their financial support.

Furthermore, I would like to express my gratitude to Liang Ji, without whom the experiments in this work would not have been feasible. I learned a lot from his knowledge of how to conduct the experiments. I am grateful for his support and commitment.

I would especially like to thank my parents, who supported me during my studies whenever I needed it. When there were problems or difficulties my parents and my brother were always the first to stand by my side to help me. Thanks for the backing. Thanks are also due to my friends and family who have had to listen to many difficulties from my student days and have stood by me in these situations.

Lastly, I would like to thank my girlfriend, who always reminds me what is really important in life. She deserves a lot of respect for the fact that she has held so tight for our relationship despite the geographical separation. Through her structured way of working and studying together at the libraries of Vienna, I could learn a lot for my approach which also helped me finishing this diploma thesis in time. Thank you for your support and sharing this adventure with me.

„The boldness of asking deep questions may require unforeseen flexibility if we are to accept the answers.“

BRIAN GREENE

Contents

List of Abbrevations and Symbols

AC	Alternating current
AF	Air/fuel
BEV	Battery electric vehicle
EGT	Exhaust gas temperature
EPA	$T_0 = 298.15K$, $p = 1.01325bar$
EV	Electric vehicle
FC	Fuel cell
HEV	Hybrid electric vehicle
ICE	Internal combustion engine
GHG	Greenhouse gases
MAD	Mean absolute deviation
MFC	Mass flow controller
PHEV	Plug-in hybrid electric vehicle
SLPM	Standard liters per minute
UHC	Unburned hydrocarbons
ZEV	Zero emission vehicle
a_2	Strain rate
A_s	Radiating surface area
b	Diameter of the thermocouple bead
B	Frequency factor
C	Carbon

CO . . . . . Carbonmonoxid

CO_2 . . . . . Carbondioxid

c_p . . . . . Specific heat capacity

d . . . . . Diameter of the duct

ϵ . . . . . Gray emissitivity

h . . . . . Heat transfer coefficient

H . . . . . Hydrogen

HC . . . . . Hydrocarbon

k . . . . . Thermal conductivity

L . . . . . Length between oxidizer and fuel duct

μ . . . . . Dynamic viscosity

N_2 . . . . . Nitrogen

ν_{O_2} . . . . . Stoichiometric coefficient oxygen

NO_x . . . . . Nitrogen oxids

Nu . . . . . Nusselt number

O_2 . . . . . Oxygen

OH . . . . . Hydroxyl group

ρ . . . . . Density

Pr . . . . . Prandtl number

Pt . . . . . Platinum

Re . . . . . Reynolds number

RF . . . . . Radiation factor

Rh . . . . . Rhodium

rpm . . . . . Rotations per minute

σ . . . . . Stefan-Boltzmann-constant

SO_x	Sulfur oxids
T_a	Activation temperature
T_g	Gas temperature
T_∞	Ambient temperature
T_{tc}	Thermocouple temperature
V	Volt
v_r	Radial flow velocity
v_z	Axial flow velocity
Ω	Ohm
w	Reaction rate
W_F	Molecular weight fuel
W_{O_2}	Molecular weight oxygen
Y_F	Mass fraction fuel
Y_{O_2}	Mass fraction oxygen

1
Introduction

Through the discovery of fire, humanity was able to usher in a new era. Over the centuries, mankind has built an ever-increasing advantage through the further development of fire and the accompanying use of electricity. The prosperity of transportation fulfills human needs of mobility and transportation. Due to the current further increase in population density and the rising global energy consumption which will double itself over the next 40 years, research on combustion and energies will stay an important topic. Never before in the history of mankind has there been such an increase in energy consumption as in the present time. However global primary energy demand will only grow up to by 30% in comparison with the current level, the development of alternative energy resources will be one of the main topics of current population. Total energy-related CO_2 emissions have increased exorbitantly with an 87% increase from the 1978 level of 18.0 bn tones to 33.7 bn tones in 2018. This contrasts with a recently published study by the Paul Scherrer Institute, which found a reduction in energy related carbon-containing CO_2 emissions over a 40-year period. In 1978, the carbon intensity of the global energy supply was 66.3 $\frac{kgCO2}{MJ}$ in 1978, the value was reduced by 13% to only 58.0 $\frac{kgCO2}{MJ}$ in 2018. Due to emerging technologies and renewable energies a further decrease of the emissions will be possible in the next decades.[1]

Emissions in the automotive technology sector go hand in hand with this issue. Even though the proportion of hybrid and electric vehicles has increased, conventional combustion engines respectively piston engines with internal combustion, still account for the majority of vehicles on the market. Latest forecast show that the number of vehicles in 2032 will have a share of 30% EVs. Including the rapid percentage increase of HEV and EV in the automotive market during the pandemic year 2020, this figure will be reached earlier. Nevertheless, the upcoming EV growth has important influence on sustainability

[1] Cf. p.5 ff. T. Kober et al. "Global energy perspectives to 2060 – WEC's World Energy Scenarios 2019". eng. In: *Energy strategy reviews* 31 (2020), p. 100523. ISSN: 2211-467X.

implications assuming that the countries are able to manage low emission electricity with the aim to lower the CO_2 emissions. Faced with this global challenge, new green technologies and alternative options for existing fuels must be adopted through the years to dramatically decrease the GHG emissions. It should be noted that the decline of internal combustion engines is not only due to the influence of EVs. Aspects like ride-sharing, self-driving vehicles, improved public transportation systems could even contribute higher and need mentioning.[2]

When speaking about alternative fuels, the usage of biofuels is getting more important due to easily infrastructural adjustments to the current fuel dispenser. EVs, such as BEVs and PHEVs show as well as hydrogen infrastructural problems as well as in modifications of vehicles as of their refueling stations. Biofuel expansions aim to reduce the GHG emissions and are already being widely used as ethanol blends or biodiesel in modern types of vehicles. To serve as a prime example the US state California tries to convince customers into PHEVs by introducing allocation of free parking for these types of vehicles, a price cut of 5000$ and additional money for the charging supply infrastructure.[3]

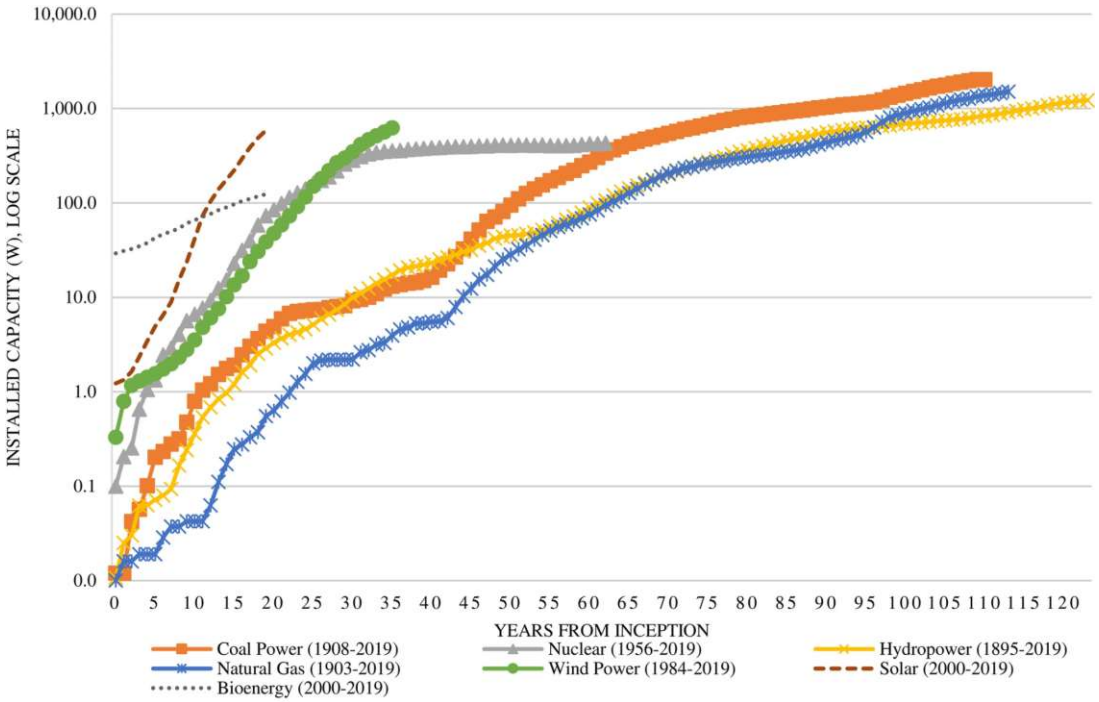

Fig. 1.1: Evolution of energy sources through the years[4]

[2]Cf. p.2 ff. N. Rietmann et al. "Forecasting the trajectory of electric vehicle sales and the consequences for worldwide CO2 emissions". eng. In: *Journal of cleaner production* 261 (2020), p. 121038. ISSN: 0959-6526.

[3]Cf. p.1 ff. Y. Balali and S. Stegen. "Review of energy storage systems for vehicles based on technology, environmental impacts, and costs". eng. In: *Renewable & sustainable energy reviews* 135 (2021), p. 110185. ISSN: 1364-0321.

The Figure 1.1 shows in a logarithmic relationship how primary energy resources have changed over the years since their first inception. While nuclear energy has shown only a linear asymptotic behavior over the last decades since its introduction, natural gas, coal and hydrogen as well as bioenergy have experienced a marginal increase. The most promising growth curve is seen in the alternative energy resources wind and sun, which will overtake fossil fuels in the future if they continue to increase rapidly. The renewable energies are now projected to make 28% of global electric power generation by major energy source in 2021, while the economics of scale is promoting a further growth of renewables in the upcoming decades.[5]

The use of biofuels continues to be in full development and further optimization of these is crucial to turning the emissions issue around. The association of the ZEV nomenclature with EVs has fortunately been pushed out of people's minds in recent years. Among other things, 60% of the world's electrical energy comes from fossil fuels and is thus anything but sustainable. Considering GHG emissions in a global impact on earth's atmosphere and not only on local air quality, there are no evident environmental benefits when comparing a EVs and an internal combustion engine running on biofuel blends from a life-cycle perspective. Only through the parallel improvement of the new powertrain technologies, like BEVs, FCs, HEVs and ICEs with biofuel blends, going hand in hand with a sustainable acquisition of the energy sources they require, seriously sustainable impulses can be set in the direction of „green mobility".[6, 7]

Finding the most suitable technology must be region dependent with a focus on applying the most efficient local conditions optimally utilized and efficiently using regional resources. Only a diversity of vehicle types and powertrain solutions is understood to be the most reasonable and balanced. Globally only combined solutions, not competitive ones, will make a difference in sustainable transportation technology in the long run.[8, 9]

[4] p.24 R. Cherif et al. "Riding the Energy Transition: Oil beyond 2040". eng. In: *Asian economic policy review* 16.1 (2021), pp. 117–137. ISSN: 1832-8105.

[5] Cf. p.10 f. 8.

[6] Cf. p.1 ff. N. Duarte Souza Alvarenga Santos et al. "Internal combustion engines and biofuels: Examining why this robust combination should not be ignored for future sustainable transportation". eng. In: *Renewable sustainable energy reviews* 148 (2021), p. 111292. ISSN: 1364-0321.

[7] Cf. p.316 ff. O. A. Towoju and F. A. Ishola. "A case for the internal combustion engine powered vehicle". In: *Energy Reports* 6 (2020). The 6th International Conference on Power and Energy Systems Engineering, pp. 315–321. ISSN: 2352-4847. DOI: https://doi.org/10.1016/j.egyr.2019.11.082. URL: https://www.sciencedirect.com/science/article/pii/S2352484719309977.

[8] Cf. G. Kalghatgi. "Is it really the end of internal combustion engines and petroleum in transport?" eng. In: *Applied energy* 225 (2018), pp. 965–974. ISSN: 0306-2619.

[9] Cf. M. Balaji et al. "Scope for improving the efficiency and environmental impact of internal combustion engines using engine downsizing approach: A comprehensive case study". eng. In: *IOP conference series. Materials Science and Engineering*. Vol. 1116. 1. Bristol: IOP Publishing, 2021, p. 12070.

In order to pursue the goal of a sustainable future, a diversity of solutions must be considered and the real major cause of global emissions, not only the automotive sector, must be addressed. Despite the energetic combustion approach, the production of the blends, the construction of corresponding efficient machines, must also be considered, where reference is made to further literature[10, 11, 12, 13].
We could face a change in energy supply and the whole transportation market on the basis of technological, political and societal influence in the future. The transition away from fossil energies has important implications for the climate change to keep global temperature rise below 1.5°C. This goes hand in hand with ongoing research into combustion processes for a better understanding and more targeted application of existing fuel blends and novel alternative fuel components. Research in the field of biogenic fuels and alternative energies is a clear focus here.

Combustion is basically a converting process where reactants are converted into products, releasing heat for utilization. At the global level the combustion system consists of the oxidizer and the fuel. By the laws of equilibrium thermodynamics, the thermal and compositional properties of these products can be determined. In a non-premixed system the separated reactants need to get brought together with transportation systems to a common region where the reaction can be held.[14]

In this diploma thesis extinction and autoignition experiments are presented and a comparative both numerical and simulate study is performed. The investigated fuel mixtures will be different volume mixtures of Heptane with Decane, Ethanol and Isobutanol.

[10] Cf. R. C. Ray. *Sustainable biofuels : opportunities and challenges*. eng. Applied Biotechnology Reviews. London, England: Academic Press, 2021. ISBN: 0128223928.
[11] Cf. K. Pandey et al. *Recent Advances in Mechanical Engineering : Select Proceedings of ICRAME 2020*. eng. 1st ed. 2021. Lecture Notes in Mechanical Engineering. Singapore: Springer Singapore Imprint: Springer, 2021. ISBN: 9811577110. URL: 10.1007/978-981-15-7711-6.
[12] Cf. I. Mporas et al. *Energy and Sustainable Futures : Proceedings of 2nd ICESF 2020*. eng. 1st ed. 2021. Springer Proceedings in Energy. Cham: Springer International Publishing Imprint: Springer, 2021. ISBN: 3030639169. URL: 10.1007/978-3-030-63916-7.
[13] Cf. S.-Y. No. *Application of Liquid Biofuels to Internal Combustion Engines*. eng. 1st ed. 2019. Green Energy and Technology. Singapore: Springer Singapore Imprint: Springer, 2019. ISBN: 981136737X. URL: 10.1007/978-981-13-6737-3.
[14] Cf. p.6 f. C. K. Law. *Combustion Physics*. eng. Vol. 9780521870528. Cambridge: Cambridge University Press, 2006. ISBN: 0521154219.

2
Definitions and theoretical framework

Combustion is a study of chemical reaction streams in which a conversion of chemical energy into thermal energy occurs. Combustion is an interdisciplinary topic that combines thermodynamics, chemical kinetics, fluid mechanics, and transport phenomena and takes overall also place in nature. In order for a combustion reaction to take place, the fuel must react with the oxygen present in the air to form reaction products, to be noted that the resulting products have a lower enthalpy.[15, 16]
Combustion has major interest fields which can be given as the following ones:

- **Energy sector** As mentioned in chapter 1 the dwindling of fossil energy resources in the transportation sector will also held part into the global energy sector, since better alternatives are coming up. In ICE fossil fuel as petroleum still takes the most important role.

- **Pollution and Health** Combustion produces pollutants such as soot, SO_x, NO_x, UHC, CO. Due to condensation the liquid particles on particular surfaces can lead to dangerous products. Main problem is the anthropogenic CO_2 load.

- **Safety** The inhalation of smoke and the toxic products which concern human health are as bad as the destruction structural fires can evoke.

- **Defense and Space** The national defense is interested in combustion research for jet engines, rockets and guns. To conduct experiments without the buoyancy force investigations on combustion have to be conducted in space.[17]

[15] Cf. p.6. ff. 27.
[16] Cf. p.1 f. A. Mukhopadhyay and S. Sen. *Fundamentals of combustion engineering*. eng. New York, NY: CRC Press, 2019. ISBN: 0429158211. URL: https://www.taylorfrancis.com/books/9780429158216.
[17] Cf. p.2. ff. 27.

2.1 Disciplines comprising combustion

Combustion affects many different fields

- **Thermodynamics** The combustion processes can easily be terminated while having a look on the rules of equilibrium. In this state the thermal and compositional products can be determined and the amount of transformed chemical energy to thermal energy can be specified.
- **Transport** Fresh reactants are mostly supplied to the continuing flame through the process of diffusion and the heat is moving to colder regions to force an ignition of the yet unburned reaction partners.
- **Fluid mechanics** Combustion reactions usually consist of strongly locally exothermic and temperature as well as density fluctuating chemical reactions within a fluid.
- **Chemical kinetics** Chemical equilibrium tells us only about the final stage of the experiments without mentioning factors like chemical time scales, multiple chain reactions. Therefore, chemical kinetics manages providing a relation between kinetic rate coefficients and equilibrium constants.[18, 19]

[18] Cf. p.55 ff. 33.
[19] Cf. p.6 ff. 27.

2.2 Strain rate

A steady state system as it is one in the counterflow burner must be stabilized by a flame holder. The energy released by the reaction exceeds by far the energy coming from kinetic movement of particles. To determine the strain rate, one starts by establishing the continuity equation in cylindrical coordinates (r, Θ, z). Due to the functional principle of a counterflow burner one can assume a considering steady, axisymmetric flow of gas from an upper duct with large diameter directed toward a disc at the lower part. The upper and lower part causing boundaries and are separated with the length L. Furthermore, the axial component z and the radial component r are non-dimensional with respect to L. The analysis is carried out for small values of L/d. While the component v_r describes the radial flow velocity, v_z describes the axial flow velocity. The axial axle starts with $z = O$ at the fuel duct boundary and has value $z = 1$ at the oxidizer boundary. At the injection plane the fluid velocity is represented as U_2 and the temperature of the fluid as T_2. The surface of the disc has a constant temperature of T_1. Simplifying the following equations, the values for density ρ, viscosity μ, thermal conductivity k and heat capacity c_p are considered as uniform. Further assumptions need to be taken to compute the energy conservation, mass conservation and momentum conservation: Neglecting buoyancy, single diffusion coefficient D and $\Theta = (T - T_1)/(T_2 - T_1)$:[20, 21]

Continuity equation can be given as the following:[22]

$$\frac{\partial \rho}{\partial t} + \frac{1}{r}\frac{\partial}{\partial r}(\rho r v_r) + \frac{1}{r}\frac{\partial}{\partial \Theta}(\rho r v_\Theta) + \frac{\partial}{\partial z}(\rho v_z) = 0 \tag{2.1}$$

Assuming an incompressible flow and axisymmetric flow, the equation becomes the following:

$$\frac{1}{r}\frac{\partial}{\partial r}(r v_r) + \frac{\partial}{\partial z} v_z = 0 \tag{2.2}$$

[20] Cf. p.835 f. K. Seshadri et al. "Activation-energy asymptotic theory of autoignition of condensed hydrocarbon fuels in non-premixed flows with comparison to experiment". eng. In: *Combustion theory and modelling* 12.5 (2008), pp. 831–855. ISSN: 1364-7830.

[21] Cf. p.756 ff. J. O. Hirschfelder. *Molecular theory of gases and liquids*. eng. New York: Wiley, 1965 - 1954.

[22] Cf. p.88 33.

Knowing the mass conservation equation derives to the radial equation 2.3 and axial equation 2.4 of motion with respect to the properties of a newtonian fluid exemplified for the radial component:[23]

$$\rho\left(\frac{\partial v_r}{\partial t}+v_r\frac{\partial v_r}{\partial r}+\frac{v_\Theta}{r}\frac{\partial v_r}{\partial \Theta}+v_z\frac{\partial v_z}{\partial z}-\frac{v_\Theta^2}{r}\right)=-\frac{\partial p}{\partial r}+\mu\left[\frac{\partial}{\partial r}\left(\frac{\partial}{r\partial r}(rv_r)\right)+\frac{1}{r^2}\frac{\partial^2 v_r}{\partial \Theta^2}+\frac{\partial^2 v_r}{\partial z^2}-\frac{2}{r^2}\frac{\partial v_\Theta}{\partial \Theta}\right]$$

$$v_r\frac{\partial v_r}{\partial r}+v_z\frac{\partial v_r}{\partial z}=-\frac{\partial p}{\partial r}+\frac{1}{Re}\left[\frac{\partial}{\partial r}\left(\frac{\partial}{r\partial r}(rv_r)\right)+\frac{\partial^2 v_r}{\partial z^2}\right] \tag{2.3}$$

$$v_r\frac{\partial v_z}{\partial r}+v_z\frac{\partial v_z}{\partial z}=-\frac{\partial p}{\partial z}+\frac{1}{Re}\left(\frac{\partial}{\partial r}\left[\frac{\partial}{r\partial r}(rv_z)\right]+\frac{\partial^2 v_z}{\partial z^2}\right) \tag{2.4}$$

The pressure for low speed flows can be given as:[24]

$$p(z)=P(z)-r^2Q(z) \tag{2.5}$$

Reynolds number due to injection velocity U_2 for $z=1$ and Prandtl number at the oxidizer duct are given as the following:

$$\begin{aligned} Re&=\frac{U_2\rho L}{\mu}\\ Pr&=\frac{\mu c_p}{k}\end{aligned} \tag{2.6}$$

Energy conversation equation:

$$v_r\frac{\partial \Theta}{\partial r}+v_z\frac{\partial \Theta}{\partial z}=\frac{1}{Re\,Pr}\left[\frac{\partial}{\partial r}\left(\frac{1}{r}\frac{\partial}{\partial r}(r\Theta)\right)+\frac{\partial^2\Theta}{\partial z^2}\right] \tag{2.7}$$

[23] Cf. p.848 R. B. Bird et al. *Transport phenomena*. eng. 2., rev. ed.. New York, NY [u.a.]: Wiley Sons, 2007. ISBN: 0470115394.

[24] Cf. p.251 K. Seshadri and F. Williams. "Laminar flow between parallel plates with injection of a reactant at high reynolds number". eng. In: *International journal of heat and mass transfer* 21.2 (1978), pp. 251–253. ISSN: 0017-9310.

All flow quantities besides the pressure are functions of the axial coordinate. Solutions are found for the radial velocity components showed in equation 2.8:[25]

$$v_r = rU(z) \tag{2.8}$$

Equation 2.2 hands down the velocity and hence the derivations of the velocity:

$$\begin{aligned} \frac{1}{r}\frac{\partial}{\partial r}(r^2U) + \frac{\partial}{\partial z}v_z = 0 \\ U(z) = -\frac{1}{2}\frac{\partial v_z}{\partial z} \end{aligned} \tag{2.9}$$

$$\begin{aligned} \frac{\partial v_r}{\partial r} = U(z) \quad & \frac{\partial v_r}{\partial z} = 0 \\ \frac{\partial v_z}{\partial r} = 0 \quad & \frac{\partial v_z}{\partial z} = -2U(z) \end{aligned} \tag{2.10}$$

And for the derivation of pressure:

$$\begin{aligned} \frac{\partial p}{\partial r} &= -2rQ(z) \\ \frac{\partial p}{\partial z} &= P'(z) - r^2Q'(z) \end{aligned} \tag{2.11}$$

Inserting 2.8 and 2.10 into equation 2.3 leads to 2.12 and for equation 2.4 to 2.13:[26]

$$\begin{aligned} rU * U + v_z\frac{r\partial U}{\partial z} &= -(-2rQ) + \frac{1}{Re}[\frac{\partial}{\partial r}\frac{1}{r}2rU + \frac{r\partial^2 U}{\partial z^2}] \\ U^2 + v_zU' &= 2Q + \frac{1}{Re}U'' \\ 0 &= (\frac{\partial v_z}{\partial z})^2 - 2v_z\frac{\partial^2 v_z}{\partial z^2} - 8Q + \frac{2}{Re}\frac{\partial^3 v_z}{\partial z^3} \end{aligned} \tag{2.12}$$

$$v_z\frac{\partial v_z}{\partial z} = -\frac{\partial P}{\partial z} + \frac{1}{Re}\frac{\partial^2 v_z}{\partial z^2} \tag{2.13}$$

[25] Cf. p.251 45.

[26] Cf. p.596 ff. I. Proudman. "An example of steady laminar flow at large Reynolds number". eng. In: *Journal of fluid mechanics* 9.4 (1960), pp. 593–602. ISSN: 0022-1120.

The following boundaries apply at z=0 and z=1:[27]

$$\begin{aligned} v_z = 0 \quad & \frac{\partial v_z}{\partial z} = 0 \quad \Theta = 1 \\ v_z = -1 \quad & \frac{\partial v_z}{\partial z} = 0 \quad \Theta = 0 \end{aligned} \tag{2.14}$$

Considering large numbers for Re and $RePr$ a thin boundary layer of thickness of the order $\delta << 1$ is established at the surface of the stagnation plane. Investigations for the flow inside this boundary layer have been made in previous literature.[28]
Indicating the strain rate the flow outside the boundary layer needs to be observed. The equations describing this inviscid, rotational zone obtained from 2.12 and 2.13 are:

$$\begin{aligned} (\frac{\partial v_z}{\partial z})^2 - 2v_z\frac{\partial^2 v_z}{\partial z^2} - 8Q = 0 \\ v_z\frac{\partial v_z}{\partial z} + \frac{\partial P}{\partial z} = 0 \end{aligned} \tag{2.15}$$

The equations in 2.15 have to fulfill all of the assumed boundary conditions mentioned in 2.2. There exists solutions that satisfies these boundary conditions:

$$\begin{aligned} v_z = z^2 - 2z \quad & v_r = r(1-z) \\ Q = \frac{1}{2} \quad & \frac{\partial P}{\partial z} = -2z(z^2 - 3z + 2) \end{aligned} \tag{2.16}$$

The strain rate is defined as the axial gradient of the axial component of the flow velocity.

$$a = -\frac{\partial v_z}{\partial z}\frac{U_2}{L} = 2(1-z)\frac{U_2}{L} \tag{2.17}$$

The velocity of the fuel stream V_1 is negligible in the experiments performed in this thesis because there literally exists no fuel stream, the fuel is just evaporated from the fuel-cup as shown in figure 3.3. For a given strain rate a_2 the velocity can be easily computed:

$$U_2 = \frac{2a_2}{L} \tag{2.18}$$

[27] Cf. p.1548 f. 34.
[28] Cf. R. Seiser et al. "Ignition in the viscous layer between counterflowing streams: asymptotic theory with comparison to experiments". eng. In: *Combustion and flame* 122.3 (2000), pp. 339–349. ISSN: 0010-2180.

2.3 Damköhler number

Turbulent flows can be described by a Reynolds number, whereas a Damköhler number characterises the reaction zone. The essential parameter for the description of extinction and autoignition is the Damköhler number Da. A mixture fraction field describes the turbulent mixing in the flow, while the Damköhler number is used to describe the flame. The Damköhler number is defined as the ratio of the integral time scale to the characteristic chemical reaction time. The time scale or flow time is the reciprocal of the strain rate and the chemical reaction time depends on the chemical kinetic rate parameters.[29]

At very high number for Da ($Da >> 1$) the characteristic chemical reaction time is much smaller than the turbulent flow time which subsequently leads to shielding of the inner flame from turbulent disturbances. Furthermore, the flame front for high Damköhler numbers gets only distorted at its outer surface while the inner surface remains as a thin layer. Opposite this at low numbers for Da ($Da < 1$) the flow corresponds to the distributed reactions regime.[30]
The Damköhler number can be given either by the general definitions or by including the strain rate a_2:[31, 32, 33]

$$D = \frac{\tau_{flow}}{\tau_{chem}} = \frac{l_0/u'}{\delta_L/S_L} = \frac{\nu_{O_2} Y_F B \rho_2}{a_2 W_F} \exp\left(-\frac{T_a}{T_2}\right) \tag{2.19}$$

S-Shaped curve

Directly related to the Damköhler number is the course of the s-shaped curve, which shows a plot of the maximum reaction temperature regarding the limits of extinction and autoignition of the mentioned fuel. The limit of extinction and autoignition show the two different burning limits in laminar diffusion counterflow flames who depend on different burning and flow conditions. In non-premixed flows the Damköhler number predicts the maximum temperature in a flow field and visualizes the combustion limits.[34]

[29] Cf. p.831 44.
[30] Cf. p.214 ff. 33.
[31] Cf. p.131 R. Grana et al. “Kinetic modelling of extinction and autoignition of condensed hydrocarbon fuels in non-premixed flows with comparison to experiment”. eng. In: *Combustion and flame* 159.1 (2012), pp. 130–141. ISSN: 0010-2180.
[32] Cf. p.4 P. Qiu et al. “Reduced-order modeling of turbulent flow reactors by tracing the Damköhler numbers”. eng. In: *Chemical engineering science* 248 (2022), pp. 117112–. ISSN: 0009-2509.
[33] Cf. p.833 44.
[34] Cf. p.1008 f. A. Liñán. “The asymptotic structure of counterflow diffusion flames for large activation energies”. eng. In: *Acta astronautica* 1.7 (1974), pp. 1007–1039. ISSN: 0094-5765.

In the shown figure 2.1 the vertical axis represents the maximum temperature of the reaction zone, while the horizontal axis shows the corresponding Damköhler numbers.

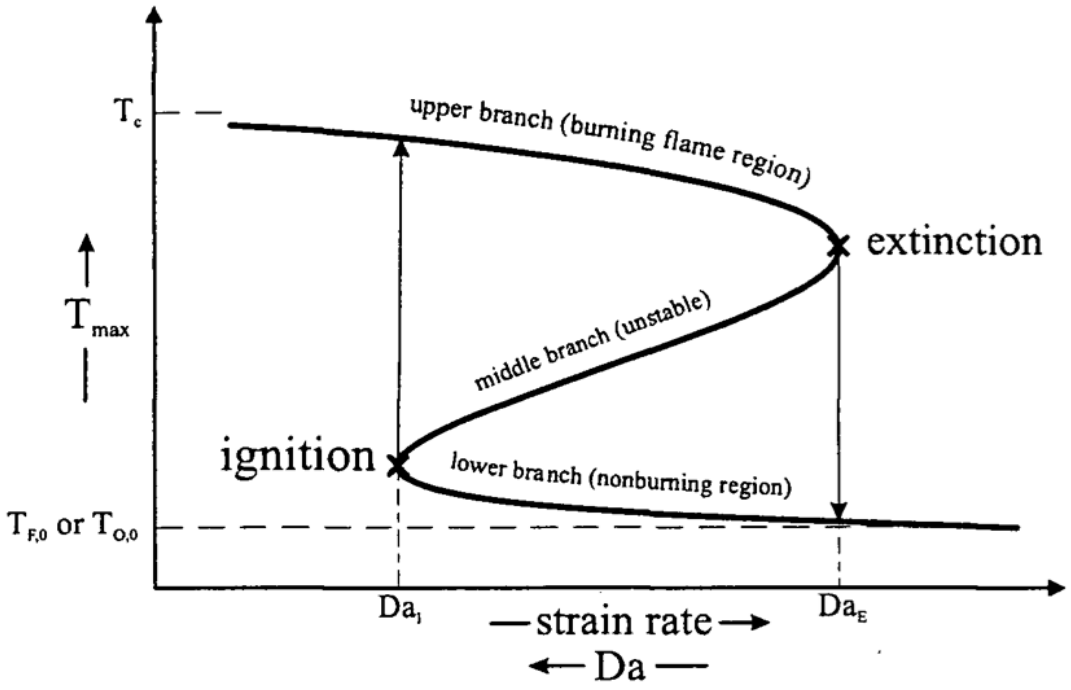

Fig. 2.1: S-shaped curve with the maximum temperature T_{max} as a function of the strain rate a_2 and Damköhler number D_a[35]

For steady counterflows the characteristic s-curve provides three possible solutions at a certain strain rate. The lower branch solution provides the temperature of the liquid before ignition takes place. The chemical reaction is frozen in this region for the first approximation until the Damköhler number reaches a sufficiently large value. The temperature rises above the frozen flow value causing nonlinear effects of the Arrhenius exponent. This effect leads to a rapid increase in the product concentration and ignition takes place. The middle branch is a physically unstable region which is also known as the partial burning regime. Here two frozen flow regions act as a sink by separating the flow regions through a thin reaction region. The reaction temperature of the mixture will be the higher ones of the flow field and the reaction rate is negligible because it is not sufficiently fast. The upper branch is characterized by a diffusion-controlled regime which occurs on both sides of the thin reaction zone due to the reached equilibrium.[36, 37]

[35] p.23 S. H. Humer. "Development of a surrogate diesel fuel". eng. PhD thesis. TU Wien, 2007.
[36] Cf. p.1010 ff. 28.
[37] Cf. R. Seiser. "Nonpremixed combustion of liquid hydrocarbon fuels". eng. PhD thesis. Graz University of Technology, 2000.

2.4 Investigated Fuels

The experimental investigations carried out in this thesis comprise two different categories of fuels and their mixtures. On the one hand, the hydrocarbon-based fuels Heptane and Decane are used, on the other hand the alcohol-based biofuels Ethanol and Isobutanol are dealt with.

2.4.1 Properties of the investigated hydrocarbons

Hydrocarbons are straight chain building molecules with the summarizing formula C_nH_{2n+2}. **Heptane** has a density of 0.684 $\frac{g}{cm^3}$ a boiling point of 99°C and a vapor pressure of 3.1bar. Heptane can be classified as a straight-chain neutral aliphatic hydrocarbon which is derived from crude oil and plays an important role in modern combustion engines. n-Heptane is described as an organic substance by the presence of C-chains as the main chain. the molecular structure can be described as a covalent bond of the C-atoms, where each c-atom is additionally bonded to as many H-atoms as is only possible by the free electrons. Due to its importance investigations on the ignition and combustion characteristics have been extensively investigated. Heptane showed a great reactivity and has a big energy content. Heptane is a petroleum distillate and it shows an almost insolubility in water.[38, 39]

Decane has a similar structure in comparison to Heptane, but it has a longer chain length due to its 10 C-atoms. It has a vapor pressure of 2.11bar, a boiling point of 174°C and a density of 0.727$\frac{g}{cm^3}$. n-Decane is insoluble in water and its vapor can be narcotic in higher doses. Decane can be obtained from natural gas and petroleum by fractional distillation of crude oil. As all saturated hydrocarbons it can also be gained isolation or by suitable conversion reactions such as the Fischer-Tropsch synthesis. The Fischer-Tropsch technology can be briefly summarized as converting a synthetic gas with carbon monoxide into a liquid hydrocarbon product Due to its oxygen content of 0 mass% it shows no solubility with water. Decane is a key component of jet-fuel and engine fuel in general.[40, 41]

[38] Cf. N. I. of Standards and T. (NIST). *Heptane*. URL: https://webbook.nist.gov/cgi/inchi/InChI%5C%3D1S/C7H16/c1-3-5-7-6-4-2/h3-7H2%5C%2C1-2H3 (Accessed 11/29/2021).

[39] Cf. p.845 S. Clough. "Heptane". In: *Encyclopedia of Toxicology (Third Edition)*. Ed. by P. Wexler. Third Edition. Oxford: Academic Press, 2014, pp. 845–847. ISBN: 978-0-12-386455-0. DOI: https://doi.org/10.1016/B978-0-12-386454-3.00396-1. URL: https://www.sciencedirect.com/science/article/pii/B9780123864543003961.

[40] Cf. N. I. of Standards and T. (NIST). *Decane*. URL: https://webbook.nist.gov/cgi/inchi/InChI%5C%3D1S/C10H22/c1-3-5-7-9-10-8-6-4-2/h3-10H2%5C%2C1-2H3 (Accessed 11/29/2021).

[41] Cf. PubChem. *Compound Summary Decane*. URL: https://pubchem.ncbi.nlm.nih.gov/compound/Decane#section=Consumer-Uses (Accessed 12/02/2021).

2.4.2 Properties of the investigated alcohols

Alcohols can be built in general by the formula $C_nH_{2n}OH$.
Isobutanol also known as 2-methylpropan-1-ol is a four-carbon alcohol with a boiling point of 108°C, a vapor pressure of 0.23bar, and a relative density of 0.802$\frac{g}{cm^3}$ at 15°C. Unlike n-Butanol with its straight-chain structure, Isobutanol has a branched-chain structure and its hydroxyl group is located at the terminal carbon.[42]
Isobutanol plays an important role as an alternative fuel due to his advantages such as relatively high energy content, mitigated flammability and compatibility with gasoline. Isobutanol is worth more to refiners than Methanol because it has 26% more energy. Unlike Ethanol that is 100% miscible with water, Isobutanol has only a limited solubility of 10.6% which corresponds to 85.0 $\frac{g}{L}$ at 25°C with water. Isobutanol convinces with its safety not to allow any corrosion of engines and pipelines. The production of Isobutanol can either be produced by an industrial carbonylation of propylene or it can be fabricated in existing cornstarch Ethanol fermentation plants as a biofuel via fermentation of glucose coming from biomass. Therefore, Isobutanol is proving to be an ideal candidate to replace fossil fuels in gasoline engines. The lower oxygen content of the molecules allows greater amounts of additives blended with gasoline than Ethanol.[43, 44]

Studies on efficiency and emission values of an Isobutanol additive in spark-ignition engines show that a 50Vol.%Isobutanol–50Vol.%Gasoline mixture improves fuel conversion efficiency up to 6%. Further mixtures were investigated with a Isobutanol additive of either 3,5 or 7%. CO_2 values dropped by an average of 33% by using the Isobutanol-gasoline-blends. This decrease can be explained by the molecular composition of 4 C-atoms compared to the average 8 C-atoms of gasoline and the additional oxygen atom of the Isobutanol molecule, which leads to a more complete combustion of the fuel. With a 30Vol.%Isobutanol blend a decrease of 9% in the NO_x emissions were achieved in comparison to neat gasoline and the HC emissions reduced by 12%. Critical to this is the increase in CO and UHC emissions in the partial load range at speeds >3000 rpm. Due to the lower AF-ratio of 11.1 in comparison to 14.6 of pure gasoline as mentioned in table 2.1 the amount of extra fuel injected for a complete combustion causes an increase in the mentioned emission values. In contradiction to this the EGT dropped the higher the amount of Isobutanol was in the vaporized fuel mixture.

[42] Cf. p.400 f. A. Elfasakhany. "Experimental investigation on SI engine using gasoline and a hybrid iso-butanol/gasoline fuel". eng. In: *Energy conversion and management* 95 (2015), pp. 398–405. ISSN: 0196-8904.
[43] Cf. p.109 ff. V. K. Gupta. *Bioenergy research : advances and applications*. eng. Waltham, MA: Elsevier, 2014. ISBN: 0444595643.
[44] Cf. p.47 ff. A. M. Brownstein. *Renewable Motor Fuels: The Past, the Present and the Uncertain Future*. eng. Oxford: Elsevier Science Technology, 2014. ISBN: 9780128009703.

It follows that the operational temperature of catalyst works better for fuel blends and the amount of oxygen allows a greater efficiency of cleaning up the CO and UHC particles. Isobutanol provides in comparison to n-Butanol a reduction of the CO and CO_2 emissions while increasing the UHC emissions and the engine performance which is why Isobutanol takes precedence over n-Butanol in blended fuels.[45, 46]
The blended fuels of Isobutanol additives are very promising of reducing the GHG effect in the atmosphere and thus also the CO_2 emissions.

Ethanol is worldwide used as alternative fuel additive, solvent and feedstock. It is a two-carbon alcohol which is known for its large oxygen amount causing a higher complete combustion and lower exhaust emission rates than other fuels. It has a a density of 0.789 $\frac{g}{m^3}$ at EPA, a boiling point of 78°C and a vapor pressure of $1.38bar$.[47] Ethanol is completely soluble in water, which made the investigation of Ethanol–Heptane mixtures more complicated as a constant change of the fuel was necessary to keep the influence of the mixing by means of the cooling water during experiments as low as possible. Ethanol is currently either produced by alcoholic fermentation of agricultural residues such as sugarcane or corn which leads to a biomass-based renewable fuel or by ethane hydration.[48]

When compared with Ethanol Isobutanol can be described as a longer chain alcohol with lower vapor pressure, lower hygroscopicity, lower corrosivity and greater energy content. However, Ethanol has proven its strengths through its proven use as a fuel additive.

The following table 2.1 gives a summary about the most important numbers of the investigated fuel properties in comparison to similar fuels. Normal gasoline is a complex fuel mixture with hydrocarbons of higher order, cylcobenzols, alipahts, aromats. Here it will be approximated as C_8H_{15} like given in the literature. Gasoline is contrasted with Heptane and Decane. Ethanol and Isobutanol are compared with each other, and the fuel props of n-butanol are also listed to enable a comparison of the two alcohol isomers.

[45] Cf. p.399 ff. 13.
[46] Cf. p.385 ff. F. N. Alasfour. "The Effect of Using 30% Iso-Butanol-Gasoline Blend on Hydrocarbon Emissions from a Spark-Ignition Engine". eng. In: *Energy sources* 21.5 (1999), pp. 379–394. ISSN: 0090-8312.
[47] Cf. p.483 ff. M. Yusoff et al. "Comparative assessment of ethanol and isobutanol addition in gasoline on engine performance and exhaust emissions". eng. In: *Journal of cleaner production* 190 (2018), pp. 483–495. ISSN: 0959-6526.
[48] Cf. p.404 f. A. Elfasakhany. "Investigations on performance and pollutant emissions of spark-ignition engines fueled with n-butanol–, isobutanol–, ethanol–, methanol–, and acetone–gasoline blends: A comparative study". eng. In: *Renewable sustainable energy reviews* 71 (2017), pp. 404–413. ISSN: 1364-0321.

Property	Unit	Gasoline	Heptane	Decane	Ethanol	Iso-Butanol	n-Butanol
Chemical formula	-	C_8H_{15}	C_7H_{16}	C_10H_{22}	C_2H_5OH	C_4H_9OH	C_4H_9OH
Composition C/H/O	mass %	86/14/0	83.9/16.1/0	84.4/15.6/0	52.2/13.1/34.7	64.8/13.6/21.6	64.8/13.6/21.6
Oxygen content	mass %	0.0	0.0	0.0	34.7	21.6	21.6
Molecular weight	$\frac{kg}{kmol}$	111.205	100.202	142.282	46.068	74.122	74.122
Lower heating value	$\frac{MJ}{kg}$	43.5	44.9	44.6	27.0	33.3	33.1
Heat of evaporation	$\frac{kJ}{kg}$	223.2	317	277	725.4	474.3	582
Stoichiometric A/F-ratio	-	14.6	15.2	15.1	9.0	11.1	11.2
Density	$\frac{kg}{m^3}$	760	684	727	790	802	810
Saturation pressure at 38°C	kPa	31	27.4	21.1	13.8	2.3	2.27
Flash point	K	228-235	317	322	294	301	308
Autoignition temperature	K	693	496	479	707	688	658
Boiling point	K	298-488	372	447	351	381	390
Solubility in water	$\frac{ml}{100ml H_2O}$	<0.1	Insolubility in water	Insolubility in water	Fully miscible	10.6	7.7
Vapor toxicity	-	Moderate irritant	Very acute toxicity of the vapor	Acute toxicity of the vapor	Toxic even in small doses	Moderate irritant	Moderate irritant

Tab. 2.1: Investigated and comparable hydrocarbon and alcohol properties of used fuels[49, 50, 51, 52, 53]

2.4.3 Tested Fuels and Surrogates

The mentioned pure fuels in sections 2.4.1 and 2.4.2 were used to provide mixtures by volume percent mixtures 80%-20%, 50%-50% and 20%-80%. The purpose of this thesis is fundamental research on pure fuel properties and mixtures of two different fuels only. Commercial fuels especially aviation fuels, but also automotive fuels, consist of a multitude of hundreds of different hydrocarbons. Investigations taking place on these fuels would not provide satisfying data and numerical modeling due to the complexity of their combustion processes. To better elucidate the mechanisms of autoignition and extinction, surrogates of jet-fuels take normally place in the investigation. Surrogates reproduce selected aspects of combustion from the actually used fuels but these should only have been mentioned here for the sake of completeness.[56]

In this thesis, a further simplification was considered, which deals with the mixtures of pure fuels and the previously mentioned mixtures of two different fuels each. The properties of the tested fuels can be found in table 2.1. The mechanisms of autoignition and extinction of mixtures of biogenic fuels with hydrocarbon fuels is investigated at elevated pressure. Experimental investigations and numerical simulations are carried out to elucidate the fundamental behavior of these different volumetric mixtures, mentioned in appendix A.2 and B, to predict extinction and autoignition using a counterflow burner setup.

[49] Cf. p.409 14.
[50] Cf. p.194 ff. N. P. Cheremisinoff. *Handbook of Hazardous Chemical Properties*. eng. Burlington: Elsevier Science, 1999. ISBN: 1281077429.
[51] Cf. 49.
[52] Cf. 48.
[53] Cf. p.244 ff. S. McAllister et al. *Fundamentals of combustion processes*. eng. Mechanical engineering series. New York, NY [u.a.]: Springer, 2011. ISBN: 1441979425.
[56] Cf. p.1606 G. Mairinger et al. "Experimental and computational investigation of autoignition of jet fuels and surrogates in nonpremixed flows at elevated pressures". eng. In: *Proceedings of the Combustion Institute* 37.2 (2019), pp. 1605–1614. ISSN: 1540-7489.

3
Experimental setup

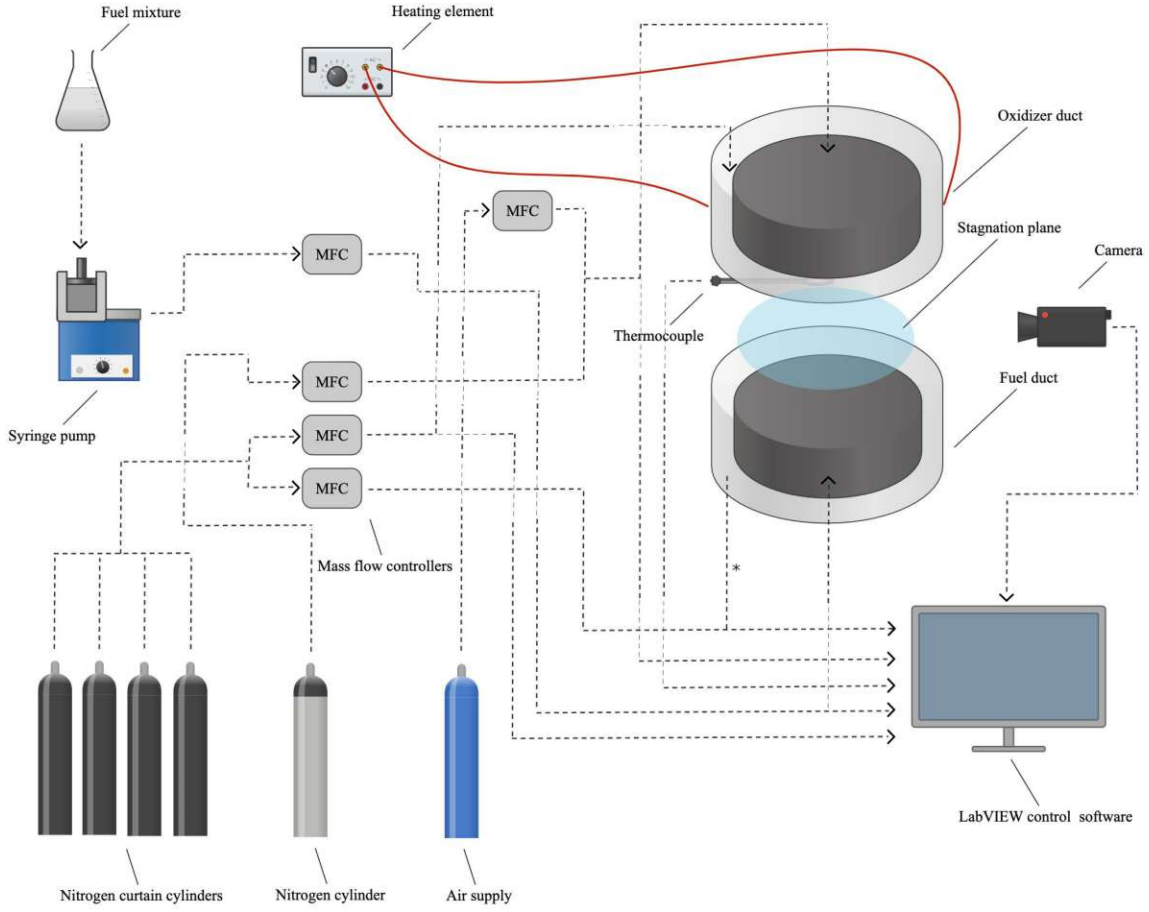

Fig. 3.1: Experimental setup of the counterflow configuration including thermocouple and heating element used for autoignition experiments

The counterflow setup shown in figure 3.1 consists of the gas supply, the pump system, the control software and the counterflow burner itself, which is the most important component. A syringe pump filled with the fuel mixture provides the liquid level in the

fuel duct which can be additionally observed by a camera. This duct faces axisymmetric the oxidizer duct. An oxidizer stream facing this fuel disc causes in optimal configuration a stagnation plane. During autoignition experiments the autoignition top of the burner is connected to a heating element and a thermocouple measures the temperature close to the ducts' outlet. The gas supply comes from N_2 cylinders and an air pipe. All measured flows are regulated by MFCs who operate together with the LabVIEW^{TM} software.

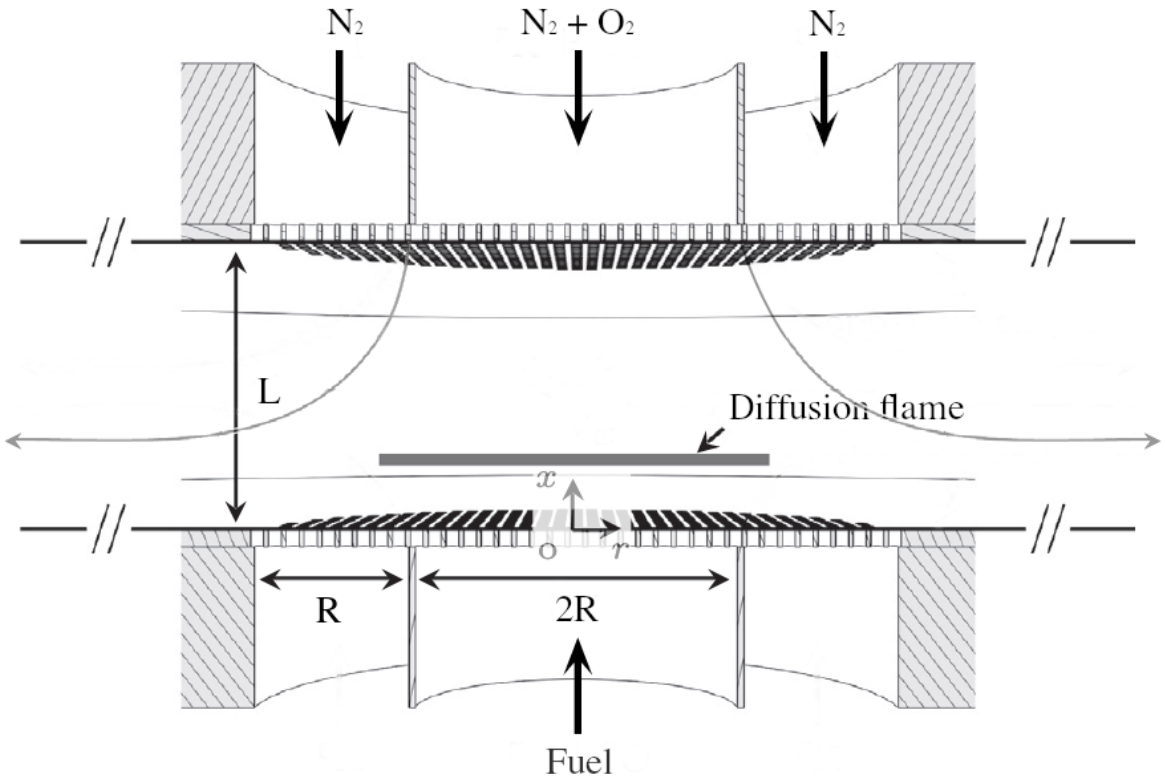

Fig. 3.2: Schematic sketch of the counterflow burner with the fuel duct at $x = 0$ and the oxidizer duct at $x = 1$[57]

The burner can be viewed as a lower and upper top. A detailed sketch of the gas flows inside the counterflow burner is provided by figure 3.2. For completeness, the path in the counterflow setup configuration in figure 3.1 marked with „*“ shows the use of a fuel curtain. For the extinction and autoignition experiments performed in this work, this is not required, although it would theoretically be available. This can also be seen in the SLPM in figure 3.6, where Port 2 is automatically assigned to the fuel curtain, although this is not used here with 0 SLPM. The mechanism inside the counterflow burner is explained in its details in section 3.1 and further subsections.

[57] Slightly modified from p.232 M. Di Renzo et al. "The breakdown of self-similarity in electrified counterflow diffusion flames". eng. In: *Combustion and flame* 205.C (2019), pp. 231–240. ISSN: 0010-2180.

3.1 Counterflow burner

The counterflow burner has been extensively used since the 1960s in combustion research. The principle of using a diffusion flame, which arises due to the mixing of oxidizer and fuel, is used in combustion applications from candle lighters to battle jets. A counterflow burner is used to reduce the three-dimensional complexity of chemical reactions and thermodynamic conditions of combustion systems into a one-dimensional diffusion problem. A non-premixed gas stream from the oxidizer duct faces a fuel duct causing a boundary layer in which a diffusion flame is established in between the two ducts. The gas stream is diluted by the inert gas N_2 to make detailed computations about peak temperature, stoichiometric AF-ratio, reaction rates and flow properties. The position of the stagnation plane in between the two ducts away from any walls allows optical access and prevents the flame from heat loss. In particular, this means neglecting diffusion in the direction orthogonal to the flow stream. Accordingly, the values for temperature and mass fraction only vary in the flow direction.[58, 59]

Since the values of the strain rate a_2 and scalar gradients are set by the flow properties and the outlet distance L which can be flexibly adjusted, this experimental setup is suitable for carrying out a wide variety of experiments. An optimal separation distance between the two nozzles could be defined by carrying out axisymmetric simulations of non-premixed counterflow flames including the surrounding annular co-flows.[60] Due to investigations of the velocity and the reactive scalars from the one-dimensional model as seen in figure 3.2, a uniform velocity profile of the oxidizer duct can be detected.[61]

The burner consists of a lower part and two different upper parts - the extinction and the autoignition top. Both have been used for carrying out the experimental investigations performed in this diploma thesis. In the following the parts and functionality of the counterflow burner are described in detail.

[58] Cf. p.1543 34.

[59] Cf. p.927 f. E. Solmaz and F. Bisetti. “Flamelet chemistry model for efficient axisymmetric counterflow flame simulations with realistic nozzle geometries and gravitational body force”. eng. In: *Combustion theory and modelling* 24.5 (2020), pp. 926–952. ISSN: 1364-7830.

[60] Cf. R. F. Johnson et al. “On the Axisymmetric Counterflow Flame Simulations: Is There an Optimal Nozzle Diameter and Separation Distance to Apply Quasi One-Dimensional Theory?” eng. In: *Combustion science and technology* 187.1-2 (2015), pp. 37–59. ISSN: 0010-2202.

[61] Cf. C. Frouzakis et al. “Two-dimensional direct numerical simulation of opposed-jet hydrogen-air diffusion flame”. eng. In: *Symposium, International, on Combustion* 27.1 (1998), pp. 571–577. ISSN: 0082-0784.

3.1.1 Lower part of the burner and syringe pump

The lower part of the burner always remains the same for both the extinction and autoignition experiments. As described in previous sections, a syringe pump directs a fuel stream of the investigated fuel mixture to the lower outlet. A phase transition takes place and the vaporized fuel is than carried to the stagnation plane to react under certain circumstances with the oxidizer stream. The lower part of the counterflow burner includes besides the here unconnected curtain duct and the fuel duct a surface-enhancing burner cooling coat, water cooling, and exhaust pipe as seen in figure 3.3. The lower part of the burner is a complex steel construction and consists of a fuel cup with a depth of 10mm and an inner diameter of 35mm. A high precision syringe pump Teledyne Isco 500D with a volumetric flow accuracy of $\pm 0.01\ \frac{ml}{min}$ provides a constant liquid flow from the reservoir to the fuel-cup by matching the liquid mass flow rate to the actual burning rate. An indicator needle made of stainless steel is welded on the bottom of the fuel cup for a visual inspection of a steady fuel level, observed through the camera pointing towards it.

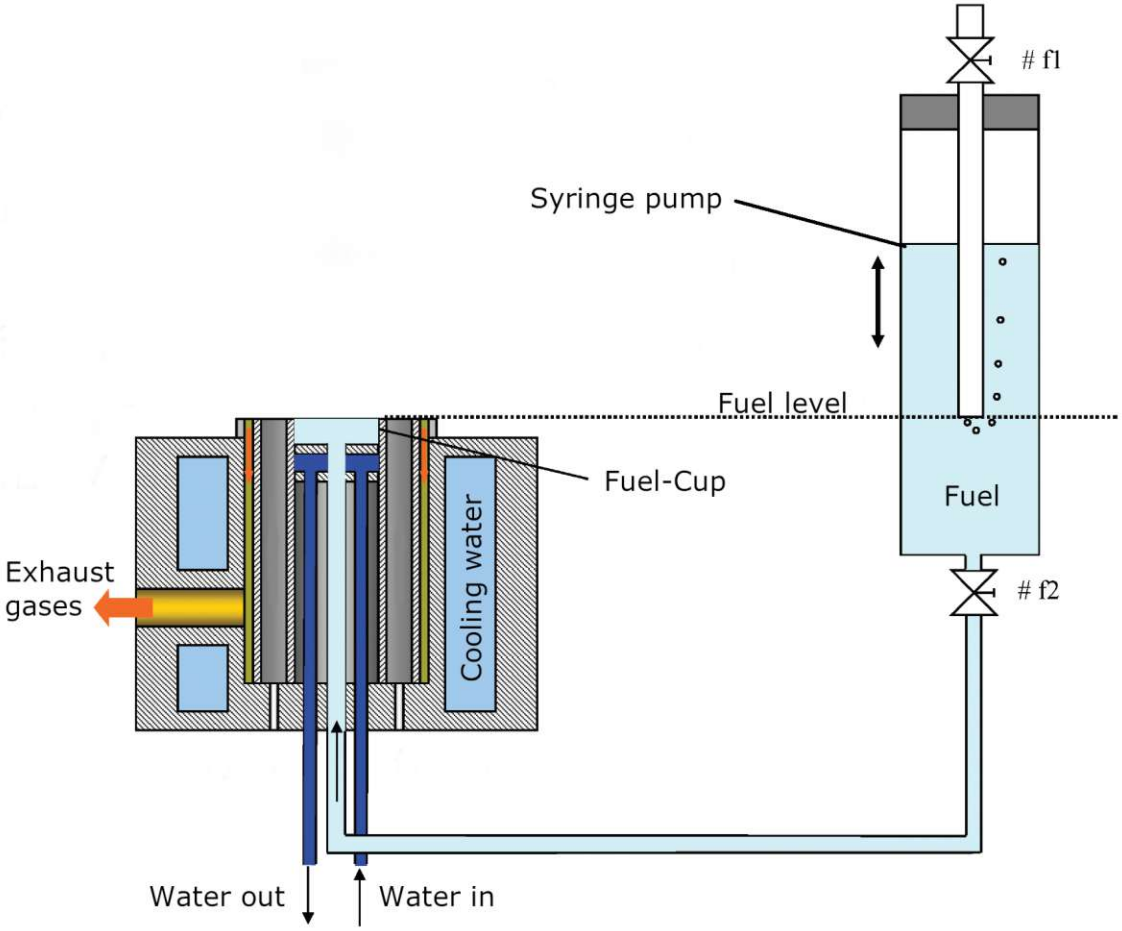

Fig. 3.3: Schematic functional sketch of the lower part of the burner including the syringe pump[62]

The exhaust pipe is connected to the lower part of the counterflow burner as seen in figure 3.3. The task of the exhaust system is to draw the hot reactive gases away from the reaction zone and to cool it down in order to prevent subsequent reactions. The reactive gases are drawn concentrically away from the stagnation plane and cooled by the water spray nozzles of the lower part. Subsequently, the reaction products are fed into an internal extraction system and safely stowed away.

3.1.2 Extinction top

The extinction top as shown in figure 3.4 is made of two stainless steel tubes, where the inner duct guides the oxidizer stream of N_2 and O_2 to the reaction zone. To ensure plug flow conditions three stainless steel mesh screens with a diameter of 25.4mm are mounted on the exit of the duct. Between the inner and outer tube an oxidizer stream protecting curtain stream of N_2 is injected. A honeycomb ring in the annular duct is used for providing a uniform curtain flow. Three set screws allow fixation of the top to the lower part.[63]

3.1.3 Autoignition top

Inside the autoignition top a silicon carbide heating element with a diameter of 19mm and a length of 259mm is surrounded by a machined quartz tube. Quartz is capable of reducing the thermal expansion and dealing with the high temperature. The oxidizer stream of N_2 and O_2 is preheated at the oxidizer duct outlet and is guided through the tube to the reaction zone. In order to ensure plug flow conditions three Inconel 600 screens held by four steel rings are places at the exit of the oxidizer duct. The heating element is a variable transformer Staco Energy^{TM} 3PN2210B with an electric output of 0-140V AC. It is connected via two electrical connections made of flat aluminum branch. An inlet and outlet pipe of the water cooling system is connected to the autoignition top to prevent overheating. Heat loss is prevented by wrapping the duct in thermal isolation. The fixation elements of the autoignition top are the same as those of the extinction top. Figure 3.5 shows an illustrative structure of the autoignition top.[64]

[62] Slightly modified from p.843 K. Seshadri et al. “Activation-energy asymptotic theory of autoignition of condensed hydrocarbon fuels in non-premixed flows with comparison to experiment”. eng. In: *Combustion theory and modelling* 12.5 (2008), pp. 831–855. ISSN: 1364-7830.
[63] Cf. p.13 f. 17.
[64] Cf. p.27 f. 23.

Fig. 3.4: Counterflow burner in extinction configuration at fixed O_2 mass fraction $Y_{O_2,2} = 0.195$ of 50%Vol.Heptane–50%Vol.Ethanol mixture

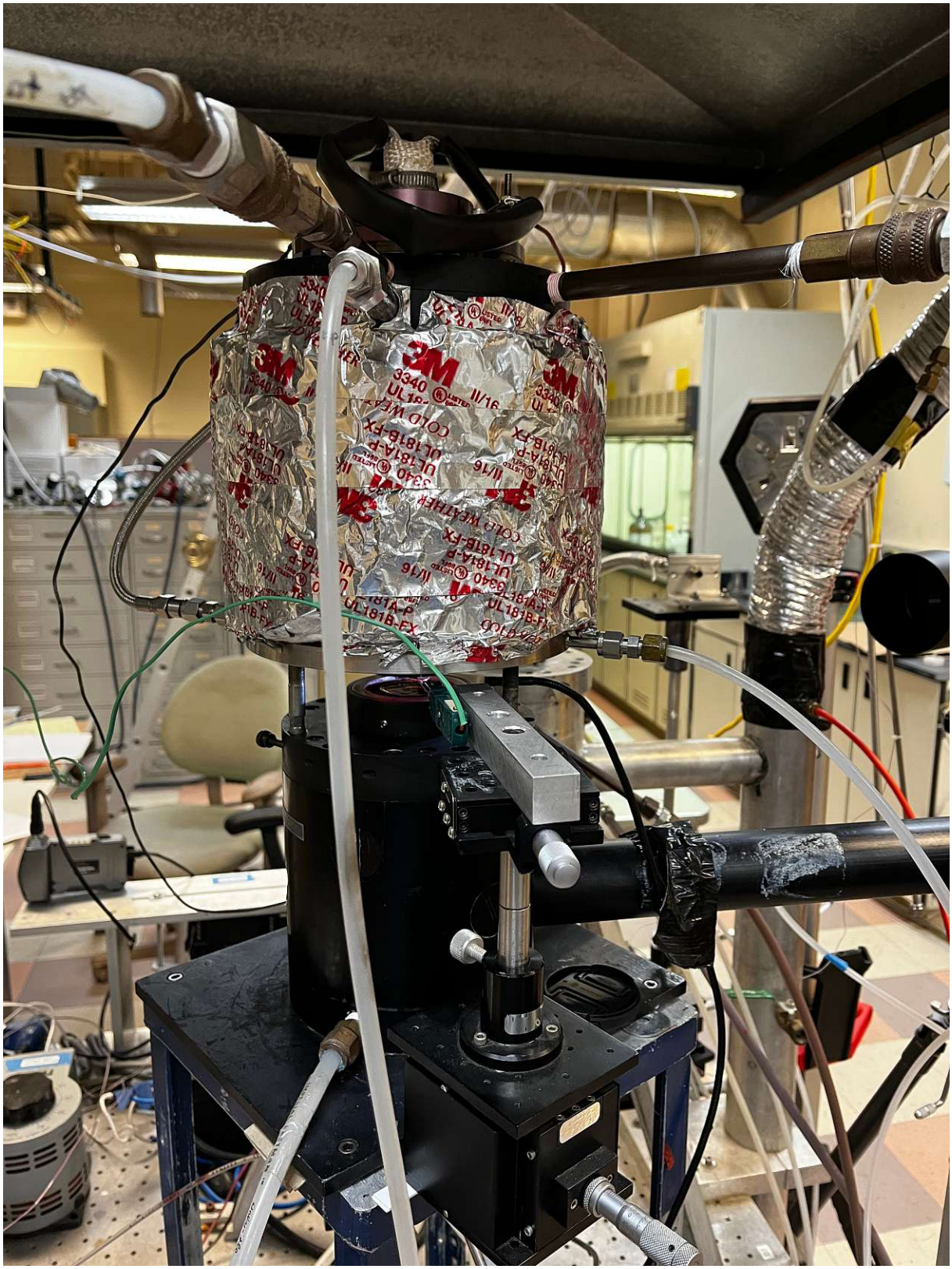

Fig. 3.5: Counterflow burner in autoignition configuration during heating up process

3.2 Gas flow

The gas flow in the experimental setup consists of pure air provided by the air pressure chamber of the University of California San Diego. Four cylinders of nitrogen are connected in series to provide the curtain flow in the counterflow burner. In addition to that one cylinder with a separate flow provides the nitrogen which is connected to the air pipe to ensure correct stoichiometric values of the inert gas mixed with pure air. The stoichiometric values for each experimental run can be taken from item number 5 in figure 3.6.

3.3 LabVIEW^{TM} control software

The software used for the counterflow burner is LabVIEW^{TM}(Laboratory Virtual Instrumentation Engineering Workbench), in whose back-end complex functions of the most diverse contexts for the experimental execution have been defined and automated. The custom code provided by former research groups provides controlling over five gaseous streams including the curtain stream and one additional liquid or vaporized stream. The allocations used here can be taken from number 6 of figure 3.7.[65, 66]

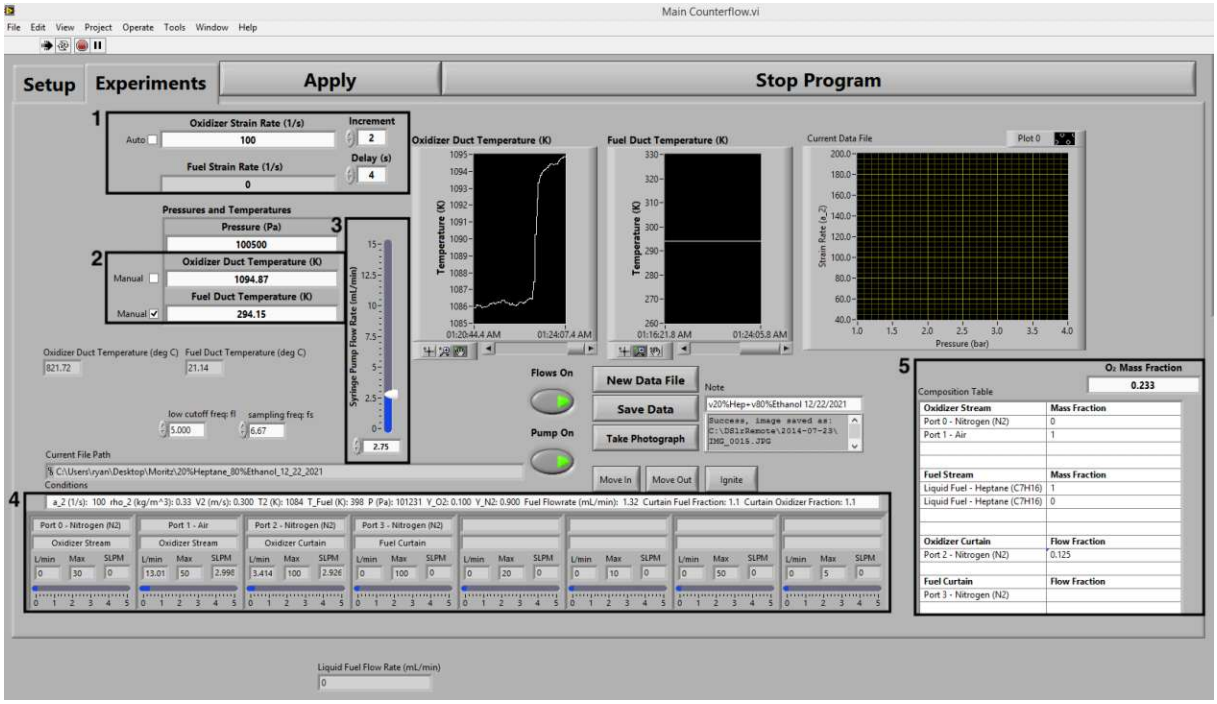

Fig. 3.6: Basic control screen of LabVIEW^{TM} during an autoignition experiment of a 20%Vol.Heptane–80%Vol.Ethanol mixture evaluated at $a_{2,AI} = 100$

[65] Cf. p.45 ff. 23.
[66] Cf. p.19 ff. 17.

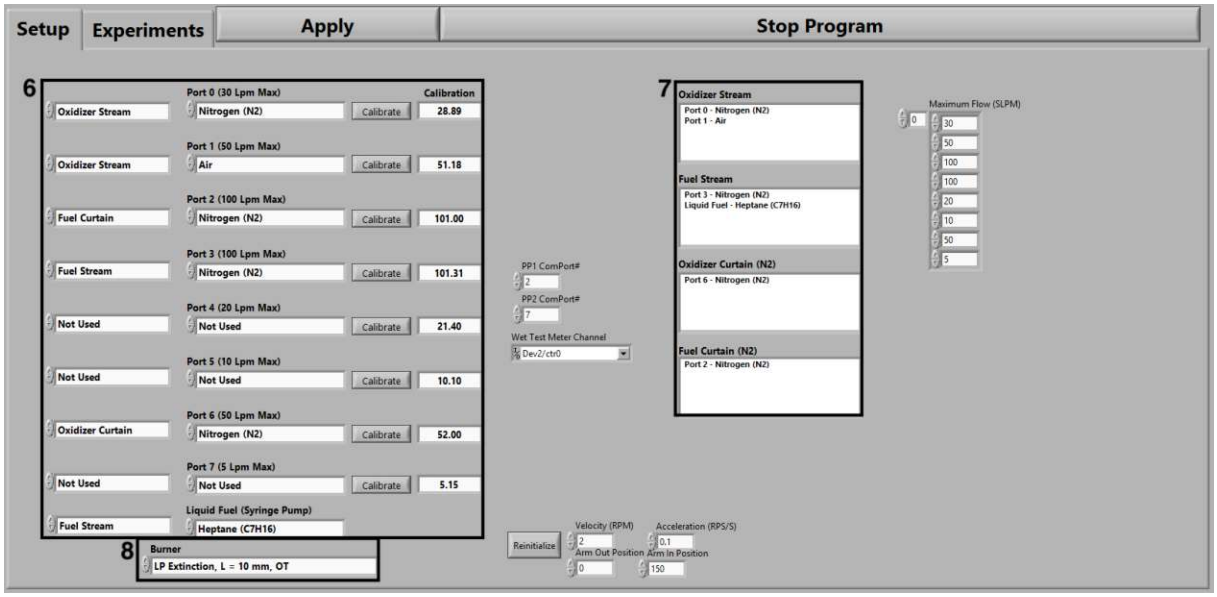

Fig. 3.7: LabVIEW^{TM} setup used for experimental extinction investigations

The software and setup can be described by the following sub-items:

1. The oxidizer strain rate a_2 can be set here. An automatic increment per adjustable time period can be selected.

2. Oxidizer and fuel duct temperatures can be read numerically. A detailed temperature curve is also displayed graphically close to number 2 and can be exported as .txt-file. The oxidizer duct temperature is recorded via the thermocouple temperature T_{tc} during autoignition experiments.

3. The pump flow rate must be precisely adjusted manually to generate a constant fuel flow causing a stagnation plane.

4. The curtain and oxidizer streams can be monitored using the flow rates shown and compared with the values of the MFC

5. An O_2 mass fraction $Y_{O_2.2}$ can be defined, according to which the respective N_2 and O_2 values of the oxidizer stream are calculated automatically. The N_2-share is controlled accordingly.

6. The setup can be used to assign the respective streams regarding their type and ports. The calibration of the SLPM and the maximum flow rates must be taken into account when choosing a port.

7. The result of the assignment can be checked with the help of the proposed software classification.

8. The experimental results depend not only on the strain rate a_2, but also on the separation distance L, which has to be set for extinction and autoignition experiments.

Figure 3.6 shows the application of the software during an autoignition experiment. Figure 3.7 illustrates the allocation of ports during the extinction experiments. Since at the end of the extinction experiments the MFC of the oxidizer curtain port was beyond repair, the second MFC display was deactivated and the required port was switched so that all three required ports were visible on one Teledyne display. The inconsistency of the two mentioned images 3.6 and 3.7 therefore has no influence on the results of this research.

3.4 Mass flow controller

The used LabVIEW^{TM} software calculates the composition of the individual gas flows with the aid of the measured values of the MFCs. The accuracy of the MFCs is a critical success variable of the combustion experiments. Many different MFCs with different SLPMs, evident in the calibration table in figure 3.7, are in general used over a wide range of combustion experiments. A targeted calibration of the MFCs is therefore mandatory and will be performed by the research group using a high precision wet-test meter at appropriate time intervals. In the presented experimental setup 3.1 the MFC for the oxidizer stream adjusts the SLPM of N_2 and O_2 gas flow. The value of the N_2 oxidizer curtain can be observed in one Port (Port 2 in 3.6) while the N_2 fuel curtain is unused for all experiments run in this thesis with a constant value of 0 SLPM. For all gases Teledyne HFC-302 modules are used as MFCs. A continuous comparison between MFC and software must be carried out manually via LabVIEW^{TM}. The interface between the software and the MFCs is made with two Teledyne PowerPod 400 modules which provide a voltage linear to the mass flow rate. They compare the values of the sensors to the signal and adjust the valves to achieve the predefined flows. At higher stoichiometric mixtures of oxygen, a further reaction of the gases is prevented by emergency shut-off valves placed after the MFCs.

3.5 Temperature measurement

Due to their robustness, ease of installation as well as simple functionality and comparatively low costs thermocouples are one of the most widespread sensors for temperature measurements. The examined results obtained by the thermocouple in high temperature environments can however be affected by thermal radiation exchange to and from the surrounding area. Here a $Pt/13\%Rh\text{-}Pt$ R-type thermocouple is used for temperature measurements as seen in figure 3.8. The diameter of the bead measures 0.457mm and is used for the computation of the radiation error mentioned in chapter 5.1. The influence of the thermocouple on the flow field is therefore neglected. A thermocouple in general measures the temperature equivalent potential difference of the heat transfer between the two junctions. This heat transfer is mainly caused by convection. For an optimal uniform temperature measurement, the two junctions must be arranged flat and oval. The bead should be bent slightly upwards in the direction of the oxidizer duct.[67]

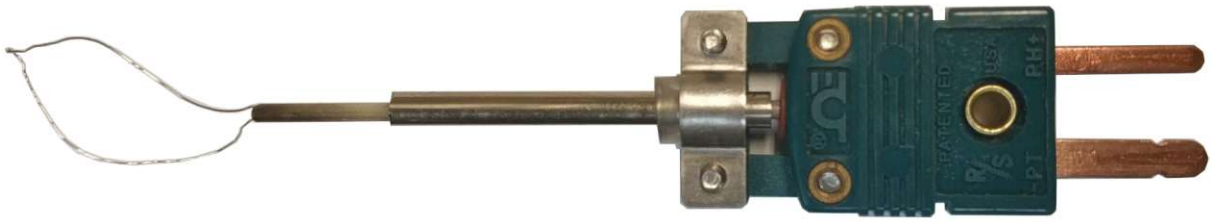

Fig. 3.8: R-type thermocouple used for autoignition experiments

[67] Cf. p.1 ff. C. Falsetti et al. "Thermal radiation, its effect on thermocouple measurements in the PANDA facility and how to compensate it". In: *Nuclear Engineering and Design* 375 (2021), p. 111077. ISSN: 0029-5493. DOI: https://doi.org/10.1016/j.nucengdes.2021.111077. URL: https://www.sciencedirect.com/science/article/pii/S0029549321000297.

3.6 Setup preparation

In order to obtain comparable experimental evaluations, a certain procedure must be followed for both the extinction and the autoignition experiments. Deviations or occurring peculiarities were documented in detail and, if necessary, repeated in case of non-usability. Although the implementation of the two series of experiments is fundamentally different, the preparatory measures are partly identical.

3.6.1 Extinction configuration preparation

The extinction top is mounted via three set screws on top of the liquid pool which are first only lightly fixed. The gas connections for the oxidizer stream and curtain stream are connected to the top. Afterwards, it follows a fine adjustment of the distance L to 12mm using a dial gauge. Four different points need to be checked for the correct separation distance between the two cylindrical outlet surfaces. The set screws are now fixed tightly.

3.6.2 Autoignition configuration preparation

The curtain duct must be cleaned over its cylindrical shell surface with a fine paper. The thermocouple must be cleaned of carbon deposits on its outer layer by means of a torch flame. After every second experiment run, the Inconel mesh screens must be remanufactured and replaced. The lower end of the oxidizer duct is cleaned of residues with sandpaper and than coated with a fine layer of quick steel. The quick steel must be dried for 4-5 hours. The liquid pool is cleaned with cotton swabs before the autoignition top is mounted on top of it. Three set screws are first only lightly fixed. The autoignition top is connected to the oxidizer stream, curtain stream and to the inlet and outlet of the autoignition top cooling pipes. The resistance of the heating element is measured and should be in the range of 5-6 Ω. The electrical connection from the heating element to the autoignition top is mounted and fixed on top of it. Afterwards, it follows again a fine adjustment of the distance L to 12mm using a dial gauge, which are checked according to the same procedure, as well as at the extinction top. The thermocouple is connected to the measuring device last and it is placed in the center directly below the oxidizer duct with a slightly upward bent nose.

To ensure that the experiments are carried out correctly and safely, the safety areas of cooling, electricity and gas must be checked both at the beginning and at the end of all types of experiments:

Cooling To ensure sufficient cooling of the product gases and thus prevent subsequent reactions by lowering the reaction temperature, cooling water must be fed into the burner through water spray noses or by a separate cooling line including an inlet and an outlet for the autoignition top. All used cooling lines must be checked for adequate flow at discharge.

Gas The N_2 curtain gas cylinders, the N_2 gas cylinder and the air pipe must be opened. To prevent the opening valves from engaging and to be able to close them immediately in the event of a safety gap, they should not be turned fully open. Valves upstream of the MFCs must be turned open slowly to allow gas flow to the MFCs and burner.

Electricity The experimental workbench has a separate power switch, which must be activated before switching on the pump or the heating element.

Taking these described general safety categories into account, follows preparing the different settings of the burner for the extinction and ignition experiments as explained above in 3.6.1 and 3.6.2.

The reservoir of the syringe pump needs to be filled sufficient with the investigated fuel. The liquid pool is prepared by flash burning the fuel cup when switching to a new fuel mixture.

The last step is to link the software to the control elements by pressing „Flows on“ and „Pump on“ at the computer. The preparations for the experiment have thus been made and the actual experimental procedure is carried out as described in the following sections 4.1 for extinction and 4.2 for autoignition.

4
Experimental investigations

4.1 Extinction

The experimental determination of the flame extinction is defined by the following approach: The temperature of the oxidizer stream T_2 is set to a constant value of 294.15K. After the fuel mixture has been ignited at a low strain rate, the liquid level is adjusted by means of a metal needle located at the bottom of the burner, so that the tip of the needle, mounted inside the fuel cup, is just out of sight. This liquid level must be maintained in order to ensure an equivalent flow rate of the syringe pump to the stoichiometric burning rate at the reactive zone of the stagnation plane. Before the actual start of the experiment, the extinction strain rate is estimated based on previous experience, previous comparable experiments, or values found in the literature. The strain rate a_2 is than adjusted to a value close to the presumed extinction strain rate $a_{2.E}$ in steps of 10. If the presumed extinction strain rate $a_{2.E}$ is according to previous experience, 20 values away, an automatic increase of the strain rate in increments of 2 with a delay of 4 seconds is set on the software side. In the first run, this increase is maintained until an exact value for the extinction of the flame could be determined. If the extinction strain rate is already known, the delay is set to 3 seconds and the increment is set to 1 for all subsequent experimental runs when the expected extinction strain rate $a_{2.E}$ is 5-10 data points away. The experiment is to be repeated for several values of the oxygen mass fraction $Y_{O_2.2}$.

For an accurate experimental evaluation, 3 extinction values are determined, taking care not to create an excess. Values with unstable surface behavior are noted and included in the measurement, since this is mainly caused by the predominant influence of the gravity force at lower strain rates. After the extinction rate $a_{2.E}$ has been determined, the strain rate a_2 is slowly reset to the start value and a new measurement is quickly started.

Extinction is defined to take place at the value of a certain strain-rate, when the stagnation plane is extinguished by a sudden transition from a reactive region to a non-reactive region. Extinction as well as autoignition depend on the value of the Damköhler number.[68]

The figures 4.1, 4.2 and 4.3 show the mass fraction of oxygen $Y_{0_2.2}$ in the oxidizer stream as a function of the strain rate at extinction $a_{2.E}$. The symbols in these figures represent obtained experimental data. The lines are interpolated plots of the observed values.

The evaluated extinction strain rates were in the range of $a_{2.E}\epsilon[60, 250]$. No new readings were taken below strain rates of 60 and at the last measured extinction strain rate which exceeded 250.

4.1.1 Extinction of Heptane–Decane mixtures

The extinction strain rates showed in figure 4.1 show the oxygen mass fraction $Y_{O_2.2}$ as a function of the strain rate at extinction $a_{2.E}$ for different mixtures of Heptane and Decane. The symbols represent experimental data. Thus, Heptane is harder to extinguish as Decane, which explains why the diffusion flame with a higher volumetric percentage of Heptane can withstand a greater strain rate before the flame is about to break out and extinguishes. This phenomenon can be well observed, for example, at a fixed strain rate $a_2 = 120$: The O_2 mass fraction $Y_{0_2.2}$ of 100%Vol.Decane requires a value of 0.185 to reach this extinction strain rate, whereas 100%Vol.Heptane only requires a O_2-share of 0.175 in the oxidizer stream for the same extinction strain rate to extinguish the burning flame. Therefore, it can be concluded that higher chain hydrocarbons extinguish easier before lighter hydrocarbons.

[68] Cf. p.131 ff. 18.

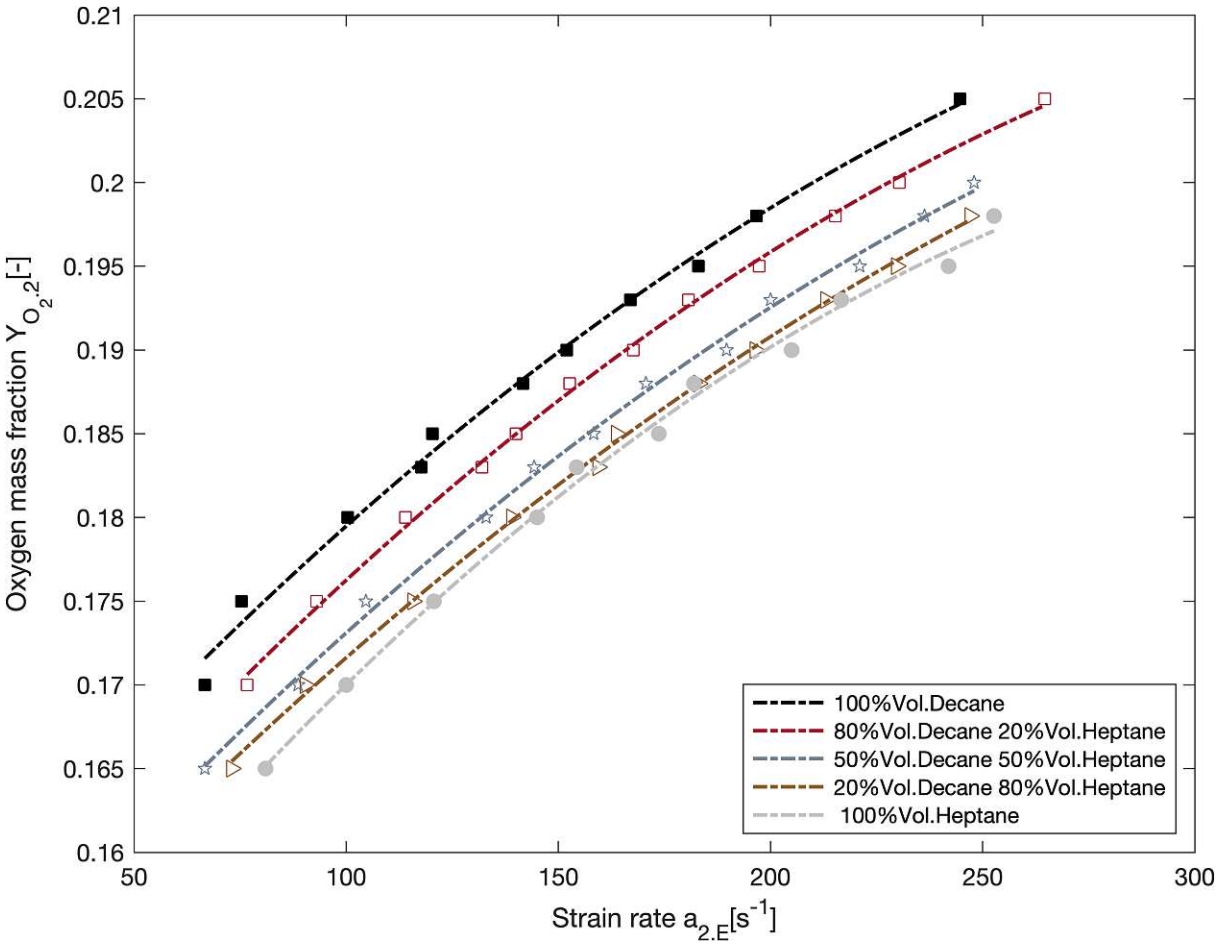

Fig. 4.1: The oxygen mass fraction $Y_{0_2.2}$ as a function of the strain rate $a_{2.E}$ at extinction for Heptane–Decane mixtures. The symbols represent experimental measurements described in detail in appendix A.1. The interpolation plots are best fit to experimental data.

In figure 4.1 it can be observed that all volumetric mixtures, between the pure fuels behave linearly as expected. In particular, the higher the volumetric Heptane content of the fuel mixture of the Heptane–Decane mixture, the higher the strain rate at a fixed O_2 mass fraction $Y_{0_2.2}$. Regardless of the volumetric mixtures generally applies the higher the O_2 mass fraction $Y_{0_2.2}$ the higher is the extinction strain rate $a_{2.E}$.

4.1.2 Extinction of Ethanol–Heptane mixtures

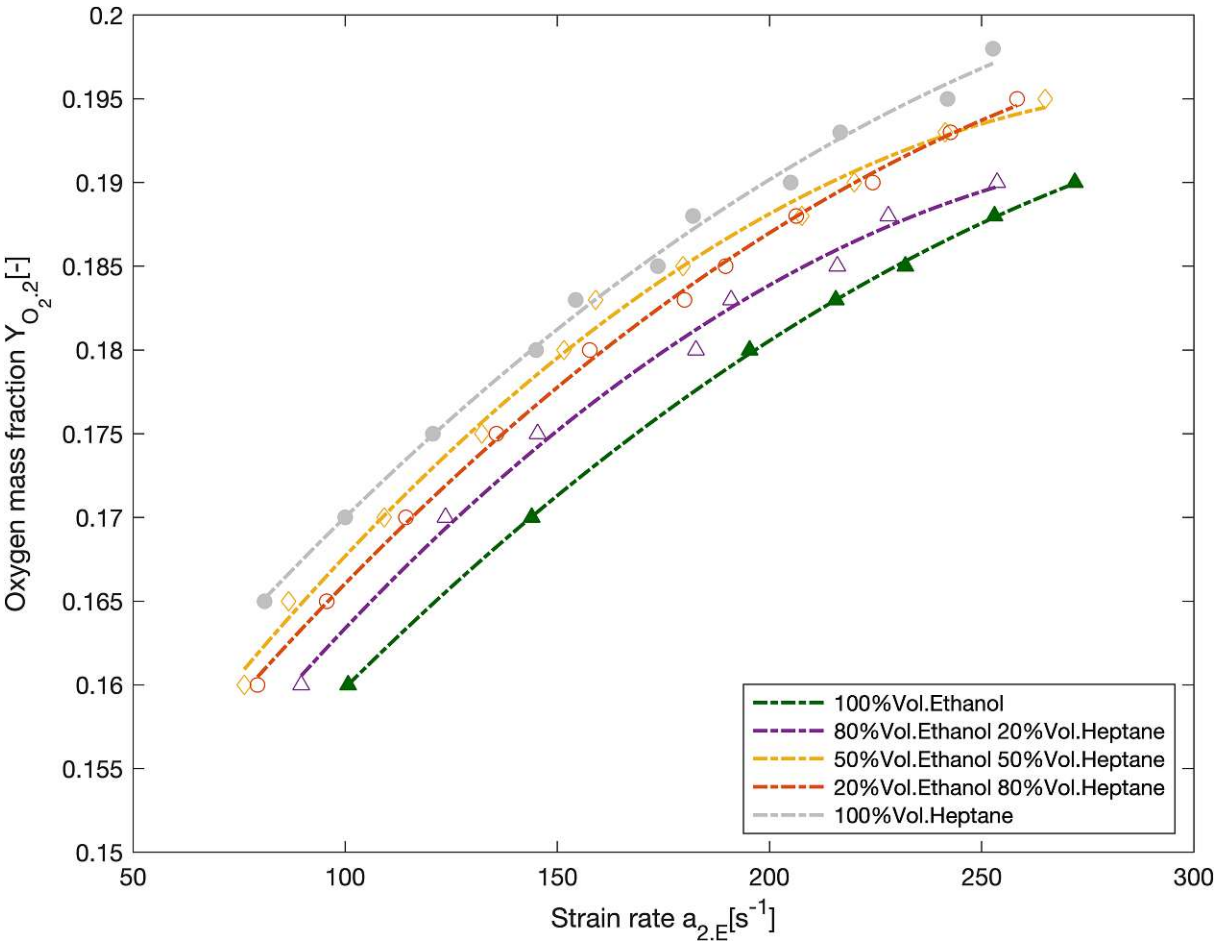

Fig. 4.2: The oxygen mass fraction $Y_{0_2.2}$ as a function of the strain rate $a_{2.E}$ at extinction for Ethanol–Heptane mixtures. The symbols represent experimental measurements described in detail in appendix A.2. The interpolation plots are best fit to experimental data.

Figure 4.2 shows that for a given fuel and oxygen mass fraction $Y_{0_2.2}$ the flame will extinguish if the strain rate is higher than the extinction strain rate $a_{2.E}$. For all mixtures of Ethanol and Heptane the value of $a_{2.E}$ increases with increasing the oxygen mass fraction $Y_{0_2.2}$. Comparing the critical conditions of extinction for a given extinction strain rate $a_{2.E}$ the value of the oxygen mass fraction $Y_{0_2.2}$ is the highest for Heptane, followed by a 50%Vol.Ethanol–50%Vol.Heptane-, 20%Vol.Ethanol–80%Vol.Heptane-, 80%Vol.Ethanol–20%Vol.Heptane-mixture and Ethanol. This means that flames burning Ethanol are the most difficult to extinguish. It should be emphasized that, according to the experimental findings, a flame burning a 50%Vol.Ethanol–50%Vol.Heptane mixture is easier to extinguish than a 20%Vol.Ethanol–80%Vol.Heptane mixture or a 80%Vol.Ethanol–20%Vol.Heptane mixture.

It seems therefor that a 50%Vol.Ethanol–50%Vol.Heptane mixture doesn't follow the expected linear trend of the critical conditions of the extinction rate in view of the trend in variable fuel blends, which can be considered for Decane-Heptane mixtures as seen in figure 4.1.

4.1.3 Extinction of Isobutanol–Heptane mixtures

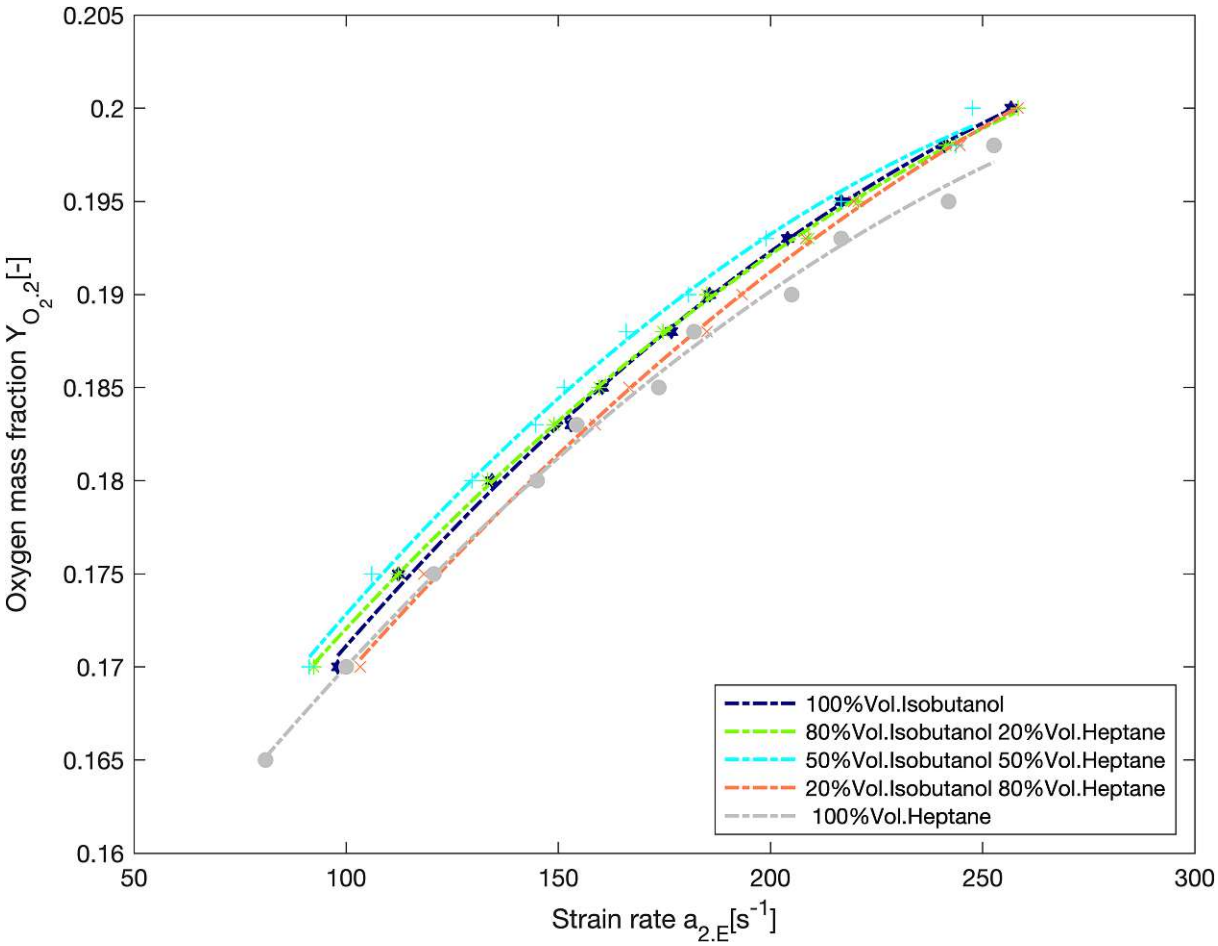

Fig. 4.3: The oxygen mass fraction $Y_{0_2.2}$ as a function of the strain rate $a_{2.E}$ at extinction for Isobutanol–Heptane mixtures. The symbols represent experimental measurements described in detail in appendix A.3. The interpolation plots are best fit to experimental data.

Comparison of figure 4.1 and figure 4.2 with figure 4.3 shows with respect to mixing ratio independent critical conditions of extinction, the value of $a_{2.E}$ increases in general with increasing the oxygen mass fraction $Y_{0_2.2}$. Figure 4.3 shows that the described nonlinear phenomena for critical conditions of extinction of burning Isobutanol–Heptane mixtures are similar to those of Ethanol-Heptane mixtures in 4.2, in particular a burning 50%Vol.Isobutanol–50%Vol.Heptane mixture is the most difficult to ignite and consists of the lowest reactivity of the investigated Isobutanol–Heptane blends. The critical conditions of extinction of burning Isobutanol–Heptane blends of different ratios are in general very similar regardless their volumetric mixing ratios.

Nevertheless, minor differences can be observed in the extinction strain rates. Figure 4.3 shows for a given value of $a_{2.E}$ the highest value of the oxygen mass fraction $Y_{0_2.2}$ is reached in descending order by 50%Vol.Isobutanol–50%Vol.Heptane mixture, Isobutanol, 80%Vol.Isobutanol–20%Vol.Heptane mixture, 20%Vol.Isobutanol–80%Vol.Heptane mixture followed by Heptane which is therefor the hardest to extinguish. For observed extinction strain rates lower than $a_{2.E} = 160$ a comparison of the critical conditions of extinction leads to the observation of a higher reactivity of a 20%Vol.Isobutanol–80%Vol.Heptane blend in comparison to pure Heptane ascertainable at the lower extinction strain rate $a_{2.E}$ of 20%Vol.Isobutanol–80%Vol.Heptane for a certain oxygen mass fraction $Y_{0_2.2}$.

4.2 Autoignition

Start of the autoignition experiment begins after completion of the preparations according to section 3.6.2 with an extinction of the investigated mixture to be able to guarantee the functioning of the instruments. At a strain rate a_2 value of 80 and an oxygen mass fraction $Y_{0_2.2}$ of 0.233 the oxygen mass fraction will slowly be reduced until the burning flame is extinguished. When the functionality is confirmed, the up-heating of the heating element is started. In order to protect the sensitive components, the continuously measured temperature rise of the fuel stream should not exceed the value 15-20 $\frac{K}{min}$. The gas flow must be continuously adjusted and the liquid pool should be filled to a visible liquid level to prevent overheating of the burner. In order to obtain comparative values of the correctness of the measuring instruments, the maximum achievable measured temperature of the thermocouple is recorded at a fixed strain rate value of $a_2 = 100$. Since there must be no guarantee of a uniform laminar temperature distribution in the oxidizer flow, the central position of the thermocouple may have to be adjusted slightly. For these measurements the oxygen flow temperature T_2 values for 40%, 42% and 44% maximum output voltage of the heating element are recorded.

The acquisition of the autoignition temperature at different strain rates can be started according to the following procedure: The liquid flow rate needs to be adjusted any time to match the fuel burning rate. After slowly increasing the power of the heating element while adjusting the gas flow, the temperature of the oxidizer stream T_2 is gradually increased until the autoignition temperatures $T_{2.AI}$ is reached and an ignition takes place. All measurable variables are recorded by the measuring software, while the optical examination is performed by a high-speed camera. The burning flame must be extinguished by simultaneously decreasing the O_2 mass fraction $Y_{0_2.2}$ by 0.01-0.02 and increasing the strain rate by 5-10 values in order to achieve an annihilating effect on the temperature development. The power of the heating element must also be turned down by 2% of the output voltage. Care must be taken to ensure that the temperature is lower than the autoignition temperature of the actual strain rate to not cause a spontaneous ignition. The described procedure is repeated until the autoignition temperatures $T_{2.AI}$ of strain rates $a_{2.AI}\epsilon[100, 450]$ in increasing steps of a strain rate value of 50 are obtained.

After finishing the autoignition experiments the cooling down procedure follows inversed rules as the heating up process. The temperature decrease shouldn't exceed the value 15-20 $\frac{K}{min}$. While decreasing the strain rate a_2 to the start value, the actual temperature of the oxidizer stream T_2 needs to be lower than the autoignition temperature $T_{2.AI}$. The autoignition top needs to be disconnected, cleaned and the screens may be replaced as described earlier.

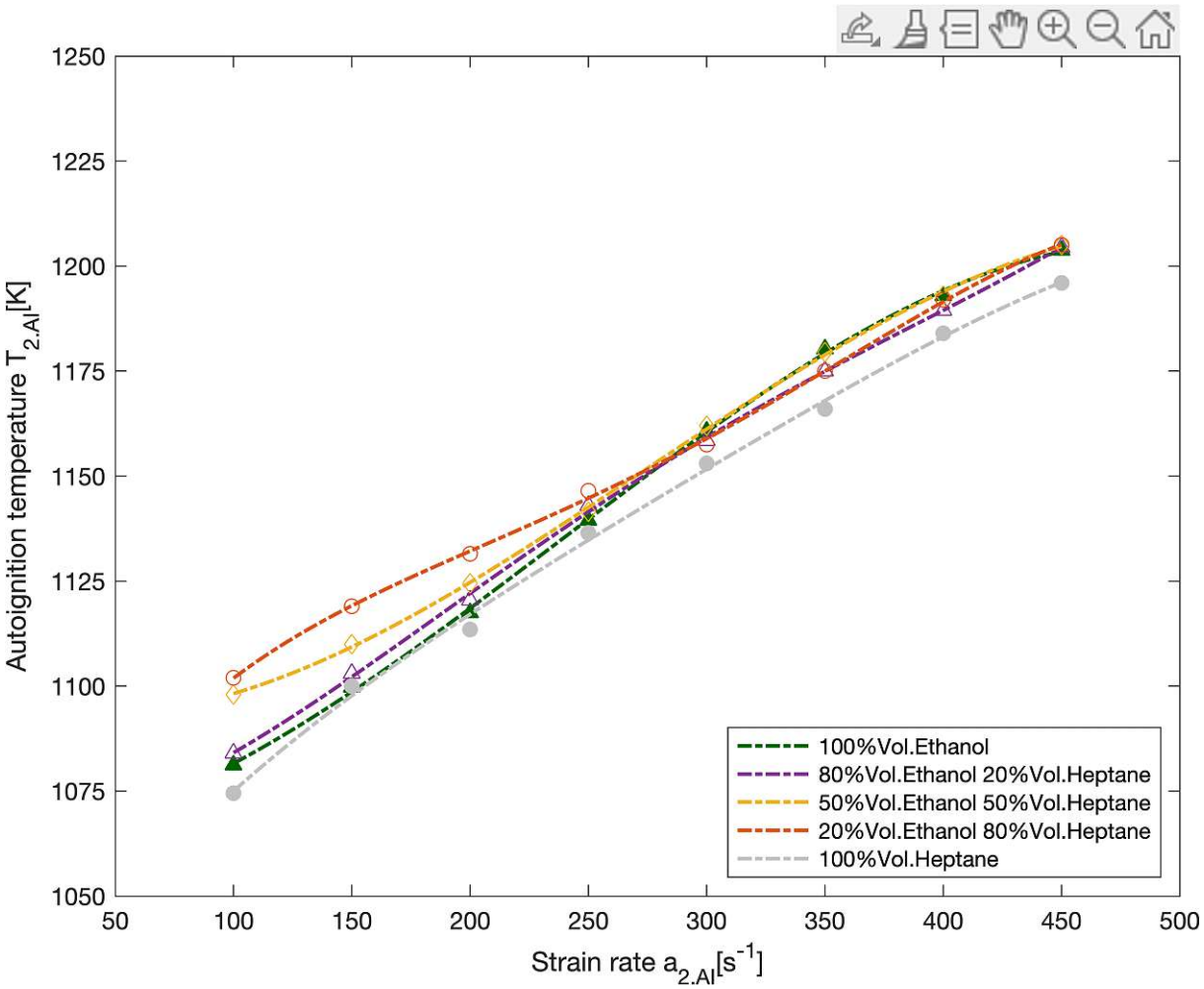

Fig. 4.4: The autoignition temperature $T_{2.AI}$ as a function of the strain rate $a_{2.E}$ for different Ethanol–Heptane mixtures. The symbols represent experimental measurements described in detail in appendix B. The interpolation plots are best fit to experimental data.

At a given strain rate $a_{2.AI}$ autoignition takes place if the temperature of the oxidizer stream T_2 exceeds the autoignition temperature $T_{2.AI}$. The strain rate at autoignition $a_{2.AI}$ is calculated from equation 2.2. Figure 4.4 shows with respect to mixing ratio independent critical conditions of autoignition, the value of $T_{2.AI}$ increases in general with increasing the strain rate $a_{2.AI}$.

Comparing the experimental values at a fixed strain rate, two opposite investigations can be observed: Comparing the experimental values at for a given strain rate $a_{2.AI} > 275$ the graph 4.4 shows that the value of $T_{2.AI}$ for Ethanol is the highest and the lowest for Heptane. Accordingly, mixtures of both fuels behave in a linear correlation. For given strain rate $a_{2.AI} < 275$ the experimental data show that the value of $T_{2.AI}$ for 20%Vol.Ethanol–80%Vol.Heptane is the highest, followed by 50%Vol.Ethanol–50%Vol.Heptane mixture, followed by 80%Vol.Ethanol–20%Vol.Heptane followed by Ethanol and lastly Heptane. According to that it indicates that for Ethanol–Heptane blends a 20%Vol.Ethanol–80%Vol.Heptane mixture is the most difficult to ignite and Heptane the easiest. The order of the autoignition behavior changed for Ethanol and Ethanol–Heptane blends. Only Heptane shows a linear progression of its autoignition temperature over all fixed strain rate values, since the fuel tested was always the easiest to ignite recognizable by its comparatively low autoignition temperature $T_{2.AI}$.

Regarding the experimental results, it seems that Ethanol itself and blends cause this in-linearity. Depending on the overall stoichiometry, the concentration of the intermediates varies in their relative concentration, since different reactions occur with different degrees of favor during the oxidation of Ethanol. The initial oxygen concentration determines the relative abundance of abstracting radicals, which form from the pathway with the fastest reactivity.[69]

Further investigations comparing the corrected autoignition temperature and numerical results especially of Ethanol–Heptane mixtures are done in the following chapter 5 to investigate the described behavior.

[69] Cf. UCSD. *The San Diego Mechanism. Chemical-Kinetic Mechanisms for Combustion Applications.* URL: `https://web.eng.ucsd.edu/mae/groups/combustion/sdmech/sandiego20161214/sandiego20161214_mechCK.txt` (Accessed 02/10/2022).

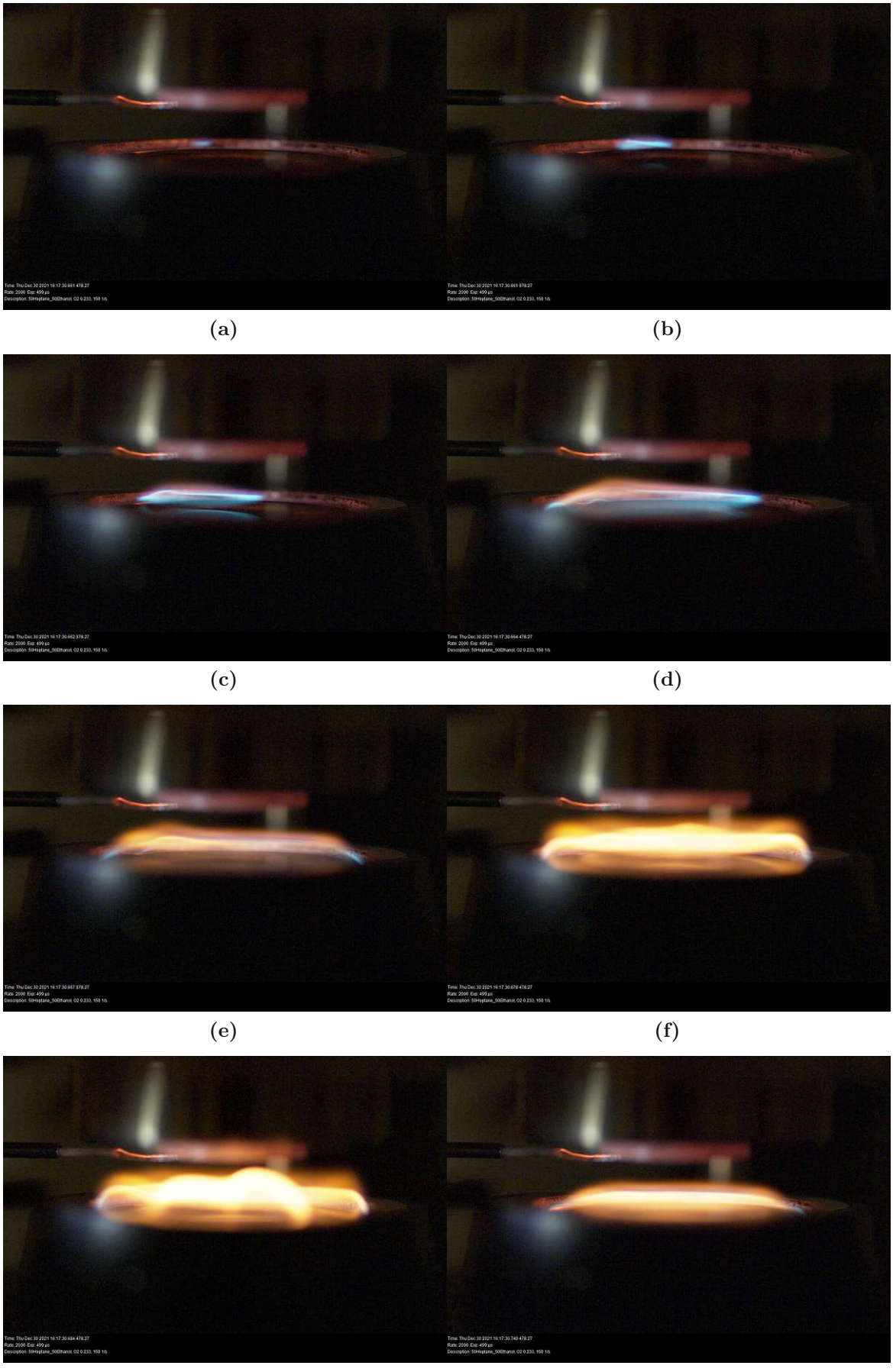

Fig. 4.5: High speed photograph of a 50%Vol.Ethanol–50%Vol.Heptane mixture of a typical autoignition event at $p = 99900bar$, $Y_{O_2.2} = 0.233$, $a_2 = 150$, $T_1 = 294.15K$ and $T_2 = 1109K$

Figure 4.5 shows a typical autoignition event at lower strain rate. On frame (a) it is shown that the ignition takes place almost in the center of the burner, what is considered a good ignition. The flame propagation should ideally start in the center to provide uniform flame propagation and comparable measurement points.
As long as the autoignition starts on the edge of the burner, and not on the rim, it can be still classified as a good ignition. At strain rates higher than 200-250 it is observed that the initial ignition point starts not anymore in the center.

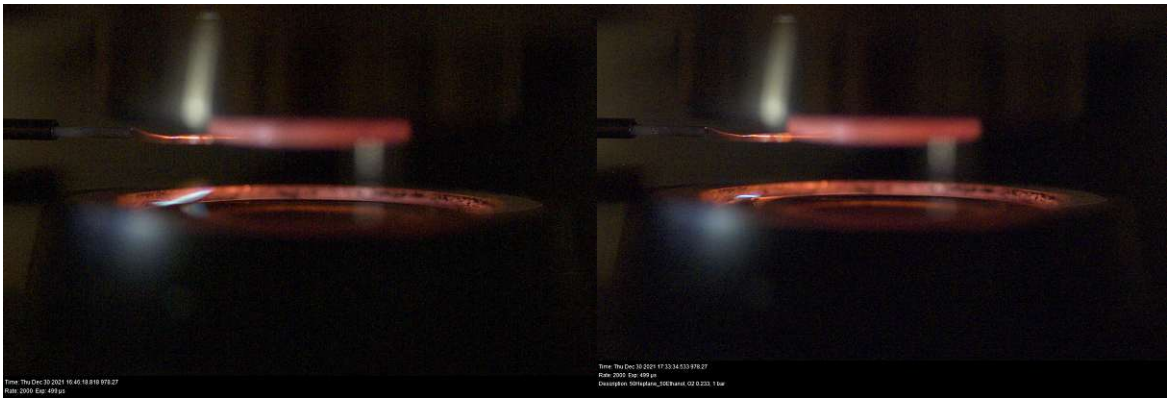

(a) **(b)**

Fig. 4.6: High speed photograph of a 50%Vol.Ethanol–50%Vol.Heptane mixture of initial autoignition frames at high strain rates (a) 300 and (b) 450

As shown in the graphic above, the ignition at a strain rate $a_2 = 300$ shows flame formation at the edge, which must be regarded as impermissible ignition. The ignition at a strain rate $a_2 = 450$ is significantly better. Compared with figure 4.5, the initial ignition point has moved further and further to the edge of the burner as the strain rate has increased.
One main cause of these uniform observations across different fuel mixing ratios is the high strain rate, which results in a high flow rate from the oxidizer outlet. Due to the high strain rate, even small fluctuations at the surface are sufficient to cause an ignition.

5
Numerical calculations

5.1 Temperature correction

The measured temperature of the thermocouple and therefor the experimental autoignition temperature needs to be numerically adjusted. Due to the high temperature difference between the thermocouple and the surrounding environment, the heat loss in form of radiation needs to be calculated:

Energy balance thermocouple

$$\dot{Q}_{cat} + \dot{Q}_{conv} + \dot{Q}_{cond} + \dot{Q}_{rad} = \frac{\partial}{\partial t}(m\, c_p\, T_{tc}) = \rho\, c_p\, V\, \frac{\partial T_{tc}}{\partial t}$$

$$\dot{Q}_{conv} >> \underbrace{\dot{Q}_{cat},\, \dot{Q}_{cond}}_{Negligible},\, \dot{Q}_{rad} \tag{5.1}$$

Convection-radiation energy balance[70, 71]

$$m\, c_p \underbrace{\frac{\partial T_{tc}}{\partial t}}_{Steady\ state} = \epsilon_{tc}\, \sigma\, A_s\, RF\, (T_{tc}^4 - T_s^4) - h\, A_s\, (T_g - T_{tc}) \tag{5.2}$$

$$h(T_g - T_{tc}) = \epsilon_{tc}\, \sigma\, (T_{tc}^4 - T_s^4)\, RF$$

Reynolds number

$$Re = \frac{U_2\, b}{\mu} = \frac{a_2\, L\, b}{\mu} \tag{5.3}$$

[70] Cf. p. 6 15.

[71] Cf. p.819 S. Venkateshan. *Heat Transfer*. eng. 3rd ed. 2021. Cham: Springer International Publishing Imprint: Springer, 2021. ISBN: 3030583384. URL: 10.1007/978-3-030-58338-5.

Nusselt number

$$\mathrm{Nu} = \begin{cases} \frac{h\,b}{k} & \text{general expression} \\ (0.24 + 0.56\,Re_b^{0.45})(\frac{T_m}{T_\infty})^{17} & \text{cylindrical problem} \\ 2 + 0.6\,Re^{0.5}\,Pr^{\frac{1}{3}} & \text{spherical problem} \end{cases}$$

Gas temperature

$$\begin{aligned} T_g &= T_{tc} + \frac{b}{\mathrm{Nu}\,k}[\epsilon_{tc}\,\sigma\,(T_{tc}^4 - T_s^4)\,RF] \\ &= T_{tc} + \frac{b\,\epsilon_{tc}\,\sigma\,(T_{tc}^4 - T_s^4)\,RF}{2 + 0.6\,Re^{0.5}\,Pr^{\frac{1}{3}}} \\ T_g &= \frac{b\,\epsilon_{tc}\,\sigma\,T_{tc}^5\,RF}{2 + 0.6\,Re^{0.5}\,Pr^{\frac{1}{3}}} - \underbrace{\frac{b\,\epsilon_{tc}\,\sigma\,T_s^4\,RF}{2 + 0.6\,Re^{0.5}\,Pr^{\frac{1}{3}}}}_{\textit{Radiation error thermocouple}} \end{aligned} \tag{5.4}$$

The energy balance of the thermocouple includes the heat transfer caused from radiation, convection, conduction and surface-induced catalytic reactions. Due to the following assumed simplifications, the conductive and catalytic parts of the heat flow equation can be neglected as seen in equation 5.1 and 5.2:

- Air environment with small catalytic activity. A constant air flow prevents the reactants from dwelling on the catalytic surface.[72]
- Ratio of the wire in comparison to the thermocouple length is very small. An increase in the wire diameter causes the radiation and conduction errors to increase significantly.[73]
- High Reynolds number provide higher heat transfer coefficients with the increase in convective heat transfer and negotiation of conduction errors.[74]
- The assumption of surface-induced reactions renders considerations of catalytic reactions at the surface obsolete.[75]

[72] Cf. p.1 46.
[73] Cf. p.9 V. Hindasageri et al. "Thermocouple error correction for measuring the flame temperature with determination of emissivity and heat transfer coefficient". eng. In: *Review of scientific instruments* 84.2 (2013), pp. 024902–024902. ISSN: 0034-6748.
[74] Cf. p.10 21.
[75] Cf. p.6 46.

Therefore, the thermocouple can be regarded as a measuring instrument which is constantly heated by a hot gas stream and small deviations are only caused by lost heat radiation. The gas temperature measured by the thermocouple can be given as heat transferred by gas convection and the radiation loss to the surrounding area. The temperature indicated by the thermocouple is T_{tc}. The radiation heat loss of the sensor by unit area is given by the right side of equation 5.2 $\epsilon\,\sigma\,(T_{tc}^4 - T_s^4)$ where T_s is the temperature of the surface visible to the thermocouple. The heat gained by the sensor on the left side of equation 5.2 can be written as $h\,(T_s - T_{tc})$, where h is the convective heat transfer coefficient between the gas and the sensor. The convective term thus almost completely maps the measurement of the characteristic gas temperature computed from the heat transfer since the radiation loss is respectively small.[76]

The remaining convection-radiation energy balance under thermal equilibrium can be simplified as shown in equation 5.2. The steady state environment of the formed stagnation plane lets the time-dependent variables truncate out.
By introducing the strain rate via the oxidizer stream velocity into the Reynolds number and using the Nusselt number for a spherical problem[77], the gas temperature can be written explicitly as in equation 5.4.

[76] Cf. p.819 f. 52.

[77] Cf. p.1542 A. Aissa et al. “Ranz and Marshall Correlations Limits on Heat Flow Between a Sphere and its Surrounding Gas at High Temperature”. In: *Thermal Science* 19.5 (2015), pp. 1521–1528. DOI: 10.2298/TSCI120912090A. URL: https://hal.univ-lorraine.fr/hal-01599788.

The following python™ code aims to interpolate the exact gas temperature of the gas stream including the radiation error. Some notes on the presented code:
The Radiation Factor is set to $RF = 2$ because the radiation loss is only happening at half space. Therefore, also the value of ϵ is reduced by half. Nu is described by the Ranz&Marshall correlation for spherical coordinates.

After initializing the parameters from the thermocouple temperature to the radiation factor, linear interpolation between the known parameters for $T_{i1} = 973K$ and $T_{i2} = 1273K$ is performed for an exact temperature determination to include the temperature deviation of the radiation output to the surrounding area. The output values given from line 4-17 were provided or measured by the UCSD research group and are used for numerical calculations of the corrected autoignition temperature.
The viscosity μ, the thermal conductivity k, the Pr and the Re are interpolated in a loop until the defined deviation in line 30 is less than or equal to 10%.

```
def GASTEMP(Ttc, a2, L=10.5e-3, Nu ='Sphere'):

    Tp =Ttc          #Temperature thermocouple       [K]
    b=0.457e-3       #Diameter thermocouple bead     [m]
    Ti1=973          #Interpolation temperature 1    [K]
    Ti2=1273         #Interpolation temperature 2    [K]
    niu1=1.133e-4    #Viscosity oxidizer stream|Ti1  [m2/s]
    niu2=1.529e-4    #Viscosity oxidizer stream|Ti2  [m2/s]
    k1=6.581e-2      #Thermal conductivity|Ti1       [W/(mK)]
    k2=7.868e-2      #Thermal conductivity|Ti2       [W/(mK)]
    Pr1=0.71         #Prandtl number|Ti1             [-]
    Pr2=0.73         #Prandtl number|Ti2             [-]
    em=0.2           #Emissitivity thermocouple      [-]
    sigma=5.67e-8    #Stefan-Boltzmann-constant      [W/(m2K4)]
    Tsurr=295.15     #Temperature surrounding area   [K]
    u=a2*L/2         #Velocity oxidizer stream       [m/s]
    RF=2             #Radiation factor               [-]

    while True:
        niu=niu1+(Tp-Ti1)/(Ti2-Ti1)*(niu2-niu1)
        k=k1+(Tp-Ti1)/(Ti2-Ti1)*(k2-k1)
        Pr=Pr1+(Tp-Ti1)/(Ti2-Ti1)*(Pr2-Pr1)
        Re=u*b/niu

        if Nu =='Cylinder':Nu=(0.24+0.56*Re**0.45)

        elif Nu =='Sphere':Nu=2+0.6*(Re**(1/2))*(Pr**(1/3))
        Tg=Ttc+em*sigma*(Ttc**4-Tsurr**4)*b/k/Nu/RF

        if abs(0.5*(Tg+Ttc)-Tp)<=0.1:
            break
        else:
            Tp=0.5*(Tg+Ttc)

        return Tg
```

5.2 Numerical simulation of extinction

The results of numerical calculations seen in the following sections are performed using one-step chemistry with parameters so chosen, that the plots make a best fit to the numerical simulations of reacting systems with detailed kinetic mechanisms performed in OpenSMOKE++. OpenSMOKE++ is written in object-oriented C++, consists of thousands of chemical species and reactions including low temperature and high temperature mechanism. It can be easily extended and customized by the user for specific systems.[78]

In order to determine the analytically derived reaction parameters, a simplified one-step irreversible process reaction was assumed with the following reaction equation:

$$C_xH_yO_z \ + (x + \tfrac{y}{4} - \tfrac{z}{2})O_2 \ \longrightarrow xCO_2 \ + (\tfrac{y}{2})H_2O$$

The corresponding reaction rate can be given for a one-step chemistry process by[79]

$$w = \rho^2 \, [\frac{Y_F \, Y_{O_2}}{W_F \, W_{O_2}} \, B \, exp(\frac{-E}{R^0 \, T})] \tag{5.5}$$

Numerically the kinetic mechanism C1-C16 HT+LT from the CRECK Modeling Lab of Politecnico di Milano is used with 492 species and 17790 reactions for low and high temperature reactions including post-processing of sensitivity analysis, rate of production analysis and reaction path analysis.[80] The CounterFlowDiffusion1D solver used in this thesis is initialized by the strain rate/velocity and the compositions of the mixtures of the liquid fuels. A steady-state simulation building a computational grid with flow, energy, and species fields at initial conditions forms the cornerstone of the process. Followed by the definition of the dynamic boundary conditions a dynamic simulation is run until either autoignition or extinction occurs.

[78] Cf. A. Cuoci et al. "OpenSMOKE++: An object-oriented framework for the numerical modeling of reactive systems with detailed kinetic mechanisms". eng. In: *Computer physics communications* 192 (2015), pp. 237–264. ISSN: 0010-4655.

[79] Cf. p.833 44.

[80] Cf. T. C. M. Group. *C1-C16 HT+LT mechanism (Version 2003, March 2020).* URL: `http://creckmodeling.chem.polimi.it/menu-kinetics/menu-kinetics-detailed-mechanisms/107-category-kinetic-mechanisms/403-mechanisms-1911-tot-ht-lt` (Accessed 03/21/2022).

The dynamic simulation increases the strain rate until extinction occurs. The extinction experiments can't be computed with the submitted CounterFlowDiffusion1D solver. Even after parameter variations the highest fuel temperature stays the same as the boundary temperature, which means no ignition can take place. Derived from that no extinction of the mixture can be simulated either. This phenomenon has already been mentioned in previous thesis which include the subject of the extinction of different fuel mixtures in counterflow burners.

The CRECK-2003-Mechanism needs to be provided with species of high temperature and low temperature mechanism of liquid fuels. Solving this problem, a new kinetic mechanism must be developed at Politecnico di Milano by the CRECK Modeling Group. Therefore, a comparison between numerical simulation of extinction data and experimental extinction data is not possible in this thesis.

5.3 Numerical simulation of autoignition

Low temperature and high temperature mechanism are provided for all species using the CRECK-2003-Mechanism. High temperature mechanism is obtained from the detailed mechanism after deduction of the elementary and branched reactions for lower temperatures.[81] An initial simulation according to the real experimental setup is initiated. A dynamic simulation leads to an increase of the air temperature compared with the highest temperature. As the air temperature increases and a difference of 10K between the highest temperature and the air temperature is notified, the air temperature can be taken as the current autoignition temperature.

[81] Cf. p. 131 G. Mairinger et al. "Autoignition of condensed hydrocarbon fuels in non-premixed flows at elevated pressures". eng. In: *Combustion theory and modelling* 20.6 (2016), pp. 995–1009. ISSN: 1364-7830.

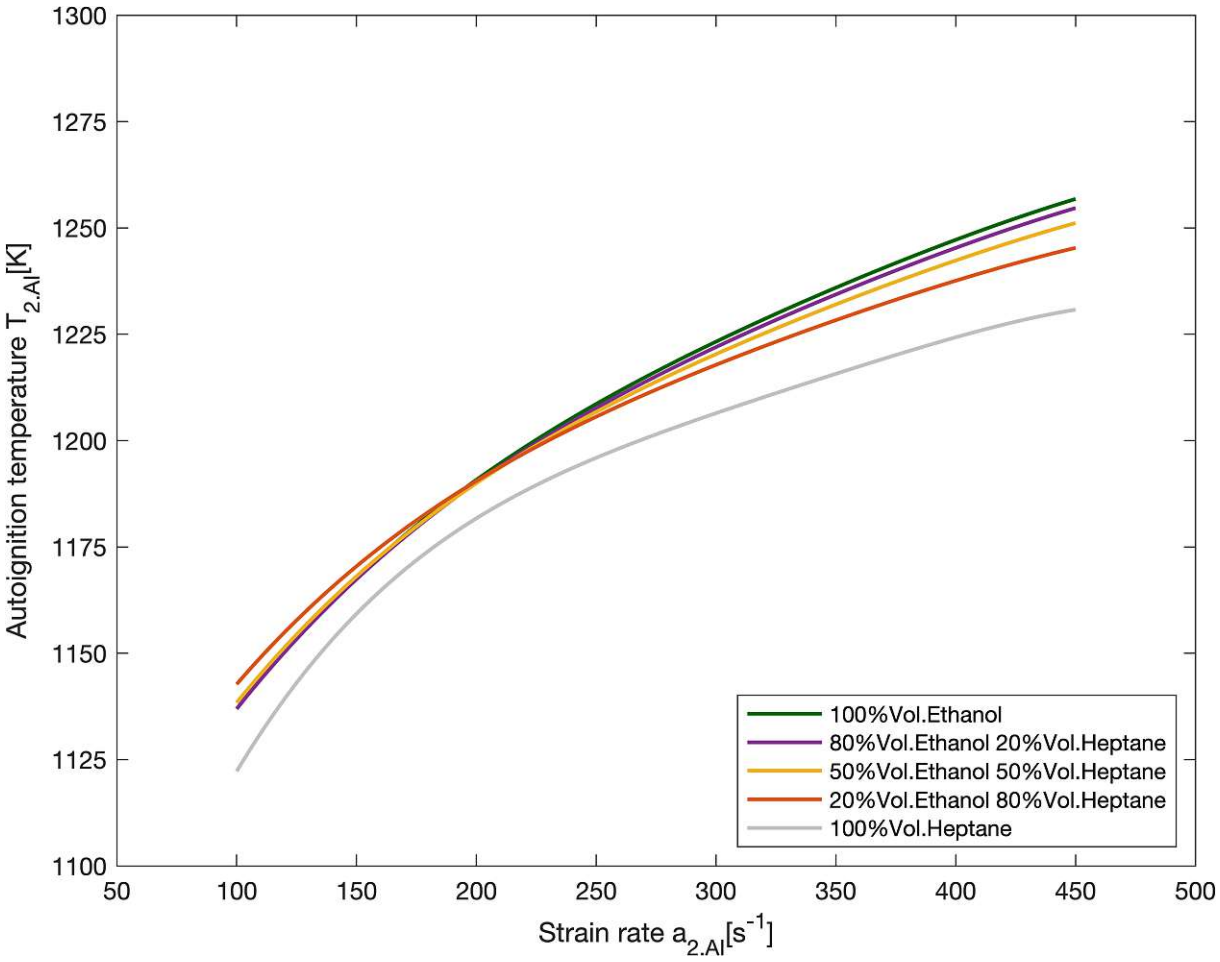

Fig. 5.1: The autoignition temperature $T_{num.AI}$ of the simulation as a function of the strain rate $a_{2.AI}$ for different Ethanol–Heptane mixtures. The plots represent numerical data described in detail in appendix C.

Figure 5.1 shows the numerical results of the autoignition simulation of different Ethanol–Heptane mixtures. Heptane is at all values $a_{2.AI}$ the easiest to ignite. For lower strain rate values a 20%Vol.Ethanol–80%Vol.Heptane mixture is the hardest to ignite, followed by a 50%Vol.Ethanol–50%Vol.Heptane mixture. 80%Vol.Ethanol–20%Vol.Heptane mixture and pure Ethanol show only very small deviations for lower strain rates. With higher strain rates the plots behave as expected with Ethanol having the highest autoignition temperature followed in order of mixtures with a higher Ethanol share. The higher the Ethanol share at a constant strain rate $a_{2.AI}$ the higher is the autoignition temperature $T_{2.AI}$.

5.4 Comparison of simulation and corrected experimental autoignition data

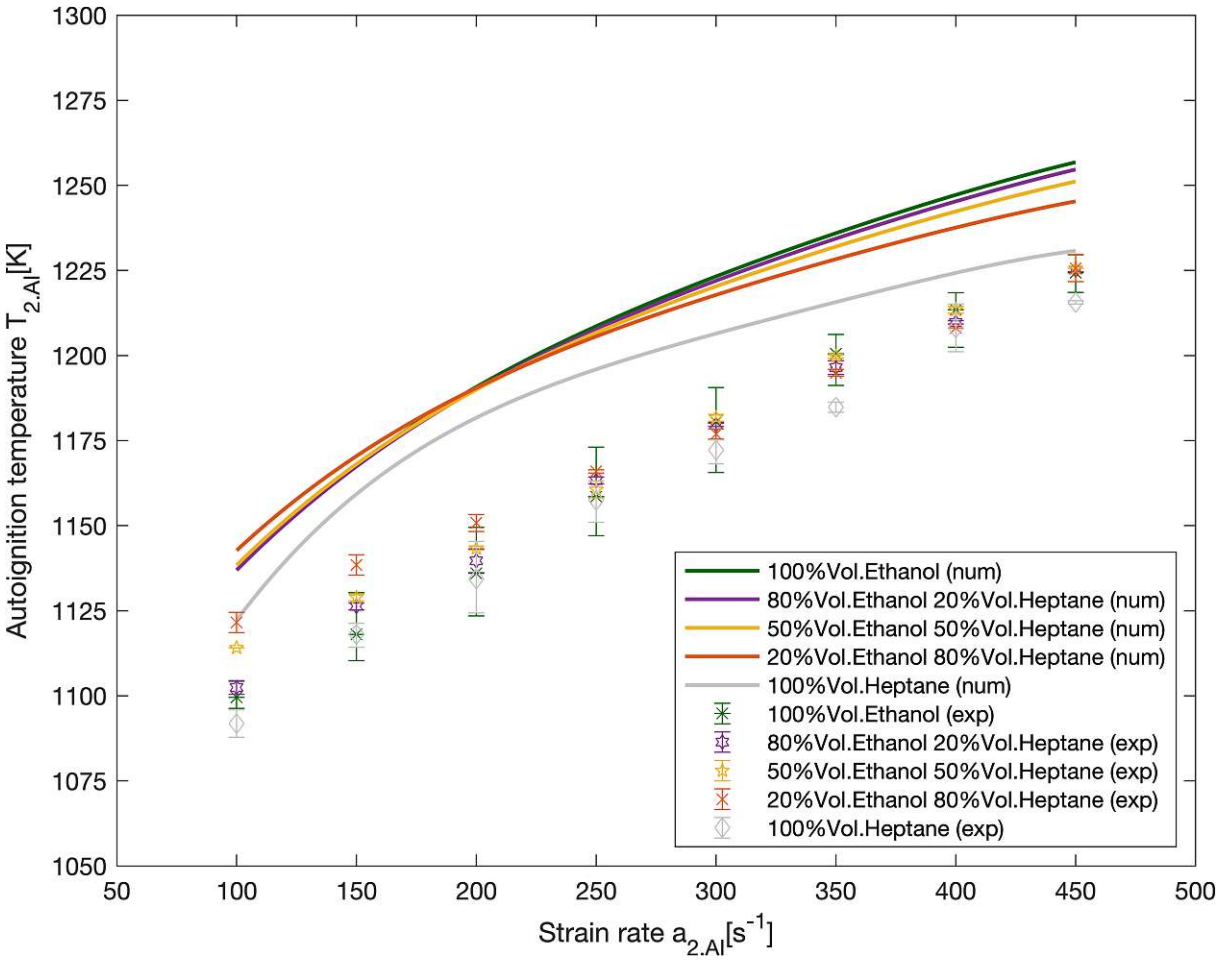

Fig. 5.2: Comparison between the autoignition temperature $T_{num.AI}$ of the simulation and the corrected autoignition temperature T_g. Both are functions of the strain rate $a_{2.AI}$ for different Ethanol–Heptane mixtures. The symbols represent numerical corrected experimental measurements and its error bars described in detail in appendix B.

Figure 5.2 shows that the numerical autoignition temperature $T_{num.AI}$ is over all strain rates and volumetric mixtures always higher than the corresponding experimental corrected gas temperature T_g. While increasing the strain rate $a_{2.AI}$ every fuel blend or pure fuel shows a higher autoignition temperature $T_{2.AI}$ and becomes therefore harder to ignite. Figure 5.3 shows that for pure Ethanol and Heptane the deviations of the measurements are the highest. In addition to that it can be observed, that the experimental interpolation plot for Heptane fits the numerical plot the best as this is the best approximation of the gradient over all strain rates.

In figure 5.2 a 20%Vol.Ethanol–80%Vol.Heptane blend has the highest autoignition temperature for lower strain rates $a_{2.AI}$ for both the numerical and the experimental plot. The numerical plot changes its autoignition behavior for the different Ethanol contents into the assumed order described in section 5.3, already at a lower strain rate than the corrected experimental measuring points. As a commonality of both plots it can be observed that at strain rate $a_{2.AI} = 100$ the pure fuels Heptane and Ethanol have the lowest autoignition temperature and are therefore the easiest to ignite. This behavior is discussed in the following chapter 6.

Figures 5.2 and 5.3 show that the numerical and corrected experimental data don't fit precisely, but on closer examination of the error, the relative deviation remains at 2% which can be taken from ΔT in appendix B and $\varnothing\Delta T$ in appendix C.

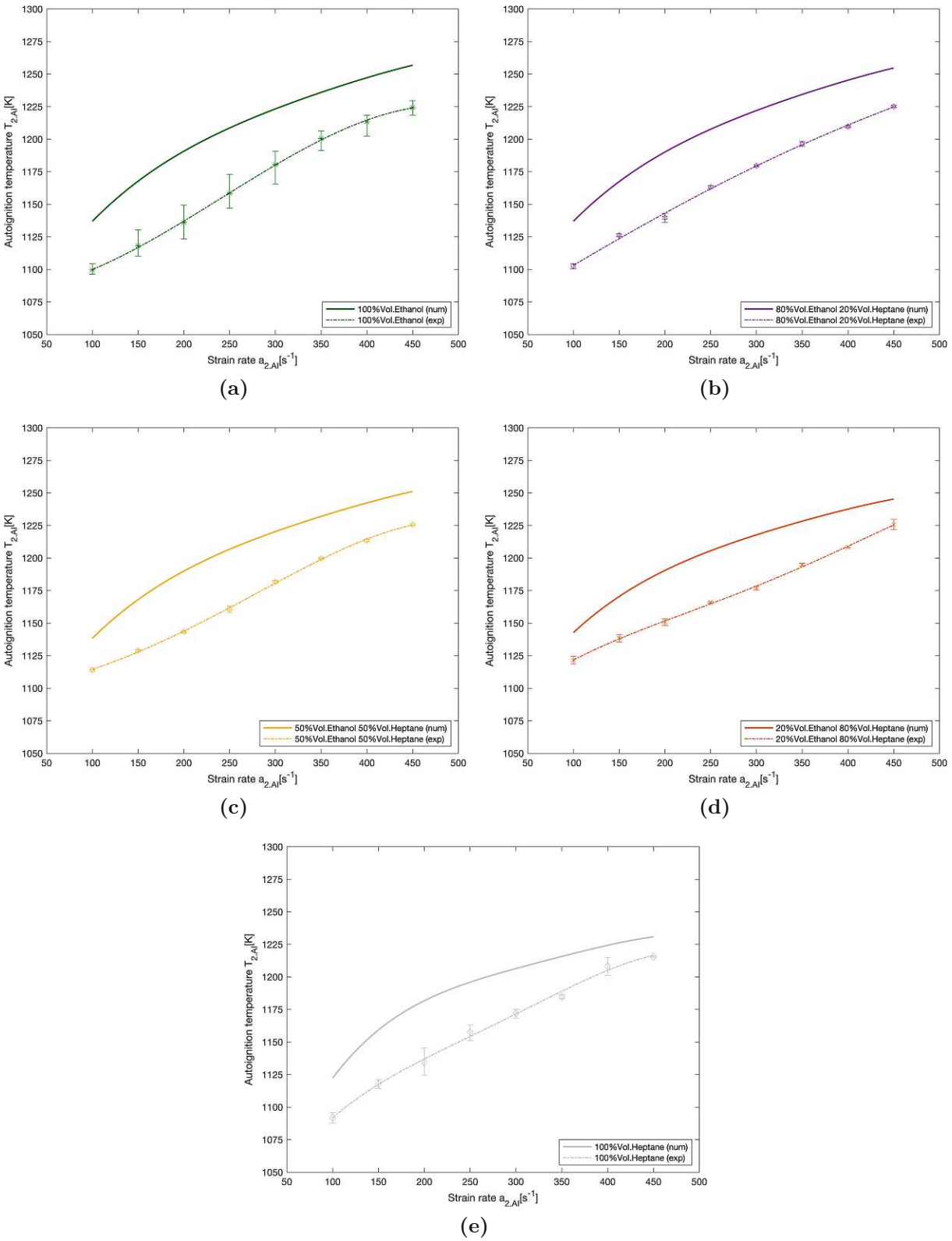

Fig. 5.3: Detailed comparison between the autoignition temperature $T_{num.AI}$ of the simulation and the corrected experimental autoignition temperature T_g of the thermocouple as functions of the strain rate $a_{2.AI}$ for different Ethanol shares.

6
Discussion

The extinction plots in figure 4.2 for Ethanol-Heptane blends and figure 4.3 for Isobutanol-Heptane blends as well as the autoignition behavior 4.4 of Ethanol-Heptane mixtures show very clearly that a „cross-over“ for lower strain rates exists. This phenomenon is well known in literature and is described in several studies for other fuels.[82, 83, 84]

The results of the extinction plots for blends of Isobutanol and Heptane in figure 4.3 show outcomes that deviate from the expected linear extinction plots as described earlier in section 4.1.3. Previous studies show that the errors in well-designed counterflow experiments are less than 5%.[85]
Thus, the computed deviations showed in appendix A.3 aren't large for Isobutanol-Heptane mixtures, the data points for the mixtures are quite similar and no specific characteristics can be observed. Despite this, it seems that both the low and high temperature chemistry of Heptane is being hemmed in mixtures with Isobutanol shares over all strain rates causing a 50%Vol.Isobutanol–50%Vol.Heptane mixture to have the least reactivity. A numerical kinetic study needs to be done by modifying the kinetic chemical mechanism in future works with the cooperation of the CRECK Modeling Group.

Analyzing the critical conditions of extinction of Ethanol-Heptane mixtures in figure 4.2 it can be derived that a 50%Vol.Ethanol–50%Vol.Heptane mixture seems to follow a different kinetic chemical mechanism than the other volumetric compositions. Attributing the experimental uncertainties to the observed differences can not explain that behavior alone.

[82] Cf. 44.
[83] Cf. 18.
[84] Cf. 30.
[85] Cf. p.1548 34.

Previous studies show that critical conditions of extinction are calculated using the high temperature mechanism because low temperature chemistry has low influence on extinction. From this consideration it may be concluded that a 50%Vol.Ethanol–50%Vol.Heptane mixture somehow prevents a molecular transport as it has a significant influence on the critical conditions of extinction of straight chain alkanes proven in a previous study.[86]

The autoignition behavior of Ethanol–Heptane blends can be discussed in more detail, since a combined numerical and experimental study is carried out in this thesis. In figure 5.2 both the numerical and the experimental autoignition behavior show the „cross-over“ of the plots from a lower to a higher strain rate. It seems that at low strain rates the autoignition low temperature chemistry of Heptane is being hemmed for all volumetric mixtures. As the strain rate increases it could be that this effect vanishes and high temperature chemistry and molecular transport play the significant part of the autoignition behavior as expected. For lower strain rates it seems that the low temperature chemistry in all different volumetric Ethanol–Heptane blends is hemmed causing a higher autoignition temperature than for both pure fuels itself. It seems that already small shares of Ethanol are able to inhibit the low temperature chemistry of Heptane in these fuel mixtures. Reaction path analysis should be carried out to investigate if the frequency factor in the formation of the hydroxyl group(OH-radical), which plays a dominant part in the low temperature chemistry of Heptane and its mixtures, leads to a competing reaction path which may be faster than the expected ones and causes the observed autoignition behavior.[87]

To proof these hypotheses further investigations should be carried out. In order to understand whether the „cross-over“ section depends significant on the molecular transport, the formation of OH-radicals at low temperature chemistry or even the saturation pressure, the influencing variables must be examined separately by experts and investigated in future studies. In addition to that the chemical kinetic mechanism needs to be correspondingly adjusted. This can only be done by the CRECK Modeling Group by the Politecnico di Milano in cooperation with the combustion research group at UCSD.

[86] Cf. p.132 ff. 18.
[87] Cf. p.996 ff. 30.

7
Concluding remarks

The investigations performed in this diploma thesis aim to investigate the extinction and autoignition behavior of different liquid fuel compositions of both pure fuels and 80%Vol.–20%Vol.-, 50%Vol.–50%Vol.- and 20%Vol.–80%Vol.-mixtures. Extinction experiments are carried out for Decane–Heptane-, Isobutanol–Heptane- Ethanol–Heptane-blends. For a detailed analysis the idea for the autoignition experiments is to perform both a numerical and experimental investigation of Ethanol–Heptane mixtures.

The experimental extinction experiments cannot be compared to a numerical study because the kinetic solver used here cannot account for liquid fuels. Modifications will have to be made in future research to decently complete this study of reaction kinetics on extinction of the investigated fuels.
The common finding of the extinction experiments for all fuels and volumetric mixtures is that an increase of the oxygen mass fraction $Y_{O_2.2}$ leads to an increase in the extinction strain rate $a_{2.E}$. Heptane is the hardest to extinguish followed in a linear trend by Decane–Heptane mixtures with a higher share of Heptane. Thus, the experimental investigations show that higher chain hydrocarbons extinguish easier before lighter hydrocarbons.
The critical conditions of extinction of burning Isobutanol-–Heptane blends of different ratios are in general very similar regardless their volumetric mixing ratios shown by the relatively small deviations between them. Nonlinear effects occur, in particular a burning 50%Vol.Isobutanol–50%Vol.Heptane flame being the easiest to extinguish and consists of the lowest reactivity of the investigated Isobutanol–Heptane blends.
Comparing the critical conditions for a given extinction strain rate $a_{2.E}$ the value of the oxygen mass fraction $Y_{O_2.2}$ is the highest for Heptane, followed by a 50%Vol.Ethanol–50%Vol.Heptane-, 20%Vol.Ethanol–80%Vol.Heptane-, 80%Vol.Ethanol–20%Vol.Heptane mixture and Ethanol.

According to the experimental findings, a flame burning a 50%Vol.Ethanol–50%Vol.Heptane mixture is easier to extinguish than a 20%Vol.Ethanol–80%Vol.Heptane mixture or a 80%Vol.Ethanol–20%Vol.Heptane mixture.

It is noteworthy that for every mixing ratio of Ethanol and Heptane fuels the autoignition temperature $T_{2.AI}$ increases whit an increased strain rate $a_{2.AI}$. Thus, the fuel mixture become harder to ignite. Heptane is at all strain rate values $a_{2.AI}$ the easiest to ignite. The results indicate that at higher strain rates, Ethanol has the highest autoignition temperature $T_{2.AI}$ followed by descending shares of Ethanol in the mixture. At lower strain rates both numerical and experimental results observe in contrast, opposite results. Analyzing the autoignition behavior of mixtures of Ethanol and Heptane, it seems that already small shares of Ethanol inhibit the low temperature chemistry of Heptane. This leads to a „cross-over“ in the plots for the experimental and numerical results.

Further research on the significant parameters causing the „cross-over“ section in the autoignition behavior must be examined separately and investigated in future studies.

Bibliography

[1] A. Aissa, M. Abdelouahab, A. Noureddine, M. El Ganaoui, and B. Pateyron. "Ranz and Marshall Correlations Limits on Heat Flow Between a Sphere and its Surrounding Gas at High Temperature". In: *Thermal Science* 19.5 (2015), pp. 1521–1528. DOI: 10.2298/TSCI120912090A. URL: https://hal.univ-lorraine.fr/hal-01599788.

[2] F. N. Alasfour. "The Effect of Using 30% Iso-Butanol-Gasoline Blend on Hydrocarbon Emissions from a Spark-Ignition Engine". eng. In: *Energy sources* 21.5 (1999), pp. 379–394. ISSN: 0090-8312.

[3] M. Balaji, M. Sarfas, G. S. B. Vishaal, G. V. Madhusudhan, S. Gupta, and S. Kanchan. "Scope for improving the efficiency and environmental impact of internal combustion engines using engine downsizing approach: A comprehensive case study". eng. In: *IOP conference series. Materials Science and Engineering*. Vol. 1116. 1. Bristol: IOP Publishing, 2021, p. 12070.

[4] Y. Balali and S. Stegen. "Review of energy storage systems for vehicles based on technology, environmental impacts, and costs". eng. In: *Renewable & sustainable energy reviews* 135 (2021), p. 110185. ISSN: 1364-0321.

[5] R. B. Bird, W. E. Stewart, and E. N. Lightfoot. *Transport phenomena*. eng. 2., rev. ed.. New York, NY [u.a.]: Wiley Sons, 2007. ISBN: 0470115394.

[6] A. M. Brownstein. *Renewable Motor Fuels: The Past, the Present and the Uncertain Future*. eng. Oxford: Elsevier Science Technology, 2014. ISBN: 9780128009703.

[7] N. P. Cheremisinoff. *Handbook of Hazardous Chemical Properties*. eng. Burlington: Elsevier Science, 1999. ISBN: 1281077429.

[8] R. Cherif, F. Hasanov, and A. Pande. "Riding the Energy Transition: Oil beyond 2040". eng. In: *Asian economic policy review* 16.1 (2021), pp. 117–137. ISSN: 1832-8105.

[9] S. Clough. “Heptane”. In: *Encyclopedia of Toxicology (Third Edition)*. Ed. by P. Wexler. Third Edition. Oxford: Academic Press, 2014, pp. 845–847. ISBN: 978-0-12-386455-0. DOI: https://doi.org/10.1016/B978-0-12-386454-3.00396-1. URL: https://www.sciencedirect.com/science/article/pii/B9780123864543003961.

[10] A. Cuoci, A. Frassoldati, T. Faravelli, and E. Ranzi. “OpenSMOKE++: An object-oriented framework for the numerical modeling of reactive systems with detailed kinetic mechanisms”. eng. In: *Computer physics communications* 192 (2015), pp. 237–264. ISSN: 0010-4655.

[11] M. Di Renzo, G. Pascazio, and J. Urzay. “The breakdown of self-similarity in electrified counterflow diffusion flames”. eng. In: *Combustion and flame* 205.C (2019), pp. 231–240. ISSN: 0010-2180.

[12] N. Duarte Souza Alvarenga Santos, V. Rückert Roso, A. C. Teixeira Malaquias, and J. G. Coelho Baêta. “Internal combustion engines and biofuels: Examining why this robust combination should not be ignored for future sustainable transportation”. eng. In: *Renewable sustainable energy reviews* 148 (2021), p. 111292. ISSN: 1364-0321.

[13] A. Elfasakhany. “Experimental investigation on SI engine using gasoline and a hybrid iso-butanol/gasoline fuel”. eng. In: *Energy conversion and management* 95 (2015), pp. 398–405. ISSN: 0196-8904.

[14] A. Elfasakhany. “Investigations on performance and pollutant emissions of spark-ignition engines fueled with n-butanol–, isobutanol–, ethanol–, methanol–, and acetone–gasoline blends: A comparative study”. eng. In: *Renewable sustainable energy reviews* 71 (2017), pp. 404–413. ISSN: 1364-0321.

[15] C. Falsetti, R. Kapulla, S. Paranjape, and D. Paladino. “Thermal radiation, its effect on thermocouple measurements in the PANDA facility and how to compensate it”. In: *Nuclear Engineering and Design* 375 (2021), p. 111077. ISSN: 0029-5493. DOI: https://doi.org/10.1016/j.nucengdes.2021.111077. URL: https://www.sciencedirect.com/science/article/pii/S0029549321000297.

[16] C. Frouzakis, J. Lee, A. Tomboulides, and K. Boulouchos. “Two-dimensional direct numerical simulation of opposed-jet hydrogen-air diffusion flame”. eng. In: *Symposium, International, on Combustion* 27.1 (1998), pp. 571–577. ISSN: 0082-0784.

[17] R. K. Gehmlich. “Experimental Studies on Nonpremixed Combustion at Atmospheric and Elevated Pressures”. eng. PhD thesis. 2015.

[18] R. Grana, K. Seshadri, A. Cuoci, U. Niemann, T. Faravelli, and E. Ranzi. "Kinetic modelling of extinction and autoignition of condensed hydrocarbon fuels in non-premixed flows with comparison to experiment". eng. In: *Combustion and flame* 159.1 (2012), pp. 130–141. ISSN: 0010-2180.

[19] T. C. M. Group. *C1-C16 HT+LT mechanism (Version 2003, March 2020)*. URL: `http://creckmodeling.chem.polimi.it/menu-kinetics/menu-kinetics-detailed-mechanisms/107-category-kinetic-mechanisms/403-mechanisms-1911-tot-ht-lt` (Accessed 03/21/2022).

[20] V. K. Gupta. *Bioenergy research : advances and applications*. eng. Waltham, MA: Elsevier, 2014. ISBN: 0444595643.

[21] V. Hindasageri, R. P. Vedula, and S. V. Prabhu. "Thermocouple error correction for measuring the flame temperature with determination of emissivity and heat transfer coefficient". eng. In: *Review of scientific instruments* 84.2 (2013), pp. 024902–024902. ISSN: 0034-6748.

[22] J. O. Hirschfelder. *Molecular theory of gases and liquids*. eng. New York: Wiley, 1965 - 1954.

[23] S. H. Humer. "Development of a surrogate diesel fuel". eng. PhD thesis. TU Wien, 2007.

[24] R. F. Johnson, A. C. VanDine, G. L. Esposito, and H. K. Chelliah. "On the Axisymmetric Counterflow Flame Simulations: Is There an Optimal Nozzle Diameter and Separation Distance to Apply Quasi One-Dimensional Theory?" eng. In: *Combustion science and technology* 187.1-2 (2015), pp. 37–59. ISSN: 0010-2202.

[25] G. Kalghatgi. "Is it really the end of internal combustion engines and petroleum in transport?" eng. In: *Applied energy* 225 (2018), pp. 965–974. ISSN: 0306-2619.

[26] T. Kober, H.-W. Schiffer, M. Densing, and E. Panos. "Global energy perspectives to 2060 – WEC's World Energy Scenarios 2019". eng. In: *Energy strategy reviews* 31 (2020), p. 100523. ISSN: 2211-467X.

[27] C. K. Law. *Combustion Physics*. eng. Vol. 9780521870528. Cambridge: Cambridge University Press, 2006. ISBN: 0521154219.

[28] A. Liñán. "The asymptotic structure of counterflow diffusion flames for large activation energies". eng. In: *Acta astronautica* 1.7 (1974), pp. 1007–1039. ISSN: 0094-5765.

[29] G. Mairinger, A. Frassoldati, A. Cuoci, M. Pelucchi, E. Pucher, and K. Seshadri. "Experimental and computational investigation of autoignition of jet fuels and surrogates in nonpremixed flows at elevated pressures". eng. In: *Proceedings of the Combustion Institute* 37.2 (2019), pp. 1605–1614. ISSN: 1540-7489.

[30] G. Mairinger, A. Frassoldati, R. Gehmlich, U. Niemann, A. Stagni, E. Ranzi, and K. Seshadri. "Autoignition of condensed hydrocarbon fuels in non-premixed flows at elevated pressures". eng. In: *Combustion theory and modelling* 20.6 (2016), pp. 995–1009. ISSN: 1364-7830.

[31] S. McAllister, J.-Y. Chen, and A. C. Fernandez-Pello. *Fundamentals of combustion processes*. eng. Mechanical engineering series. New York, NY [u.a.]: Springer, 2011. ISBN: 1441979425.

[32] I. Mporas, P. Kourtessis, A. Al-Habaibeh, A. Asthana, V. Vukovic, and J. Senior. *Energy and Sustainable Futures : Proceedings of 2nd ICESF 2020*. eng. 1st ed. 2021. Springer Proceedings in Energy. Cham: Springer International Publishing Imprint: Springer, 2021. ISBN: 3030639169. URL: 10.1007/978-3-030-63916-7.

[33] A. Mukhopadhyay and S. Sen. *Fundamentals of combustion engineering*. eng. New York, NY: CRC Press, 2019. ISBN: 0429158211. URL: https://www.taylorfrancis.com/books/9780429158216.

[34] U. Niemann, K. Seshadri, and F. A. Williams. "Accuracies of laminar counterflow flame experiments (vol 162, pg 1540, 2015)". eng. In: *Combustion and flame* 162.12 (2015), pp. 4673–4673. ISSN: 0010-2180.

[35] S.-Y. No. *Application of Liquid Biofuels to Internal Combustion Engines*. eng. 1st ed. 2019. Green Energy and Technology. Singapore: Springer Singapore Imprint: Springer, 2019. ISBN: 981136737X. URL: 10.1007/978-981-13-6737-3.

[36] K. Pandey, R. Misra, P. Patowari, and U. Dixit. *Recent Advances in Mechanical Engineering : Select Proceedings of ICRAME 2020*. eng. 1st ed. 2021. Lecture Notes in Mechanical Engineering. Singapore: Springer Singapore Imprint: Springer, 2021. ISBN: 9811577110. URL: 10.1007/978-981-15-7711-6.

[37] I. Proudman. "An example of steady laminar flow at large Reynolds number". eng. In: *Journal of fluid mechanics* 9.4 (1960), pp. 593–602. ISSN: 0022-1120.

[38] PubChem. *Compound Summary Decane*. URL: https://pubchem.ncbi.nlm.nih.gov/compound/Decane#section=Consumer-Uses (Accessed 12/02/2021).

[39] P. Qiu, F. Wang, Q. Guo, A. Richter, J. Xu, and Z. Dai. "Reduced-order modeling of turbulent flow reactors by tracing the Damköhler numbers". eng. In: *Chemical engineering science* 248 (2022), pp. 117112–. ISSN: 0009-2509.

[40] R. C. Ray. *Sustainable biofuels : opportunities and challenges*. eng. Applied Biotechnology Reviews. London, England: Academic Press, 2021. ISBN: 0128223928.

[41] N. Rietmann, B. Hügler, and T. Lieven. "Forecasting the trajectory of electric vehicle sales and the consequences for worldwide CO2 emissions". eng. In: *Journal of cleaner production* 261 (2020), p. 121038. ISSN: 0959-6526.

[42] R. Seiser, K. Seshadri, E. Piskernik, and A. Liñán. "Ignition in the viscous layer between counterflowing streams: asymptotic theory with comparison to experiments". eng. In: *Combustion and flame* 122.3 (2000), pp. 339–349. ISSN: 0010-2180.

[43] R. Seiser. "Nonpremixed combustion of liquid hydrocarbon fuels". eng. PhD thesis. Graz University of Technology, 2000.

[44] K. Seshadri, S. Humer, and R. Seiser. "Activation-energy asymptotic theory of autoignition of condensed hydrocarbon fuels in non-premixed flows with comparison to experiment". eng. In: *Combustion theory and modelling* 12.5 (2008), pp. 831–855. ISSN: 1364-7830.

[45] K. Seshadri and F. Williams. "Laminar flow between parallel plates with injection of a reactant at high reynolds number". eng. In: *International journal of heat and mass transfer* 21.2 (1978), pp. 251–253. ISSN: 0017-9310.

[46] C. Shaddix. "Correcting thermocouple measurements for radiation loss: A critical review". eng. In: Sandia National Labs., Livermore, CA (US). United States: American Society of Mechanical Engineers, New York, NY (US), 1999.

[47] E. Solmaz and F. Bisetti. "Flamelet chemistry model for efficient axisymmetric counterflow flame simulations with realistic nozzle geometries and gravitational body force". eng. In: *Combustion theory and modelling* 24.5 (2020), pp. 926–952. ISSN: 1364-7830.

[48] N. I. of Standards and T. (NIST). *Decane*. URL: `https://webbook.nist.gov/cgi/inchi/InChI%5C%3D1S/C10H22/c1-3-5-7-9-10-8-6-4-2/h3-10H2%5C%2C1-2H3` (Accessed 11/29/2021).

[49] N. I. of Standards and T. (NIST). *Heptane*. URL: `https://webbook.nist.gov/cgi/inchi/InChI%5C%3D1S/C7H16/c1-3-5-7-6-4-2/h3-7H2%5C%2C1-2H3` (Accessed 11/29/2021).

[50] O. A. Towoju and F. A. Ishola. "A case for the internal combustion engine powered vehicle". In: *Energy Reports* 6 (2020). The 6th International Conference on Power and Energy Systems Engineering, pp. 315–321. ISSN: 2352-4847. DOI: https://doi.org/10.1016/j.egyr.2019.11.082. URL: https://www.sciencedirect.com/science/article/pii/S2352484719309977.

[51] UCSD. *The San Diego Mechanism. Chemical-Kinetic Mechanisms for Combustion Applications*. URL: https://web.eng.ucsd.edu/mae/groups/combustion/sdmech/sandiego20161214/sandiego20161214_mechCK.txt (Accessed 02/10/2022).

[52] S. Venkateshan. *Heat Transfer*. eng. 3rd ed. 2021. Cham: Springer International Publishing Imprint: Springer, 2021. ISBN: 3030583384. URL: 10.1007/978-3-030-58338-5.

[53] M. Yusoff, N. Zulkifli, H. Masjuki, M. Harith, A. Syahir, L. Khuong, M. Zaharin, and A. Alabdulkarem. "Comparative assessment of ethanol and isobutanol addition in gasoline on engine performance and exhaust emissions". eng. In: *Journal of cleaner production* 190 (2018), pp. 483–495. ISSN: 0959-6526.

A
Results extinction experiments

A.1 Extinction of Heptane–Decane mixtures

Mixture	Heptane	Decane
	100%-Vol.	0%-Vol.

$Y_{O_2.2}[-]$	$a_{2.E}[\frac{1}{s}]$	∅ Strain rate•$[\frac{1}{s}]$	| Relative deviation• |	∅MAD$[\frac{1}{s}]^{\otimes}$
0.165	83	81	2.469%	+2
	80		1.235%	-1
	80		1.235%	-1
0.170	100	99.40	0.604%	+0.6
	101		1.610%	+1.6
	99		0.402%	-0.4
	98		1.408%	-1.4
	99		0.402%	-0.4
0.175	120	119.80	0.167%	+0.2
	122		1.836%	+2.2
	120		0.167%	+0.2
	120		0.167%	+0.2
	117		2.337%	-2.8
0.180	145	143.80	0.834%	+1.2
	147		2.225%	+3.2
	143		0.556%	-0.8
	141		1.947%	-2.8
	143		0.556%	-0.8
0.183	157	154.33	1.728%	+2.67
	155		0.432%	+0.67
	151		2.160%	-3.33
0.185	172	172.20	0.116%	-0.2
	174		1.045%	+1.8
	175		1.626%	+2.8
	170		1.278%	-2.2
	170		1.278%	-2.2
0.188	181	182	0.549%	-1
	180		1.099%	-2
	185		1.648%	+3
0.190	205	202.20	1.385%	+2.8
	204		0.890%	+1.8
	206		1.879%	+3.8
	197		2.572%	-5.2
	199		1.583%	-3.2

• Computed values

$^{\otimes}$ MAD between the average strain rate $\varnothing a_{2.E}$ and the actual strain rate $a_{2.E}$.

Table continues on next page

Mixture	Heptane	Decane
	100%-Vol.	0%-Vol.

$Y_{O_2.2}[-]$	$a_{2.E}[\frac{1}{s}]$	∅ Strain rate$^{\bullet}[\frac{1}{s}]$	| Relative deviation$^{\bullet}$ |	∅MAD$[\frac{1}{s}]^{\otimes}$
0.193	217	216.67	0.154%	+0.33
	219		1.077%	+2.33
	214		1.231%	-2.67
0.195	242	237.60	1.852%	+4.4
	241		1.431%	+3.4
	243		2.273%	+5.4
	230		3.199%	-7.6
	232		2.357%	-5.6
0.198	253	254.40	0.550%	-1.4
	252		0.943%	-2.4
	253		0.550%	-1.4
	260		2.201%	+5.6
	254		0.157%	-0.4

$^{\bullet}$ Computed values
$^{\otimes}$ MAD between the average strain rate $\varnothing a_{2.E}$ and the actual strain rate $a_{2.E}$.

Tab. A.1: Experimental extinction results 100%Vol.Heptane carried out at $T_2 = 294.15K$ and p_{atm}.

Mixture	Heptane	Decane
	80%-Vol.	20%-Vol.

$Y_{O_2.2}[-]$	$a_{2.E}[\frac{1}{s}]$	⌀ Strain rate$^{\bullet}[\frac{1}{s}]$	| Relative deviation$^{\bullet}$ |	⌀MAD$[\frac{1}{s}]^{\otimes}$
0.165	69*	73	5.479%	-4
	74*		1.370%	+1
	76*		4.110%	+3
0.170	89*	90.33	1.476%	-1.33
	89*		1.476%	-1.33
	93*		2.952%	+2.67
0.175	116*	115.67	0.288%	+0.33
	114*		1.441%	-1.67
	117*		1.153%	+1.33
0.180	141	139	1.439%	+2
	139		0%	±0
	137*		1.439%	-2
0.183	160*	159.33	0.418%	+0.67
	160*		0.418%	+0.67
	158*		0.837%	-1.33
0.185	164	163.67	0.204%	+0.33
	163		0.407%	-0.67
	164		0.204%	+0.33
0.188	182	183	0.546%	-1
	184		0.546%	+1
	183		0%	±0
0.190	199	196.33	1.358%	+2.67
	195		0.679%	-1.33
	195		0.679%	-1.33
0.193	213	213	0%	±0
	213		0%	±0
	213		0%	±0
0.195	221*		-	-
	230	229.67	0.145%	+0.33
	230		0.145%	+0.33
	229		0.290%	-0.67
0.198	248	247	0.405%	+1
	248		0.405%	+1
	245		0.810%	-2

$^{\bullet}$ Computed values
* Boyling observed on surface
* No representative value due to observed overflow
$^{\otimes}$ MAD between the average strain rate $\varnothing a_{2.E}$ and the actual strain rate $a_{2.E}$.

Tab. A.2: Experimental extinction results 80%Vol.Heptane and 20%Vol.Decane carried out at $T_2 = 294.15K$ and p_{atm}.

Mixture	Heptane	Decane
	50%-Vol.	50%-Vol.

$Y_{O_2.2}[-]$	$a_{2.E}[\frac{1}{s}]$	∅ Strain rate$^{\bullet}[\frac{1}{s}]$	| Relative deviation$^{\bullet}$ |	∅MAD$[\frac{1}{s}]^{\otimes}$
0.165	64	66.67	4.000%	-2.67
	66		1.000%	-0.67
	70		5.000%	+3.33
0.170	91	88.67	2.632%	+2.33
	88		0.752%	-0.67
	87		1.880%	-1.67
0.175	107	104.67	2.229%	+2.33
	105		0.318%	+0.33
	102		2.548%	-2.67
0.180	132	133	0.752%	-1
	134		0.752%	+1
	133		0%	±0
0.183	147	144.33	1.848%	+2.67
	144		0.231%	-0.33
	142		1.617%	-2.33
0.185	160	158.33	1.053%	+1.67
	160		1.053%	+1.67
	155		2.105%	-3.33
0.188	171	170.67	0.195%	+0.33
	170		0.391%	-0.67
	171		0.195%	+0.33
0.190	190	189.67	0.176%	+0.33
	190		0.176%	+0.33
	189		0.351%	-0.67
0.193	202	200	1.000%	+2
	201		0.500%	+1
	197		1.500%	-3
0.195	224	221	1.357%	+3
	220		0.452%	-1
	219		0.905%	-2
0.198	235	236.33	0.564%	-1.67
	237		0.282%	+0.67
	237		0.282%	+0.67
0.200	247	248	0.403%	-1
	247		0.403%	-1
	250		0.806%	+2

$^{\bullet}$ Computed values

$^{\otimes}$ MAD between the average strain rate $\varnothing a_{2.E}$ and the actual strain rate $a_{2.E}$.

Tab. A.3: Experimental extinction results 50%Vol.Heptane and 50%Vol.Decane carried out at $T_2 = 294.15K$ and p_{atm}.

Mixture	Heptane	Decane
	20%-Vol.	80%-Vol.

$Y_{O_2.2}[-]$	$a_{2.E}[\frac{1}{s}]$	⌀ Strain rate$^{\bullet}[\frac{1}{s}]$	| Relative deviation$^{\bullet}$ |	⌀MAD$[\frac{1}{s}]^{\otimes}$
0.170	76*	76.33	0.437%	-0.33
	76*		0.437%	-0.33
	77*		0.873%	+0.67
0.175	92*	93	1.075%	-1
	94*		1.075%	+1
	93*		0%	±0
0.180	115*	114	0.877%	+1
	112*		1.754%	-2
	115*		0.877%	+1
0.183	134*	132	1.515%	+2
	134*		1.515%	+2
	128*		3.030%	-4
0.185	138	140	1.429%	-2
	138		1.429%	-2
	144		2.857%	+4
0.188	154	152.67	0.873%	+1.33
	149		2.402%	-3.67
	155		1.528%	+2.33
0.190	166	167.67	0.994%	-1.67
	167		0.398%	-0.67
	170		1.392%	+2.33
0.193	182	180.67	0.738%	+1.33
	180		0.369%	-0.67
	180		0.369%	-0.67
0.195	196	197.33	0.676%	-1.33
	197		0.169%	-0.33
	199		0.845%	+1.67
0.198	215	215.33	0.155%	-0.33
	217		0.774%	+1.67
	214		0.619%	-1.33
0.200	228	230.33	1.013%	-2.33
	233		1.158%	+2.67
	230		0.145%	-0.33
0.205	266	264.67	0.504%	+1.33
	265		0.126%	+0.33
	263		0.630%	-1.67

$^{\bullet}$ Computed values
* Boyling observed on surface
$^{\otimes}$ MAD between the average strain rate $\varnothing a_{2.E}$ and the actual strain rate $a_{2.E}$.

Tab. A.4: Experimental extinction results 20%Vol.Heptane and 80%Vol.Decane carried out at $T_2 = 294.15K$ and p_{atm}.

Mixture	Heptane	Decane
	0%-Vol.	100%-Vol.

$Y_{O_2.2}[-]$	$a_{2.E}[\frac{1}{s}]$	∅ Strain rate$^{\bullet}[\frac{1}{s}]$	| Relative deviation$^{\bullet}$ |	∅MAD$[\frac{1}{s}]^{\otimes}$
0.170	70*	66.67	5.000%	+3.33
	66*		1.000%	-0.67
	64*		4.000%	-2.67
0.175	78*	75.33	3.540%	+2.67
	77*		2.212%	+1.67
	71*		5.752%	-4.33
0.180	102*	100.33	1.661%	+1.67
	97*		3.322%	-3.33
	102*		1.661%	+1.67
0.183	122*	117.67	3.683%	+4.33
	114		3.116%	-3.67
	117		0.567%	-0.67
0.185	121	120.33	0.554%	+0.67
	120		0.277%	-0.33
	120		0.277%	-0.33
0.188	143*	141.67	0.941%	+1.33
	141*		0.471%	-0.67
	141*		0.471%	-0.67
0.190	153	152	0.658%	+1
	151		0.658%	-1
	152		0%	±0
0.193	168	167	0.599%	+1
	167		0%	±0
	166		0.599%	-1
0.195	187	183	2.186%	+4
	183		0%	±0
	179		2.186%	-4
0.198	198	196.67	0.678%	+1.33
	195		0.847%	-1.67
	197		0.169%	+0.33
0.205	243	244.67	0.681%	-1.67
	246		0.545%	+1.33
	245		0.136%	+0.33

$^{\bullet}$ Computed values
* Unstable behavior of the surface at the beginning until the extinction strain rate is reached.
$^{\otimes}$ MAD between the average strain rate $\varnothing a_{2.E}$ and the actual strain rate $a_{2.E}$.

Tab. A.5: Experimental extinction results 100%Vol.Decane carried out at $T_2 = 294.15K$ and p_{atm}.

A.2 Extinction of Ethanol–Heptane mixtures

Mixture	Ethanol	Heptane
	100%-Vol.	0%-Vol.

$Y_{O_2.2}[-]$	$a_{2.E}[\frac{1}{s}]$	⌀ Strain rate$^{\bullet}[\frac{1}{s}]$	| Relative deviation$^{\bullet}$ |	⌀MAD$[\frac{1}{s}]^{\otimes}$
0.150	67*	66.67	0.500%	+0.33
	66*		1.000%	-0.67
	67*		0.500%	+0.33
0.160	102*	100.67	1.325%	+1.33
	98*		2.649%	-2.67
	102*		1.325%	+1.33
0.170	149	144	3.472%	+5
	145		0.694%	+1
	138		4.167%	-6
0.180	195	195.33	0.171%	+0.33
	198		1.365%	+2.67
	193		1.195%	-2.33
0.183	217	215.67	0.618%	+1.33
	214		0.773%	-1.67
	216		0.155%	+0.33
0.185	235	232	1.293%	+3
	231		0.431%	-1
	230		0.862%	-2
0.188	256	253	1.186%	+3
	250		1.186%	-3
	253		0%	±0
0.190	265	272	2.574%	-7
	269		1.103%	-3
	282		3.676%	+10
0.200	379	375	1.067%	+4
	376		0.267%	+1
	370		1.333%	-5

$^{\bullet}$ Computed values
* Boyling observed on surface
$^{\otimes}$ MAD between the average strain rate $\varnothing a_{2.E}$ and the actual strain rate $a_{2.E}$.

Tab. A.6: Experimental extinction results 100%Vol.Ethanol carried out at $T_2 = 294.15K$ and p_{atm}.

Mixture	Ethanol	Heptane
	80%-Vol.	20%-Vol.

$Y_{O_2.2}[-]$	$a_{2.E}[\frac{1}{s}]$	⌀ Strain rate$^{\bullet}[\frac{1}{s}]$	| Relative deviation$^{\bullet}$ |	⌀MAD$[\frac{1}{s}]^{\otimes}$
0.160	91*	89.67	1.487%	+1.33
	89*		0.743%	-0.67
	89*		0.743%	-0.67
0.170	124*	123.67	0.270%	+0.33
	125*		1.078%	+1.33
	122*		1.348%	-1.67
0.175	143*	145.33	1.606%	-2.33
	146*		0.459%	+0.67
	147*		1.147%	+1.67
0.180	186	182.67	1.825%	+3.33
	186		1.825%	+3.33
	176		3.650%	-6.67
0.183	201	191	5.236%	+10
	185		3.141%	-6
	187		2.094%	-4
0.185	224	216	3.704%	+8
	214		0.926%	-2
	210		2.778%	-6
0.188	235	228	3.070%	+7
	225		1.316%	-3
	224		1.754%	-4
0.190	256	253.67	0.920%	+2.33
	253		0.263%	-0.67
	252		0.657%	-1.67
0.195	304	304.67	0.219%	-0.67
	308		1.094%	+3.33
	302		0.875%	+2.67

$^{\bullet}$ Computed values

* Observed unstable behavior at surface while operating with low oxygen mass fraction

$^{\otimes}$ MAD between the average strain rate $\varnothing a_{2.E}$ and the actual strain rate $a_{2.E}$.

Tab. A.7: Experimental extinction results 80%Vol.Ethanol and 20%Vol.Heptane carried out at $T_2 = 294.15K$ and p_{atm}.

Mixture	Ethanol	Heptane
	50%-Vol.	50%-Vol.

$Y_{O_2.2}[-]$	$a_{2.E}[\frac{1}{s}]$	⌀ Strain rate•$[\frac{1}{s}]$	| Relative deviation• |	⌀MAD$[\frac{1}{s}]^{\otimes}$
0.160	80	76.20	4.987%	+3.8
	77		1.050%	+0.8
	75		1.575%	-1.2
	74		2.887%	-2.2
	75		1.575%	-1.2
0.165	87	86.67	0.385%	+0.33
	91		5.000%	+4.33
	97⋆		-	-
	82		5.385%	-4.67
0.170	116	109.20	6.227%	+6.8
	117		7.143%	+7.8
	111		1.648%	+1.8
	103		5.678%	-6.2
	99		9.341%	-9.8
0.175	141	132.20	6.657%	+8.8
	140		5.900%	+7.8
	137		3.631%	+5.2
	122		7.716%	-9.8
	121		8.472%	-11.2
0.180	167	151.6	10.158%	+15.4
	164		8.179%	+12.4
	146		3.694%	-5.6
	141		6.992%	-9.6
	140		7.652%	-10.6
0.183	160	159	0.629%	+1
	162		1.887%	+3
	156		1.887%	-3
	160		0.629%	+1
	157		1.258%	-2
0.185	191	179.60	6.347%	+10.4
	194		8.018%	+14.4
	181⋆		-	-
	172		4.232%	-7.6
	171		4.788%	-8.6
	170		5.345%	-9.6

• Computed values

$^{\otimes}$ MAD between the average strain rate $\varnothing a_{2.E}$ and the actual strain rate $a_{2.E}$.

Table continues on next page

Mixture	Ethanol	Heptane			
	50%-Vol.	50%-Vol.			
$Y_{O_2.2}[-]$	$a_{2.E}[\frac{1}{s}]$		⌀ Strain rate$^{\bullet}[\frac{1}{s}]$	| Relative deviation$^{\bullet}$ |	⌀MAD$[\frac{1}{s}]^{\otimes}$
0.188	218		207.60	5.010%	+10.4
	213			2.601%	+5.4
	206			0.771%	-1.6
	200			3.661%	-7.6
	201			3.179%	-6.6
0.190	220		220	0%	±0
	222			0.909%	+2
	206*			-	-
	226			2.727%	+6
	220			0%	±0
	212			3.636%	-8
0.193	257		241.40	6.462%	+15.6
	253			4.805%	+11.6
	235			2.651%	-6.4
	231			4.308%	-10.4
	231			4.308%	-10.4
0.195	277		265	4.528%	+12
	274			3.396%	+9
	262			1.132%	-3
	258			2.642%	-7
	254			4.151%	-11
0.200	322		319.67	0.730%	+2.33
	322			0.730%	+0.33
	315			1.460%	-4.67

$^{\bullet}$ Computed values

* No representative value due to observed overflow

$^{\otimes}$ MAD between the average strain rate $\varnothing a_{2.E}$ and the actual strain rate $a_{2.E}$.

Tab. A.8: Experimental extinction results 50%Vol.Ethanol and 50%Vol.Heptane carried out at $T_2 = 294.15K$ and p_{atm}.

Mixture	Ethanol	Heptane
	20%-Vol.	80%-Vol.

$Y_{O_2.2}[-]$	$a_{2.E}[\frac{1}{s}]$	⌀ Strain rate$^{\bullet}[\frac{1}{s}]$	| Relative deviation$^{\bullet}$ |	⌀MAD$[\frac{1}{s}]^{\otimes}$
0.160	82	79.33	3.361%	+2.67
	76		4.202%	-3.33
	80		0.840%	+0.67
0.165	98	95.67	2.439%	+2.33
	94		1.742%	-1.67
	95		0.697%	-0.67
0.170	115	114.33	0.583%	+0.67
	106*		-	-
	115		0.583%	+0.67
	113		1.166%	-1.33
0.175	138	135.67	1.720%	+2.33
	133		1.966%	-2.67
	136		0.246%	+0.33
0.180	158	157.67	0.211%	+0.33
	158		0.211%	+0.33
	157		0.423%	-0.67
0.183	183	180	1.667%	+3
	180		0%	±0
	177		1.667%	-3
0.185	185	189.67	2.460%	-4.67
	192		1.230%	+2.33
	192		1.230%	+2.33
0.188	208	206.33	0.808%	+1.67
	204		1.131%	-2.33
	207		0.323%	+0.67
0.190	229	224.33	2.080%	+4.67
	221		1.486%	-3.33
	223		0.594%	-1.33
0.193	243	242.67	0.137%	+0.33
	243		0.137%	+0.33
	242		0.275%	-0.67
0.195	259	258.33	0.258%	+0.67
	259		0.258%	+0.67
	257		0.516%	-1.33
0.200	308	306.33	0.544%	+1.67
	306		0.109%	-0.33
	305		0.435%	-1.33

$^{\bullet}$ Computed values

* No representative value due to observed overflow

$^{\otimes}$ MAD between the average strain rate $\varnothing a_{2.E}$ and the actual strain rate $a_{2.E}$.

Tab. A.9: Experimental extinction results 20%Vol.Ethanol and 80%Vol.Heptane carried out at $T_2 = 294.15K$ and p_{atm}.

A.3 Extinction of Isobutanol–Heptane mixtures

Mixture	Isobutanol	Heptane
	100%-Vol.	0%-Vol.

$Y_{O_2.2}[-]$	$a_{2.E}[\frac{1}{s}]$	∅ Strain rate$^{\bullet}[\frac{1}{s}]$	| Relative deviation$^{\bullet}$ |	∅MAD$[\frac{1}{s}]^{\otimes}$
0.160	◎	-	-	
	◎	-	-	
	◎	-	-	
0.170	98	95.60	2.510%	+3.6
	99		3.556%	+3.4
	97		1.464%	+1.4
	92		3.766%	-3.6
	92		3.766%	-3.6
0.175	110	111.60	1.434%	-1.6
	115		3.047%	+3.4
	112		0.358%	+0.4
	111		0.538%	-0.6
	110		1.434%	-1.6
0.180	133	132.40	0.453%	+0.6
	137		3.474%	+4.6
	133		0.453%	+0.6
	128		3.323%	-4.4
	131		1.057%	-1.4
0.183	154	153	0.654%	+1
	152		0.654%	-1
	153		0%	±0
0.185	162	158.80	2.015%	+3.2
	160		0.756%	+1.2
	159		0.126%	+0.2
	155		2.393%	-3.8
	158		0.504%	-0.8
0.188	176	176.33	0.187%	-0.33
	177		0.379%	+0.67
	176		0.187%	-0.33
0.190	184	185.20	0.648%	-1.2
	186		0.432%	+0.8
	187		0.972%	+1.8
	185		0.108%	+0.2
	184		0.648%	-1.2

$^{\bullet}$ Computed values
$^{\circledcirc}$ Liquid wasn't ignitable
$^{\otimes}$ MAD between the average strain rate $\varnothing a_{2.E}$ and the actual strain rate $a_{2.E}$.
Table continues on next page

Mixture	Isobutanol	Heptane
	100%-Vol.	0%-Vol.

$Y_{O_2.2}[-]$	$a_{2.E}[\frac{1}{s}]$	∅ Strain rate$^{\bullet}[\frac{1}{s}]$	| Relative deviation$^{\bullet}$ |	∅MAD$[\frac{1}{s}]^{\otimes}$
0.193	202	204	0.980%	-2
	204		0%	±0
	206		0.980%	+2
0.195	217	217.20	0.092%	-0.2
	216		0.552%	-1.2
	216		0.552%	-1.2
	219		0.829%	+1.8
	218		0.368%	+0.8
0.198	239	241	0.830%	-2
	243		0.830%	+2
	241		0%	±0
0.200	257	257	0%	±0
	255		0.778%	-2
	258		0.389%	+1
	258		0.389%	+1
	257		0%	±0

$^{\bullet}$ Computed values

$^{\otimes}$ MAD between the average strain rate $\varnothing a_{2.E}$ and the actual strain rate $a_{2.E}$.

Tab. A.10: Experimental extinction results 100%Vol.Isobutanol carried out at $T_2 = 294.15K$ and p_{atm}.

Mixture	Isobutanol	Heptane
	80%-Vol.	20%-Vol.

$Y_{O_2.2}[-]$	$a_{2.E}[\frac{1}{s}]$	⌀ Strain rate•$[\frac{1}{s}]$	| Relative deviation• |	⌀MAD$[\frac{1}{s}]^{\otimes}$
0.160	◎	-	-	
	◎	-	-	
	◎	-	-	
0.170	94◎	90.80	3.524%	+3.2
	90◎		0.881%	-0.8
	93◎		2.423%	+2.2
	87		4.185%	-3.8
	90		0.881%	-0.8
0.175	113	111.20	1.619%	+2.2
	112		0.719%	+0.8
	112		0.719%	+0.8
	108		2.878%	-3.2
	111		0.180%	-0.2
0.180	134	132	1.515%	+2
	130		1.515%	-2
	136		3.030%	+4
	130		1.515%	-2
	130		1.515%	-2
0.183	150	149	0.671%	+1
	149		0%	±0
	148		0.671%	-1
0.185	160	156.60	2.171%	+3.4
	159		1.533%	+2.4
	160		2.171%	+3.4
	150		4.215%	-6.6
	154		1.660%	-2.6
0.188	176	174.67	0.763%	+1.33
	175		0.191%	+0.33
	173		0.954%	-1.67
0.190	184	184.40	0.217%	-0.4
	185		0.325%	+0.6
	186		0.868%	+1.6
	184		0.217%	-0.4
	183		0.759%	-1.4

• Computed values
◎ Liquid wasn't ignitable
⊗ MAD between the average strain rate $\varnothing a_{2.E}$ and the actual strain rate $a_{2.E}$.
Table continues on next page

Mixture	Isobutanol	Heptane
	80%-Vol.	20%-Vol.

$Y_{O_2.2}[-]$	$a_{2.E}[\frac{1}{s}]$	∅ Strain rate$^{\bullet}[\frac{1}{s}]$	| Relative deviation$^{\bullet}$ |	∅MAD$[\frac{1}{s}]^{\otimes}$
0.193	210	209	0.478%	+1
	209		0%	±0
	208		0.478%	-1
0.195	218	219.60	0.729%	-1.6
	221		0.638%	+1.4
	223		1.548%	+3.4
	220		0.182%	+0.4
	216		1.639%	-3.6
0.198	243	241.33	0.692%	+1.67
	239		0.967%	-2.33
	242		0.278%	+0.67
0.200	260	258	0.775%	+2
	258		0%	±0
	257		0.388%	-1
	259		0.388%	+1
	256		0.775%	-2

$^{\bullet}$ Computed values

$^{\otimes}$ MAD between the average strain rate $\varnothing a_{2.E}$ and the actual strain rate $a_{2.E}$.

Tab. A.11: Experimental extinction results 80%Vol.Isobutanol and 20%Vol.Heptane carried out at $T_2 = 294.15K$ and p_{atm}.

Mixture	Isobutanol	Heptane
	50%-Vol.	50%-Vol.

$Y_{O_2.2}[-]$	$a_{2.E}[\frac{1}{s}]$	⌀ Strain rate•$[\frac{1}{s}]$	| Relative deviation• |	⌀MAD$[\frac{1}{s}]^{\otimes}$
0.160	◎	-	-	
	◎	-	-	
	◎	-	-	
0.170	93	91.20	1.974%	+1.8
	92		0.877%	+0.8
	89		2.412%	-1.2
	93		1.974%	+1.8
	89		2.412%	-1.2
0.175	106	107.60	1.487%	-1.6
	106		1.487%	-1.6
	106		1.487%	-1.6
	110		2.230%	+2.4
	110		2.230%	+2.4
0.180	128	130.80	2.141%	-2.8
	130		0.612%	-0.8
	131		0.153%	+0.2
	133		1.682%	+2.2
	132		0.917%	+1.2
0.183	146	144.67	0.922%	+2.67
	145		0.230%	+0.33
	143		1.152%	-1.67
0.185	153	154.20	0.778%	-1.2
	154		0.130%	-0.2
	147		4.669%	-7.2
	158		2.464%	+3.8
	159		3.113%	+4.8
0.188	166	166	0%	±0
	167		0.602%	+1
	165		0.602%	-1
0.190	182	183.20	0.655%	-1.2
	181		1.201%	-2.2
	179		2.293%	-4.2
	188		2.620%	+4.8
	186		1.528%	+2.8

• Computed values

◎ Liquid wasn't ignitable

⊗ MAD between the average strain rate $\varnothing a_{2.E}$ and the actual strain rate $a_{2.E}$.

Table continues on next page

Mixture	Isobutanol	Heptane
	50%-Vol.	50%-Vol.

$Y_{O_2.2}[-]$	$a_{2.E}[\frac{1}{s}]$	⌀ Strain rate$^{\bullet}[\frac{1}{s}]$	| Relative deviation$^{\bullet}$ |	⌀MAD$[\frac{1}{s}]^{\otimes}$
0.193	200	199	0.503%	+1
	199		0%	±0
	198		0.503%	-1
0.195	220	219.60	0.182%	+0.4
	213		3.005%	-6.6
	217		1.184%	-2.6
	226		2.914%	+6.4
	222		1.093%	+2.4
0.198	245	243.67	0.547%	+1.33
	240		1.505%	-3.67
	246		0.958%	+2.33
0.200	248	250.60	1.038%	-2.6
	248		1.038%	-2.6
	247		1.437%	-3.6
	258		2.953%	+7.4
	252		0.559%	+1.4

$^{\bullet}$ Computed values

$^{\otimes}$ MAD between the average strain rate $\varnothing a_{2.E}$ and the actual strain rate $a_{2.E}$.

Tab. A.12: Experimental extinction results 50%Vol.Isobutanol and 50%Vol.Heptane carried out at $T_2 = 294.15K$ and p_{atm}.

Mixture	Isobutanol	Heptane
	20%-Vol.	80%-Vol.

$Y_{O_2.2}[-]$	$a_{2.E}[\frac{1}{s}]$	⌀ Strain rate•$[\frac{1}{s}]$	| Relative deviation• |	⌀MAD$[\frac{1}{s}]^{\otimes}$
0.160	◎	-	-	
	◎	-	-	
	◎	-	-	
0.170	103*	99.60	3.414%	+3.4
	105*		5.422%	+5.4
	102*		2.410%	+2.4
	92		7.631%	-7.6
	96		3.614%	-3.6
0.175	116*	116.40	0.344%	-0.4
	119		2.234%	+2.6
	120		3.093%	+3.6
	114		2.062%	-2.4
	113		2.921%	-3.4
0.180	144	140.80	2.273%	+3.2
	145		2.983%	+4.2
	145		2.983%	+4.2
	132		6.250%	-8.8
	138		1.989%	-2.8
0.183	159	158.67	0.210%	+0.33
	158		0.420%	-0.67
	159		0.210%	+0.33
0.185	166	165	0.606%	+1
	166		0.606%	+1
	167		1.212%	+2
	165		0%	±0
	161		2.424%	-4
0.188	185	185	0%	±0
	186		0.541%	+1
	184		0.541%	-1
0.190	194	194	0%	±0
	192		1.031%	-2
	194		0%	±0
	196		1.031%	+2
	194		0%	±0

• Computed values

* Observed unstable behavior at surface while operating with low oxygen mass fraction

◎ Liquid wasn't ignitable

⊗ MAD between the average strain rate $\varnothing a_{2.E}$ and the actual strain rate $a_{2.E}$.

Table continues on next page

Mixture	Isobutanol	Heptane
	20%-Vol.	80%-Vol.

$Y_{O_2.2}[-]$	$a_{2.E}[\frac{1}{s}]$	∅ Strain rate$^{\bullet}[\frac{1}{s}]$	| Relative deviation$^{\bullet}$ |	∅MAD$[\frac{1}{s}]^{\otimes}$
0.193	208	208.33	0.160%	-0.33
	209		0.320%	+0.67
	208		0.160%	-0.33
0.195	215	224	4.018%	-9
	223		0.446%	-1
	221		1.339%	-3
	230		2.679%	+6
	231		3.125%	+7
0.198	243	244.67	0.681%	-1.67
	247		0.954%	+2.33
	244		0.272%	-0.67
0.200	260	263	1.141%	-3
	257		2.281%	-6
	258		1.901%	-5
	270		2.662%	+7
	270		2.662%	+7

$^{\bullet}$ Computed values

$^{\otimes}$ MAD between the average strain rate $\varnothing a_{2.E}$ and the actual strain rate $a_{2.E}$.

Tab. A.13: Experimental extinction results 20%Vol.Isobutanol and 80%Vol.Heptane carried out at $T_2 = 294.15K$ and p_{atm}.

B
Investigations autoignition experiments

B.1 Experimental autoignition of Ethanol–Heptane mixtures

Ethanol[%Vol.]	Heptane[%Vol.]	Strain rate[$\frac{1}{s}$]	T_{tc}[K]	T_g[K]	ΔT[K]	MAD[K]$^{\otimes}$	p[kPa]
80	20	100	1086	1104.55	18.55	+2.0	100500
		150	1104	1122.54	18.54	+1.0	100500
		200	1117	1135.44	18.44	-3.5	100500
		250	1144	1163.30	19.30	+1.0	100500
		300	1159	1178.53	19.53	+0.5	100500
		350	1173	1192.78	19.78	-2.0	100500
		400	1190	1210.26	20.26	+0.5	100500
		450	1204	1224.61	20.61	-0.5	100500
80	20	100	1082	1100.31	18.31	-2.0	100300
		150	1102	1120.42	18.42	-1.0	100300
		200	1124	1142.85	18.85	+3.5	100300
		250	1142	1161.18	19.18	-1.0	100300
		300	1158	1177.47	19.47	-0.5	100300
		350	1177	1197.02	20.02	+2.0	100300
		400	1189	1209.20	20.20	-0.5	100300
		450	1205	1225.67	20.67	+0.5	100400
50	50	100	1095	1114.09	19.09	±0	100100
		150	1111	1129.95	18.95	+1.0	100100
		200	1125	1143.91	18.91	+0.5	100100
		250	1144	1163.30	19.30	+2.5	100100
		300	1161	1180.65	19.65	-1.0	100100
		350	1180	1200.20	20.20	+0.5	100100
		400	1192	1212.38	20.38	-1.0	100100
		450	1205	1225.67	20.67	±0	100100
50	50	100	1095	1114.09	19.09	±0	99000
		150	1109	1127.83	18.83	-1.0	99000
		200	1124	1142.85	18.85	-0.5	99000
		250	1139	1158.00	19.00	-2.5	99000
		300	1163	1182.77	19.77	+1.0	99000
		350	1179	1199.14	20.14	-0.5	99000
		400	1194	1214.50	20.50	+1.0	99000
		450	1205	1225.67	20.67	±0	99000

$^{\otimes}$ MAD between the average thermocouple temperature $\varnothing T_{tc}$ and the actual thermocouple temperature T_{tc}.

Table continues on next page

Ethanol[%Vol.]	Heptane[%Vol.]	Strain rate[$\frac{1}{s}$]	T_{tc}[K]	T_g[K]	ΔT[K]	MAD[K]$^{\otimes}$	p[kPa]
20	80	100	1099	1118.34	19.34	-3	100200
		150	1116	1135.26	19.26	-3.0	100200
		200	1129	1148.15	19.15	-2.5	100200
		250	1147	1166.47	19.47	-0.5	100200
		300	1156*	1175.36	19.36	-1.5	100200
		350	1176*	1195.96	19.96	+1.0	100200
		400	1192	1203.90	21.90	±0	100200
		450	1209*	1229.91	20.91	+4.0	100200
20	80	100	1105	1124.71	19.71	+3	100200
		150	1122	1141.62	19.62	+3.0	100200
		200	1134	1153.45	19.45	+2.5	100200
		250	1146	1165.41	19.41	+0.5	100200
		300	1159*	1178.53	19.53	+1.5	100200
		350	1174	1193.84	19.84	-1.0	100200
		400	1192*	1212.38	20.38	±0	100200
		450	1201	1221.42	20.42	-4.0	100200

* During experiment high speed photographs showed a water bubble leading to turbulence flows on the stagnation plane and an increase of the surface level causing an ignition. Nevertheless, the value corresponds to a good measurement of the autoignition temperature.

$^{\otimes}$ MAD between the average thermocouple temperature $\varnothing T_{tc}$ and the actual thermocouple temperature T_{tc}.

Tab. B.1: Autoignition results Ethanol–Heptane mixtures carried out at $Y_{O_2.2} = 0.233$ and $T_1 = 294.15K$

B.2 Average autoignition values of Ethanol

Ethanol[%Vol.]	Strain rate[$\frac{1}{s}$]	T_{tc}[K]	$\varnothing T_{tc}$[K]	$\varnothing T_g$[K]	$\varnothing \Delta T$[K]	$\varnothing$MAD[K]$^{\otimes}$
100	100	1086				+4.75
		1081				-0.25
		1080				-1.25
		1078	1081.25	1099.52	18.27	-3.25
	150	1092				-7.75
		1095				-4.75
		1100				+0.25
		1112	1099.75	1118.04	18.29	+12.25
	200	1131				+13.50
		1121				+3.50
		1113				-4.50
		1105	1117.50	1135.97	18.47	-12.50
	250	1136				-3.50
		1154				+14.50
		1128				-11.50
		1140	1139.50	1158.53	19.03	+0.50
	300	1171				+10.25
		1159				-1.75
		1167				+6.25
		1146	1160.75	1180.39	19.64	-14.75
	350	1171				-9.25
		1182				+1.75
		1186				+5.75
		1182	1180.25	1200.47	20.22	+1.75
	400	1195				+2.00
		1195				+2.00
		1198				+5.00
		1184	1193.00	1213.44	20.44	-11.00
	450	1198				-5.75
		1209				+5.25
		1204				+1.75
		1204	1203.75	1224.34	20.59	+1.75

The Ethanol autoignition evaluations were provided by UCSD from work done by previous research groups. Therefore, only the arithmetic mean value was used for the gas temperature and the radiation error. The investigations were carried out at $Y_{O_2,2} = 0.233$ and $T_1 = 294.15K$.

$^{\otimes}$MAD between the average thermocouple temperature $\varnothing T_{tc}$ and the actual thermocouple temperature T_{tc}.

Tab. B.2: Former autoignition results of Ethanol

B.3 Average autoignition values of Heptane

Heptane[%Vol.]	Strain rate[$\frac{1}{s}$]	T_{tc}[K]	$\varnothing T_{tc}$[K]	$\varnothing T_g$[K]	$\varnothing \Delta T$[K]	$\varnothing$MAD[K]$^{\otimes}$
100	100	1070				-4.00
		1072				-2.00
		1078				+4.00
		1076	1074.00	1091.84	17.84	+2.00
	150	1096				-3.75
		1100				+0.25
		1103				+3.25
		1100	1099.75	1118.04	18.29	+0.25
	200	1106				-10.00
		1123				+7.00
		1127				+11.00
		1108	1116.00	1134.38	18.38	-8.00
	250	1144				+5.50
		1135				-3.50
		1143				+4.50
		1132	1138.50	1157.47	18.97	-6.50
	300	1149				-4.00
		1154				+1.00
		1156	1153.00	1172.18	19.18	+3.00
	350	1164				-1.50
		1167	1165.50	1184.84	19.34	+1.50
	400	1181				-7.00
		1195	1188.00	1208.14	20.14	+7.00
	450	1196				+0.50
		1195	1195.50	1215.59	20.09	-0.50

The Heptane autoignition evaluations were provided by UCSD from work done by previous research groups. Therefore, only the arithmetic mean value was used for the gas temperature and the radiation error. The investigations were carried out at $Y_{O_2,2} = 0.233$ and $T_1 = 294.15K$.

$^{\otimes}$ MAD between the average thermocouple temperature $\varnothing T_{tc}$ and the actual thermocouple temperature T_{tc}.

Tab. B.3: Former autoignition results of Heptane

C
Numerical calculations

Investigated fuel	100%Vol. Heptane							
Strain rate$[\frac{1}{s}]$	100	150	200	250	300	350	400	450
$T_{num.AI}$[K]	1122.12	1159.71	1181.39	1195.70	1206.75	1215.95	1223.91	1230.89
$\varnothing T_g$[K]	1091.84	1118.04	1134.38	1157.47	1172.18	1184.84	1208.14	1215.59
ΔT[K]	30.28	41.67	47.01	38.23	34.57	31.11	15.77	15.30
$v_2[\frac{m}{s}]$	0.5	0.75	1.0	1.25	1.5	1.75	2.0	2.25
Investigated fuel	80%Vol. Heptane		20%Vol. Ethanol					
Strain rate$[\frac{1}{s}]$	100	150	200	250	300	350	400	450
$T_{num.AI}$[K]	1142.67	1170.66	1190.32	1205.55	1217.94	1228.40	1237.45	1245.36
$\varnothing T_g$[K]	1121.53	1138.44	1150.80	1165.94	1176.95	1194.90	1208.14	1225.67
ΔT[K]	21.14	32.22	39.52	39.61	40.99	33.50	29.31	19.69
$v_2[\frac{m}{s}]$	0.5	0.75	1.0	1.25	1.5	1.75	2.0	2.25
Investigated fuel	50%Vol. Heptane		50%Vol. Ethanol					
Strain rate$[\frac{1}{s}]$	100	150	200	250	300	350	400	450
$T_{num.AI}$[K]	1138.34	1168.26	1189.84	1206.67	1220.45	1232.08	1242.22	1251.19
$\varnothing T_g$[K]	1114.09	1128.89	1143.38	1160.65	1181.71	1199.67	1213.44	1225.67
ΔT[K]	24.25	39.37	46.46	46.02	38.74	32.41	28.78	25.52
$v_2[\frac{m}{s}]$	0.5	0.75	1.0	1.25	1.5	1.75	2.0	2.25
Investigated fuel	20%Vol. Heptane		80%Vol. Ethanol					
Strain rate$[\frac{1}{s}]$	100	150	200	250	300	350	400	450
$T_{num.AI}$[K]	1136.89	1167.59	1189.97	1207.57	1222.10	1234.45	1245.16	1254.72
$\varnothing T_g$[K]	1102.43	1121.48	1139.15	1162.24	1178.00	1194.90	1209.73	1225.14
ΔT[K]	34.46	46.11	50.82	45.33	44.10	39.55	35.43	29.58
$v_2[\frac{m}{s}]$	0.5	0.75	1.0	1.25	1.5	1.75	2.0	2.25
Investigated fuel	100%Vol. Ethanol							
Strain rate$[\frac{1}{s}]$	100	150	200	250	300	350	400	450
$T_{num.AI}$[K]	1136.87	1167.93	1190.61	1208.54	1223.37	1236.02	1247.08	1256.85
$\varnothing T_g$[K]	1099.52	1118.04	1135.97	1158.53	1180.39	1200.47	1213.44	1224.34
ΔT[K]	37.35	49.89	54.64	50.01	42.98	35.55	33.64	32.51
$v_2[\frac{m}{s}]$	0.5	0.75	1.0	1.25	1.5	1.75	2.0	2.25

The numerical calculations were performed in OpenSMOKE++ using one-step chemistry. $\varnothing T_g$ is the corrected average gas temperature including the radiation error.

Tab. C.1: Numerical calculation results of Ethanol–Heptane mixtures carried out at $Y_{O_2,2} = 0.233$ and $T_1 = 298.15K$.

List of Figures

List of Tables

List of Equations